siam

13th Annual Meeting of the Bulgarian Section of SIAM
December 18-20, 2018
Sofia

BGSIAM'18

EXTENDED ABSTRACTS

HOSTED BY THE INSTITUTE OF MECHANICS
BULGARIAN ACADEMY OF SCIENCES

13th Annual Meeting of the Bulgarian Section of SIAM
December 18-20, 2018, Sofia

BGSIAM'18 Extended abstracts

ISSN: 1313-3357 (print)
ISSN: 1314-7145 (electronic)

Printed in Sofia, Bulgaria

PREFACE

The Bulgarian Section of SIAM (BGSIAM) was formed in 2007 with the purpose to promote and support the application of mathematics to science, engineering and technology in Republic of Bulgaria. The goals of BGSIAM follow the general goals of SIAM:

- To advance the application of mathematics and computational science to engineering, industry, science, and society;
- To promote research that will lead to effective new mathematical and computational methods and techniques for science, engineering, industry, and society;
- To provide media for the exchange of information and ideas among mathematicians, engineers, and scientists.

During BGSIAM'18 conference a wide range of problems concerning recent achievements in the field of industrial and applied mathematics will be presented and discussed. The meeting provides a forum for exchange of ideas between scientists, who develop and study mathematical methods and algorithms, and researchers, who apply them for solving real life problems. The conference support provided by SIAM is highly appreciated.

The strongest research groups in Bulgaria in the field of industrial and applied mathematics, advanced computing, mathematical modelling and applications will be presented at the meeting according to the accepted extended abstracts. Many of the participants are young scientists and PhD students.

LIST OF PLENARY INVITED SPEAKERS:

- Owe Axelsson (Czech Academy of Sciences)
  "An inner-product free iteration method for an equation of motion and a bound-constrained optimal control PDE problem"
- Mauro Ballicchia (Polytechnic University of Marche, Italy)
  "Recent advances in the Wigner signed particles: theory and applications"
- Vesselin Iossifov (University of Applied Sciences Berlin, Germany)
  "Programming Techniques for Energy-efficient Software"
- Raytcho Lazarov (Texas A&M University, USA)
  "Recent advances in numerical methods for fractional differential equations with non-smooth data: a concise overview"
- Blagovest Sendov (Bulgarian Academy of Sciences)
  "Algorithmic problems in the geometry of polynomials"

The present volume contains extended abstracts of the presentations (Part A) and list of participants (Part B).

Krassimir Georgiev
Chair of BGSIAM Section

Michail Todorov
Vice-Chair of BGSIAM Section

Ivan Georgiev
Secretary of BGSIAM Section

Sofia, December 2018

Contents

Part A
Extended abstracts[1]

[1] Arranged alphabetically according to the family name of the first author.

Design of a multi-objective optimization model for wireless sensor networks

A.Alexandrov, V.Monov

Wireless sensor networks (WSNs) have had a worldwide attention in the last years, especially with the development of smart sensors and the IoT technology[5][6].
Due to the specific problems in multihop based WSN, the design of the communication protocols poses many new challenges. The development of energy-efficient and reliable communication protocols [1], [2],[3] is very important. The minimum energy routing problem tries to optimize the WSN performance by minimizing its energy consumption[3].
One of the ways to solve this problem is to use the shortest path algorithm for the sensor networks[4], but in the real WSN environment very often the shortest path is not the most energy efficient path.
The aim of this research is to develop a multi-objective optimization model of WSN with cluster topology. The new model can help to find the most energy efficient path between the sensor nodes and the Cluster Head (CH) in WSN.
The presented design includes two objective parameters related to distance and energy restrictions. More specifically, we consider the distance between a sensor node and the CH, and the energy of the node, needed to transfer sensor data to CH.
The optimization model was developed under the following assumptions:
i) The location of the CH does not change during the process of collecting data from the sensor nodes.
ii) Sensor nodes are aware of their geographical coordinates in the field.
iii) Each sensor has resource constraints (with regard to energy and linking distance), and the CH has no energy constraints.
In Fig. 1, we present a sample design of WSN cluster.

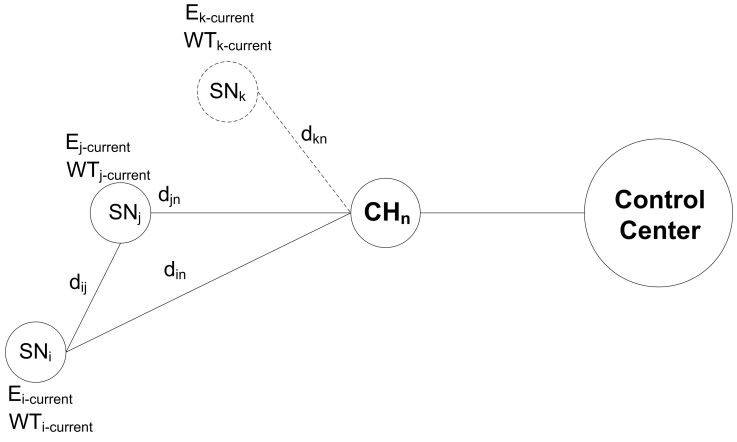

Fig.1 WSN cluster nodes design

In the WSN model on Fig.1 there are several sensor nodes who transmit the sensor data to the CH head directly or through neighbor sensor nodes. Most of the sensor nodes energy is consumed during the active mode WT when they transmit data to the CH. Therefore, we consider only the energy $E_{current}$ used in the active (transmission) mode. The energy consumed by the sensor nodes in sleep mode is at a very low level and in the presented model we do not consider it. We assume that all of the initial sensor energy levels E_{begin} are the same and that the used transmission energy is in direct proportion to the sensor nodes time period $WT_{current}$ in active mode and the distance $d_k n$ between the nodes and the CH.
In the proposed model, we consider a few types of resource limitations, related to the active time period, distance, and the energy use. The objective is to minimize the sum of the amounts of used energy and to maximize the WSN shelf life represented by the nodes amount of active time periods (work time) WT as is presented in equations (1) and (2) below:

$$MIN \sum E_{begin} - \sum E_{current} \tag{1}$$

$$MAX \sum WT_{begin} - \sum WT_{current} \tag{2}$$

As a final result of the research, the presented paper proposes a design of multi-objective optimization model for cluster-based WSN. The presented model focuses to an energy efficient transmission of sensor data between the nodes in WSN active mode. Based on the developed design and multi-objective optimization model can be realized an improved routing protocol who can increase sensitively the WSN's shelf life.

REFERENCES

[1] J. Lee, I. Moon, Modeling and optimization of energy efficient routing in wireless sensor networks, Applied Mathematical Modelling 38 (2014) 2280–2289

[2] A.Alexandrov, V.Monov, Method for Adaptive Node Clustering in AD HOC Wireless Sensor Networks, Springer, ISBN 978-3-319-9946-8, ISBN 978-3-319-99447-5 (ebook), DCCN 2018, CCIS 919, pp.257-263, 2018,

[3] A.Alexandrov, V.Monov "Method for WSN clock synchronization based on optimized SLTP protocol", Proc.of the 25th International Conference TELFOR 2017 Nov. 21-22 Beograde, Serbia IEEE, ISBN 978-3-319-26153-9, DOI: 10.100/978-3-219-24154-5, pp.121-125

[4] Atanasova T., Modelling of Complex Objects in Distance Learning Systems, Proceedings of the First International Conference - "Innovative Teaching Methodology", October 25-26, 2014, Tbilisi, Georgia, ISBN 978-9941-9348-7-2, pp.180-190.

[5] Tashev T.D., Hristov H.R. Modeling of Synthesis of Information Processes with Generalized Nets. J. "Cybernetics and Inform. Technologies", Sofia, Academic Publishing House "Prof. Marin Drinov", No.2, 2003, pp.92-104.

[6] Todor Balabanov, Iliyan Zankinski, Maria Barova Strategy for Individuals Distribution by Incident Nodes Participation in Star Topology of Distributed Evolutionary Algorithms, Cybernetics and Information Technologies, Volume 16, No 1, Sofia, 2016, pp.80-88. Print ISSN: 1311-9702, Online ISSN: 1314-4081

Cross-validated sequentially constructed multiple regression with centered right side

Slav Angelov, Eugenia Stoimenova

In this paper, we observe a right-centered version of a technique that we have called *Cross-validated sequentially constructed multiple regression*. It cross-validates the estimates of the coefficients in a multiple regression model while merging some of the predictors into components. The newly derived model tends to give better out-of-sample error while recalculated with additional observations. The *Right-centered cross-validated sequentially constructed multiple regression* version is designed to do the same, but for a multiple regression with centered right side. The problem is that the proposed technique is much heavier to estimate while with centered right side. We prove a theorem that directly links the solutions of the centered and not centered versions of the technique. This helps us to estimate the centered version as fast as the non-centered one. Additionally, we give some important remarks while using cross-validation techniques for centered data.
The standard multiple regression model is:

$$Y = \alpha_0 + \alpha_1.X_1 + \alpha_2.X_2 + \cdots + \alpha_k.X_k + \xi\,, \tag{1}$$

where Y is the predicted variable, α_i is the coefficient in front of predictor X_i for $i = 1, \ldots, k$, α_0 is the model intercept term, and ξ is the error term.
We interpret the value of the intercept term from Model (1) as the value of the model if all predictors are set to zero. However, in some cases the predictors cannot take such values which makes the interpretation of the intercept term inadequate. To solve this issue, we can center the right side of Model (1). We define the right-centered model as:

$$Y = \alpha'_0 + \alpha'_1.X^c_1 + \alpha'_2.X^c_2 + \cdots + \alpha'_k.X^c_k + \xi'\,, \tag{2}$$

where Y is the predicted variable, α'_i is the coefficient in front of the centered predictor $X^c_i = X_i - \mu_i$ for $i = 1, \ldots, k$, α'_0 is the model intercept term, ξ' is the error term, and μ_i is the sample mean of X_i. For Model 2, the intercept ξ' can be interpret as the value of the model when all predictors are set at their mean values. Such an interpretation is always adequate. This makes the right-centered model a preferred model in a lot of problems.
In our previous paper, we have presented a technique that estimates Model 1 in a step by step procedure that minimizes the RMSECV error - Cross-Validated Sequentially Constructed Multiple Regression (CVSCMR). *Root mean squared error after cross-validation* (RMSECV) measure:

$$RMSECV = \sqrt{\frac{\sum_{i=1}^{n} \epsilon_i^2}{n}}, \tag{3}$$

where n is the number of the observations in the primary data set, ϵ_i is the error for the i-th observation which is obtained from the regression model estimated over the primary data set without the i-th observation. RMSECV consists of out of sample errors which makes it more realistic measure for the model fit.
Let present a brief overview of the CVSCMR technique:

1. We estimate Model 1;

2. We choose the model variable which has the worst estimate based on its absolute t-value, let say X_i with a coefficient α_i. Then we find the most correlated with it model variable X_j with a coefficient α_j, and we combine them into one component by the following way $Z_{i,j} = X_i + k * X_j$ if $|\alpha_i| > |\alpha_j|$, or $Z_{i,j}(k) = X_j + k * X_i$;

3. We find k while minimizing the $RMSECV(k)$ for Model 1 with $Z_{i,j}(k)$ that replaces X_i and X_j (we explain in more details further in the paper);

4. Back to Step 1.

The procedure ends when we have achieved absolute t-values over a chosen threshold for all of the derived model variables or when the model variables are reduced to a predefined percentage from their initial number. The proposed step by step procedure for obtaining components is tested on a real example concerning accounting and macroeconomic information from the firms in the bulgarian gas distribution sector in the period 2007-2014.

Acknowledgements: This work was supported by grant DH02-13 of the Bulgarian National Science Fund.

References

[1] R Core Team (2017). R: A Language and Environment for Statistical Computing. R Foundation for Statistical Computing, Vienna, Austria. URL https://www.R-project.org/.

[2] Sen, A. and Srivastava, M. (1990). Regression Analysis: Theory, Methods, and Applications. Springer-Verlag New York Inc., New York.

Non-local non-linear perturbation analysis for a nonlinear matrix equation arising in Tree-Like stochastic processes

Vera Angelova

Consider the nonlinear matrix equation

$$F(X,S) \quad := \quad X + \sum_{i=1}^{m} A_i X^{-1} D_i - C = 0, \tag{1}$$

where $S = (A_1, A_2, \ldots, A_m, D_1, D_2, \ldots, D_m, C) \in \Psi = \underbrace{\mathcal{R}^{n\times n} \times \mathcal{R}^{n\times n} \times \dot{\times}\mathcal{R}^{n\times n}}_{2m+1}$ is the $(2m+1)$- tuple of the data matrices A_i, D_i, $C \in \mathcal{R}^{n\times n}$ for $i = 1, \ldots, m$ and $X \in \mathcal{R}^{n\times n}$ is the non-singular solution. For this equation norm-wise, mixes and component-wise condition numbers, as well as local perturbation bounds are formulated and norm-wise non-local residual bounds are derived in [1]. The local bounds are valid only asymptotically. The exigence to be small enough for the perturbations in the data in order to ensure sufficient accuracy of the local bound is an disadvantage of the local bound which is overcome in the non-local perturbation bound. As a continuation of the previous results, in this paper a non-local perturbation bound for the solution to equation (1) is formulated. The non-local bound is more pessimistic than the local bound, but it is formulated for data perturbations included in a given a priori prescribed domain which guarantees the uniqueness of the solution to the perturbed equation in a neighborhood of the exact solution.

For the aims of the forward perturbation analysis, the presence of errors of approximation and round-off errors in the computed solution to (1) is presented by equivalent perturbations δS_l in the data matrices $S_l \in \mathcal{S} := \{A_1, A_2, \ldots, A_m, D_1, D_2, \ldots, D_m, C\} = \{S_1, S_2, \ldots, S_{2m+1}\}$, $l = \overline{1, 2m+1}$, so as $S_l \longrightarrow S_l + \delta S_l$, $l = \overline{1, 2m+1}$.

Denote by $\delta S := (\delta A_1, \delta A_2, \ldots, \delta A_m, \delta D_1, \delta D_2, \ldots, \delta D_m, \delta C)$ the collection of equivalent perturbations in the data and by $\delta := [\delta_1, \delta_2, \ldots, \delta_{2m+1}]^T = [\|\delta A_1\|_F, \|\delta A_2\|_F, \ldots, \|\delta C\|_F]^T \in \mathcal{R}_+^{2m+1}$ the vector of Frobenious norms $\delta_l := \|\delta S_l\|_F$, $l = \overline{1, 2m+1}$ of the equivalent perturbations in the matrix coefficients.

Let $\Upsilon \in \Psi$ be such that for $S \in \Upsilon$ and sufficiently small perturbations δS, equation (1) and the perturbed equation

$$\begin{aligned} F(X+\delta X, S+\delta S) \quad := \quad & X + \delta X \\ & + \sum_{i=1}^{m} (A_i + \delta A_i)(X+\delta X)^{-1}(D_i + \delta D_i) - C - \delta C = 0, \end{aligned} \tag{2}$$

have solutions X and $X + \delta X$, respectively. The elements of the perturbation δX in the solution $X + \delta X$ to the perturbed equation (2) are continuous functions of the elements of the equivalent perturbations δS_l , $l = \overline{1, 2m+1}$ in the data S.

We rewrite the perturbed equation (2) in equivalent operator form, based on the partial Fréchet derivatives of $F(X, S)$ in X at the point (X, S) and then assuming invertibility of the partial

Fréchet derivative $F_X(X,S)$ of $F(X,S)$ in X at the point (X,S) an operator equation of the perturbation δX in the computed solution is obtained

$$\delta X = \Theta(\delta X, \delta S). \tag{3}$$

After applying the techniques of the Lyapunov majorants to the vector representation of the operator equation (3) and the fixed point principle, the following non-local non-linear perturbation bound for the solution to equation (1) is formulated.
Theorem. Suppose that $\delta \in \Omega$, such that

$$\Omega := \{\delta \geq 0 : \alpha_1^2 - 4\alpha_0\alpha_2 \geq 0\} \subset \mathcal{R}_+^{2m+1},$$

where α_i, $i = 0, 1, 2$ are the coefficients of the quadratic majorant equation to equation (3) after taking Frobenious norm of both sides of its vector representations. The coefficients α_i, $i = 0, 1, 2$ are functions of the spectral norms of the data matrices S, the solution X and the Frobenious norms of the perturbations in the data matrices δS.
Then, the non-local bound

$$\|\delta X\|_{\mathrm{F}} \leq \frac{2\alpha_0}{1 - \alpha_1 + \sqrt{(1-\alpha_1)^2 - 4\alpha_0\alpha_2}}$$

for the Frobenious norm of the error δX in the computed solution $X + \delta X$ is valid.
The perturbation bound proposed is an obligatory element to the numerical solution of equation (1). The effectiveness of the bound proposed is demonstrated by numerical examples.

References

[1] V.A. Angelova. Perturbation analysis for a nonlinear matrix equation arising in tree-like stochastic processes (2019) In *Advanced Computing in Industrial Mathematics*, Series: Studies in Computational Intelligence, 793, p. 37, DOI: 10.1007/978-3-319-97277-0_4.

One parameter family of elliptic curves and the equation $x^4 + y^4 + kx^2y^2 = z^2$

Stoyan Apostolov, Miroslav Stoenchev, Venelin Todorov

We consider the diophantine equation $x^4 + y^4 + kx^2y^2 = z^2$, where $k \in \mathbb{Z}$ is a parameter. Our aim is to determine for which integers k the equation has a solution in positive integers (x, y, z). Changing the variables $u = \frac{x}{y},\ v = \frac{z}{y^2},\ y \neq 0$, transforms the equation $T_k : x^4 + y^4 + kx^2y^2 = z^2$ to $H_k :\ v^2 = u^4 + ku^2 + 1$. For $k \neq \pm 2$ the family of curves H_k is nonsingular and contains a rational point, e.g. $(0, \pm 1)$, therefore ([3]) for fixed $k \neq \pm 2,\ H_k$ is birational equivalent to an elliptic curve E_k, with equation

$$E_k :\ Y^2 = X(X - k + 2)(X - k - 2).$$

The change $X = 2u^2 + 2v + k,\ Y = 2u(2u^2 + 2v + k)$ transforms birationally H_k to E_k. The inverse transformation $E_k \to H_k\ \ (X, Y) \mapsto (u, v)$ is defined by $u = \frac{Y}{2X},\ v = \frac{X-k}{2} - \left(\frac{Y}{2X}\right)^2$. The map $E_k \to E'_k\ \ (X, Y) \mapsto (x', y')$, defined by $x' = \left(\frac{Y}{2X}\right)^2,\ y' = \frac{Y(k^2-4-X^2)}{8X^2}$, is an isogeny ([6]) between the elliptic curves E_k and E'_k, where

$$E'_k : y'^2 = x'(x'^2 + kx' + 1).$$

The dual isogeny $E'_k \to E_k\ \ (x', y') \mapsto (X, Y)$ is defined by $X = \left(\frac{y'}{x'}\right)^2,\ \ Y = \frac{y'(1-x'^2)}{x'^2}$.
Let $S_k = \{(x, y, z) \in \mathbb{N}^3 \mid x^4 + y^4 + kx^2y^2 = z^2,\ \gcd(x, y, z) = 1,\ xy > 1\}$. Using the transformations $T_k \to H_k \to E_k$ and the isogenies $E_k \to E'_k \to E_k$, we obtain:

$$\text{card } S_k \geq 1 \Leftrightarrow \left| \begin{array}{c} x' = \left(\frac{x}{y}\right)^2 \\ y' = \pm\frac{x}{y}\cdot\frac{z}{y^2} \\ (x, y, z) \in S_k \end{array} \right. \Leftrightarrow \left| \begin{array}{c} x = y\sqrt{x'} \\ y = y,\ z = \frac{y'y^2}{\sqrt{x'}} \\ (x', y') \in E'_k(\mathbb{Q}) - E'_k(\mathbb{Q})_{tor} \end{array} \right. \Leftrightarrow \text{ rank } E'_k(\mathbb{Q}) \geq 1,$$

where $E'_k(\mathbb{Q})$ and $E'_k(\mathbb{Q})_{tor}$ are respectively Mordell-Weil group of rational points and its torsion subgroup for E'_k. Consequently, the initial equation has a solution in S_k, if and only if the rank of $E'_k(\mathbb{Q})$ is at least 1 (as noted in [1]), i.e.

$$\{k \in \mathbb{Z} \mid \text{card } S_k \geq 1\} = \{k \in \mathbb{Z} \mid \text{rank } E'_k(\mathbb{Q}) \geq 1\}.$$

The rational torsion points of E'_k generate only the trivial solutions $x = y = 1$, with k in the form $k = n^2 - 2$, which are not included in S_k.
The group of rational points of every elliptic curve is abelian and finitely generated. Every finitely generated abelian group is a direct sum of a free subgroup and a torsion subgroup. Hence $E'_k(\mathbb{Q}) \cong \mathbb{Z}^r \oplus E(\mathbb{Q})_{tor}$, where the integer $r \geq 0$ is called a rank of $E'_k(\mathbb{Q})$, denoted by $\text{ rank } E'_k(\mathbb{Q}) = r$. The rank is invariant under isogeny maps, therefore isogenous elliptic curves have the same rank, so rank $E_k(\mathbb{Q}) =$ rank $E'_k(\mathbb{Q})$.

In the present article, it has been proven that every element of $E'_k(\mathbb{Q}) - E'_k(\mathbb{Q})_{tor}$ generates infinite family of solutions of the initial equation. For all values of k, for which card $S_k \geq 1$, we construct with explicit formulas the corresponding infinite families of solutions. For special values of k, we have determined "φ-components" of Selmer and Shafarevich-Tate groups ([5]) for E_k and E'_k : $S^{(\varphi)}(E'_k/\mathbb{Q})$ and $Ш(E'_k/\mathbb{Q})[\varphi]$, for appropriate isogeny φ. We prove that rank $E'_k(\mathbb{Q}) \geq 1$ if and only if k fulfills any one of the following systems:

$$\left| \begin{array}{c} a,b,c - \text{odd} \\ m,n - \text{even} \\ mb^2 - nc^2 = 2 \\ k = mna^2 \pm (mb^2 + nc^2) \end{array} \right| \quad \left| \begin{array}{c} a,b,c,m,n - \text{odd} \\ mb^2 - nc^2 = 2 \\ k = mna^2 \pm (mb^2 + nc^2) \end{array} \right| \quad \left| \begin{array}{c} a - \text{odd} \\ mb^2 - nc^2 = 1 \\ k = mna^2 \pm 2(mb^2 + nc^2), \end{array} \right.$$

where a, b, c, m, n are positive integers satisfying $\gcd(a, bc) = 1,\ abc > 1$. Solutions of the initial equation for the corresponding three cases are:

$$\left| \begin{array}{c} x = bc \\ y = a \\ z = \left| \frac{(mb^2+nc^2)a^2}{2} \pm (bc)^2 \right| \end{array} \right| \quad \left| \begin{array}{c} x = bc \\ y = a \\ z = \left| \frac{(mb^2+nc^2)a^2}{2} \pm (bc)^2 \right| \end{array} \right| \quad \left| \begin{array}{c} x = 2bc \\ y = a \\ z = \left| (mb^2 + nc^2)a^2 \pm 4(bc)^2 \right| \end{array} \right.$$

Conclusion:All solutions of the initial equation are described by 5-tuples $(a, b, c, m, n) \in \mathbb{N}^5$, such that 4-tuples (m, b, n, c) are all positive integral points on affine curves $C_l : uv^2 - wt^2 = l$, for $l = 1, 2$; and $a \in \mathbb{N} :\ \gcd(a, bc) = 1,\ abc > 1$.

Remark:Important partial results are obtained in [2],[4], etc. Application of the considered type diophantine problems is in the so-called "elliptic curve cryptography", where the classical discrete logarithm problem in the multiplicative group $\mathbb{F}_q^*$ of finite field $\mathbb{F}_q$, is replaced by discrete logarithm problem in the elliptic curve group $E(\mathbb{F}_q)$.

References

[1] A. Bremner, J. Jones, On the equation $x^4 + y^4 + mx^2y^2 = z^2$, Journal of Number Theory 50, 286-298 (1995).

[2] E. Brown, $x^4 + y^4 + mx^2y^2 = z^2$: Some cases with only trivial solutions - and a solution Euler missed, Glasgow Math. J.31 (1989) 297-307.

[3] J.W.S. Cassels, Lectures on elliptic curves, Cambridge University Press, 1991.

[4] L. Euler, De casibus quibus formulam $x^4 + mxxyy + y^4$ ad quadratum reducere licet, Mem.acad.sci. St. Petersbourg 7 (1815/16, 1820), 10-22; Opera Omnia, ser. I, V, 35-47, Geneva, 1944.

[5] V. A. Kolyvagin, On the Mordell-Weil Group and the Shafarevich-Tate Group of Modular Elliptic Curves , Proceedings of the International Congress of Mathematicians, Kyoto, Japan, 1990 ,pp. 429-436.

[6] J. H. Silverman, The arithmetic of elliptic curves, Springer Verlag, New York/Berlin, 1986.

An inner-product free iteration method for an equation of motion and for a bound-constrained optimal control PDE problem

Owe Axelsson

Inner product free iteration methods can outperform more commonly used iteration methods based on Krylov subspaces, such as the classical conjugate gradient (CG) method and the generalized minimum residual (GMRES) method, at least when implemented on parallel computer platforms. This is due to the need to compute inner products in CG and GMRES, mainly for the orthogonalization of a new search direction with respect to previous search directions. Thereby each processor must send its local part of the inner product to all other processors or to a master processor, to enable the computation of the global inner product. This requires start up times for synchronization and global communication times. Since the computer chips on modern computers now have reached nearly their physical limit of speed, this type of overhead will be even more dominating for future generations of parallel computer processors, where the only way to decrease the computer time is to use more parallel processors.

There exists however iteration methods which do not require any computation of inner products except for the computation of the norm of the current residual, to see if it is sufficiently small for the required tolerance accuracy to be reached. But this check need to take place rarely, only at the end of the iteration process.

The classical such method is the Chebyshev iteration method, but as shown in a recent paper by O. Axelsson and D.K. Salkuyeh [1], there exists also other methods such as the transformed matrix iteration (TMIT) method. In [1] it has been shown that the Chebyshev and TMIT methods can outperform the GMRES and other methods and can be competitive even on a single processor machine, in elapsed computer times. This is due to that there is no computer time needed for the arithmetic computation involved in the inner products.

However, to be efficient these methods require that accurate, or even sharp bounds of the eigenvalues of the preconditioned matrix are available and that they do not correspond to a huge condition number.

In the present paper we consider an extension of methods to solve two-by-two block matrices arising in optimal control of PDEs where this is possible and which have appeared in a series of papers by O. Axelsson and M. Neytcheva, and coworkers, see e.g. [2]. This is one of the first papers where a very efficient preconditioner, later called PRESB (preconditioned square block) has been used. This method is fully parameter free and gives eigenvalue bounds $1/2 \leq \lambda \leq 1$ which hold uniformly with respect to problem, regularization and step-size parameters. The origin of the method comes from the elementary problem of solving a complex valued equation,

$$(W + iZ)(x + iy) = f + ig$$

avoiding complex arithmetics, which can be done via the real valued form

$$\begin{bmatrix} W & -Z \\ Z & W \end{bmatrix} \begin{bmatrix} x \\ y \end{bmatrix} = \begin{bmatrix} f \\ g \end{bmatrix},$$

see e.g. [3] and references therein to earlier papers. Thereby the PRESB preconditioner

$$\begin{bmatrix} W & -Z \\ Z & W+2Z \end{bmatrix}$$

is used, the action of which involves solving two systems with matrix $W + Z$, in addition a matrix vector multiplication with W and vector operations.
The present paper is concerned with extensions of this preconditioning method to two important types of applications. The first deals with a direct frequency domain analysis of an equation of motion, $M\ddot{q} + C\dot{q} + Kq = p$, where M is the inertia, K the stiffness matrix and C a viscous damping matrix. An early presentation of this problem is found in a paper by Feriani, Perotti, Simoncini [4], but the problem has later been taken up by many other researchers, such as Z.Z. Bai [5]. It has also been tested in [1]. In these studies only the frequency $\omega = \pi$ has been studied. In this talk an extension to more general values is presented, which leads to an indefinite matrix W. For other applications of time-harmonic approaches of optimal control problems, see [6] and the references therein.
The present talk deals also with an extension to an optimal control problem with bound constraints on the solution to the state equation. This is based on the method used in O. Axelsson, M. Neytcheva, A. Ström [7]. We show how this problem can be solved very efficiently by use of a polynomially preconditioned Chebyshev iteration method.

1. O. Axelsson, D. K. Salkuyeh, A new version of a preconditioning method for certain two-by-two block matrices with square blocks. *BIT Numerical Mathematics*, accepted, 2018.

2. O. Axelsson, S. Farouq, M. Neytcheva, Comparison of preconditioned Krylov subspace iteration methods for PDE-constrained optimization problems. Poisson and convection-diffusion control. *Numerical Algorithms*, 73(2016), 631-663.

3. O. Axelsson, M. Neytcheva, B. Ahmad, A comparison of iterative methods to solve complex valued linear algebraic systems. *Numerical Algorithms*, 66(2014), 811-841.

4. A. Feriani, F. Perotti, V. Simoncini, Iterative system solvers for the frequency analysis of linear mechanical systems. *Computer Methods in Applied Mechanics and Engineering*, 190(2000), 1719-1739.

5. Z.Z. Bai, M. Benzi, F. Chen, Modified HSS iteration methods for a class of complex symmetric systems. *Computing*, 87(2000), 93-111.

6. O. Axelsson, Z.-Z. Liang, A note on preconditioning methods for time-periodic eddy current optimal control problems, *Journal of Computational and Applied Mathematics*, accepted, 2018.

7. O. Axelsson, M. Neytcheva, A. Ström. An efficient preconditioning method for state box-constrained optimal control problems. *J. Numerical Mathematics*, accepted, 2018.

On the numerical solution of state- and control-constrained optimal control problems

Owe Axelsson, Maya Neytcheva, Anders Ström, Johanna Brodin, Ivo Dravins, Andreé Falgin

Optimal control problems with constraints given by a partial differential equation (OPT-PDE) arise in many different important applications, such as steering processes in fluid dynamics, acoustics, elasticity, elastoplasticity, modelling of living cells and tissues, optimal treatment in radiotherapy, particle growth to name a few.

The problem involves the minimization of a certain cost functional including both a state and a control variable, and one or more Lagrange multipliers to cope with the constraints. In this presentation we consider problems, where in addition the state or the control variable is constrained by lower and upper bounds. We consider also the inclusion of an additional regularization term in the cost functional, the L^1 norm of the control that allows to achieve sparse controls. Such problems are harder to solve. They include several regularization parameters, related to a standard Tikhonov regularization term to limit the cost of the optimal control variable, to a regularization for the state variable to handle the box constraint, to the L^1 regularization term etc.

The algebraic problem that arises after discretization is nonlinear and is solved using the so-called semi-smooth Newton method. Clearly, due to the large size of the so-obtained linear systems to be solved at each Newton step, iterative methods are the methods of choice. The latter inevitably requires utilization of robust and numerically and computationally efficient preconditioners.

In this presentation we consider three cases: OPT-PDE with bilateral state constrains, imposed using the so-called Moreau-Yosida framework (P1), OPT-PDE problem with bilateral control constraints (P2) and OPT-PDE problem with L^1 regularization (P3). The PDE constraint is stationary elliptic equation with appropriate boundary conditions, in this presentation, the Laplace equation in two space dimensions. The discretization is done by standard piece-wise linear finite elements and the domain of definition is the unit square.

To be specific, we consider a minimization of a cost functional $\mathcal{J}$, defined as

$$\mathcal{J}(y,u) = \frac{1}{2}\|y - y_d\|^2_{L^2(\Omega_0)} + \frac{\alpha}{2}\|u\|^2_{L^2(\Omega)},$$

where $\Omega \subset \mathbb{R}^d$ is a given domain. Here $\alpha > 0$ is a regularization parameter and y_d is the desired state of the variable y. By choosing α sufficiently small we ensure that y is close to y_d. The state y and the control u are related via an elliptic PDE, in this case the Poisson equation, possibly with a zero order term,

$$-\Delta y + cy = u \quad \text{in} \quad \Omega, \tag{1}$$

with boundary conditions $y = g$ on $\partial\Omega$ if $c = 0$ or $\frac{\partial y}{\partial n} = 0$ on $\partial\Omega$ if $c > 0$. We follow the 'discretize-then-optimize' approach. To solve the optimization problem, we formulate the corresponding Lagrangian functional, discretize and construct the first order necessary

(Karush-Kuhn-Tucker, KKT) conditions. The Lagrangian multiplier to handle the state equation is denoted by p. The Lagrangian functional, corresponding to $\mathcal{J}$ becomes

$$\mathcal{L}(y,u,p) \equiv \frac{1}{2}\|y-y_d\|^2_{L^2(\Omega)} + \frac{\alpha}{2}\|u\|^2_{L^2(\Omega)} + (p, -\Delta y + cy - u).$$

Problem 1 (P1: two-sided state constraints)**.** *We impose additional box constraints on the state y of the form $\underline{y} \le y \le \overline{y}$ (possibly in $\Omega_0 \subseteq \Omega$).*
To handle such constraints we use the Moreau-Yosida penalty function method, where we modify the cost functional and minimize

$$\begin{aligned}\mathcal{J}(y,u) &= \frac{1}{2}\|y-y_d\|^2_{L^2(\Omega)} + \frac{\beta}{2}\|u\|^2_{L^2(\Omega)} + \\ &+ \frac{1}{2\varepsilon}\|\max\{0, y-\overline{y}\}\|^2_{L^2(\Omega)} + \frac{1}{2\varepsilon}\|\min\{0, y-\underline{y}\}\|^2_{L^2(\Omega)} \end{aligned} \tag{2}$$

Problem 2 (P2: two-sided control constraints)**.** *Consider the case when the additional constraints are imposed on the control, $\underline{u} \le u \le \overline{u}$. Let $\underline{\lambda}, \overline{\lambda}$ - the Lagrange multipliers, related to the control constraints. The Lagrangian functional takes the form*

$$\mathcal{L}(y,u,p,\underline{\lambda},\overline{\lambda}) = \frac{1}{2}\|y-y_d\|^2_{L^2(\Omega)} + \frac{\alpha}{2}\|u\|^2_{L^2(\Omega)} + (p, -\Delta y + cy - u) + \overline{\lambda}(u-\overline{u}) - \underline{\lambda}(u-\underline{u}).$$

Usually the multipliers λ_a and λ_b are unified as $\lambda = \overline{\lambda} - \underline{\lambda}$.

Problem 3 (P3: sparse control)**.** *In this case the cost functional becomes*

$$\mathcal{J}(y,u) = \frac{1}{2}\|y-y_d\|^2_{L^2(\Omega_0)} + \frac{\alpha}{2}\|u\|^2_{L^2(\Omega)} + \beta\|u\|_{L^1(\Omega)},$$

together with the assumptions $\underline{u} \le u \le \overline{u}$, $-\infty < \underline{u} < 0 < \overline{u} < \infty$.

In all cases (P1)–(P3) we minimize a set of points, where the constraints are not satisfies. The cost functional is not differentiable and to solve the problem one applies the so-called *semi-smooth* Newton method. Theoretical results regarding the convergence of the semi-smooth Newton method are available in the related scientific literature.

We address efficient preconditioning techniques based on the arising two-by-two or three-by-three block matrices with square blocks. We also discuss the interplay between the discretization parameter, the regularization parameters, the stopping criteria for the linear and nonlinear solvers, as well as constructing good enough initial guess to ensure fast convergence of the nonlinear solver. The performance of the involved nonlinear and linear solvers are illustrated with some numerical experiments.
Comparisons with other preconditioning approaches for the target problems and some examples of our approach in constructing a preconditioner for the considered class of problems are included in the presentation.

Simulation model for investigation of the efficiency of an artificial immune algorithm for generation of S-boxes with good cryptographic properties

Tsonka Baicheva, Violeta Dutcheva, Nikolay Nikolov

In cryptography, an S-box (substitution-box) is a basic component of block ciphers. They are used to mask the relationship between the key and the ciphertext. Because of their importance, S-boxes have been studied for many years and variety of extensive experimentations have been performed. However, the construction of secure S-boxes is still a main problem to every block cipher designer. There are many different ways that have been explored in order cryptographically good (strong) S-boxes to be constructed. The most common techniques for S-box generation can be generalized into three main classes: random (pseudo-random) generation, pure mathematical (algebraic) constructions and a variety of heuristic approaches. Among the latter are immune algorithms.

In our work the performance of an immune algorithm using clonal selection for generation of S-boxes with good cryptographic properties is investigated. It is very hard to observe and analyse the work of the algorithm as it has many parallel branches and a big variety of randomly chosen parameters in the hypermutation functions. The aim of the investigation is to answer the following two questions.

1. Are there parallel branches of the algorithm through which it will not pass?
2. Are there any attractor where the algorithm get into?

To answer these questions we create a simulation model of the immune algorithm which satisfies the following main criteria.

- With a preliminary fixed big accuracy to follow the behaviour of the simulated immune algorithm.
- To has low computational complexity.
- To allow to predict the behaviour of the algorithm for a big number of iterations.

Preliminary tests with different probabilistic simulation models are carried out and Hidden Markov Model (HMM) is chosen as the most suitable. Simulations was carried out for 1000000 and 10000000 iterations of the algorithm and the following conclusions are made.

1. The implemented HMM correctly describes the performance of the simulated algorithm.
2. There are no states in the hidden layer which could be ignored because they have small probability to be taken.
3. The are no attractor where the algorithm gets into.
4. Additional parallel branches with different hypermutation functions can be added in order to increase the efficiency of the algorithm.

The simulated immune algorithm was applied for generation of $(n \times n)$ bijective S-boxes and a big variety of such S-boxes with values for nonlinearity and differential uniformity that had never been simultaneously achieved by any other heuristic approach starting from a randomly generated S-box are obtained.

Acknowledgement This work is partially supported by the Bulgarian National Science Fund Contract number DH 12/8 from 15.12.2017.

Multilayer Perceptron Training Randomized by Second Instance of Multilayer Perceptron

Todor Balabanov, Iliyan Zankinski, Kolyu Kolev

Introduction Multilayer perceptron is one of the most used types of artificial neural network. For the last four decades artificial neural networks are heavily researched and used in real industrial solutions. The power of artificial neural networks is in their operating phase. Once trained artificial neural networks are an extremely efficient tool. The training phase of the artificial neural network is the problematic part of their usage. Training is usually too slow and not always efficient enough. Multilayer perceptron is weighted directed graph organized in layers. When multilayer perceptron is fully connected each neuron from a single layer is connected with each neuron from the next layer. Neurons are the nodes in the graph where links between nodes are weighted. The calculating power of multilayer perceptron is in its weights. Finding proper velues for the weights is a global optimization problem. Each neuron collects signals as its input. Signals are coming from other neurons or from external for the multilayer perceptron environment. Signals are multiplied by the weight of the link and then their sum is calculated. The sum of the weighted signals is usually normalized by the activation function of each neuron. Such normalization is a key feature of the multilayer perceptron, because the number of neuron's input links is variable and there is no limitation of the weights range. The most used activation functions are the hyperbolic tangent and the sigmoid function. In the literature there are hundreds training algorithms, but the most popular and the most used one is the back-propagation training. Back-propagation is exact numerical method and it is based on the gradient of the multilayer perceptron output error. Speed-up of multilayer perceptron training is always desirable and this study proposes usage of second multilayer perceptron which randomizes the back-propagation training procedure of the basic multilayer perceptron.

Proposed Improvement This study proposes usage of two multilayer perceptrons in parallel. Both perceptrons have three layers (input, hidden and output). Hyperbolic tangent is used for the primary multilayer perceptron and sigmoid function is used for the secondary multilayer perceptron. With a given probability on each training cycle randomly selected weights from the secondary multilayer perceptron are copied in the primary multilayer perceptron. Both artificial neural networks have identical topology. Because of this weights are corresponding strictly in the primary and the secondary network. Both networks are trained with back-propagation training procedure. Both networks are supplied with the same input-output training examples. Because of the similarity of the shapes of the sigmoid function and the hyperbolic tangent the primary network gets extra noise and it helps in escaping local optimums. Such improvement gives better convergence during the training phase. The proposed modification is tested with two different experiments for optical character recognition of the ten arabic digits. Input of the networks is presented as 256 real values. The output has ten possibilities for each digit. The size of the hidden layer was chosen to be 266 as sum of the input and output size. In this study the size of the hidden layer is not of primary importance. The only requirement is identical topologies. Size of the hidden layer can be easily optimized

with the pruning algorithms implemented in Encog programming library. All experiments are done in two configurations for practical comparison of the achieved results. In the first configuration two identical multilayer perceptrons are used. Both of them are configured to have hyperbolic tangent as activation function. In this configuration random weights migration is kept as back-propagation training modification. In the second configuration the primary multilayer perceptron has hyperbolic tangent as activation function, but the secondary multilayer perceptron has sigmoid function as activation function. The average results of 30 independent tests show that there is significant outperformance of the second configuration. Weights migration rate was set to 1%, but some estimation strategy can be implemented for this parameter.

Conclusions All initial experiments are done with open source software solution, based on Encog Machine Learning Framework (https://www.heatonresearch.com/encog/). Randomization of the weights in the basic multilayer perceptron lead to stairs like convergence curve. As parallel to the neutral neural networks, such stress on the neurons is observed when the neural cells are overloaded and their performance is sensitively reduced. The proposed back-propagation training modification is very promising if it is used in hybrid implementations. As further work it will be interesting if more than two different activation functions are used. Some of the available activation functions (https://en.wikipedia.org/wiki/Activation_function) can lead to much more promising results.

Acknowledgments This work was supported by private funding of Velbazhd Software LLC.

Recent Advances of the Wigner Signed-Particle Approach

Mauro Ballicchia, Josef Weinbub, Ivan Dimov, and Mihail Nedjalkov

The signed-sarticle (SP) interpretation [1] of Wigner quantum mechanics provides a fundamental approach to model a wide range of phenomena, from fully coherent problems, such as interference, to scattering dominated processes, such as Brownian motion. The standard formulation of the latter considers near electrostatic conditions presented by the scalar potential V defining the electric field $\mathbf{E} = -\nabla V$. Generalizations including the magnetic field $\mathbf{B}$ are derived in terms of pseudo-differential operators, where the position dependence of $\mathbf{E}$ and $\mathbf{B}$ is replaced by an operator containing $\nabla_{\mathbf{p}}$. Thus the order of the equation with respect to the momentum derivatives varies with the position dependence of the electromagnetic field. We derive an equation for general, inhomogeneous, and time-dependent electromagnetic conditions, which has an explicit mathematical structure in the sense that the differential and integral operations are fixed and independent on $\mathbf{E}(\mathbf{r})$ and $\mathbf{B}(\mathbf{r})$. In the case of a homogeneous magnetic field the equation for the Wigner function $f_w(\mathbf{r}, \mathbf{p})$ of the phase space position and momentum variables is:

$$\left[\frac{\partial}{\partial t} + \frac{\mathbf{p}}{m} \cdot \frac{\partial}{\partial \mathbf{r}} + e\frac{\mathbf{p}}{m} \times \mathbf{B} \cdot \frac{\partial}{\partial \mathbf{p}}\right] f_w(\mathbf{r}, \mathbf{p}, t) = \int d\mathbf{p}' V_w(\mathbf{p} - \mathbf{p}', \mathbf{r}) f_w(\mathbf{r}, \mathbf{p}', t)\,. \qquad (1)$$

Here, V_w is the standard Wigner potential obtained by the Fourier transform $e^{i\mathbf{p}\cdot\mathbf{s}/\hbar}$ of the potential difference $V(\mathbf{r} + \mathbf{s}/2) - V(\mathbf{r} - \mathbf{s}/2)$.

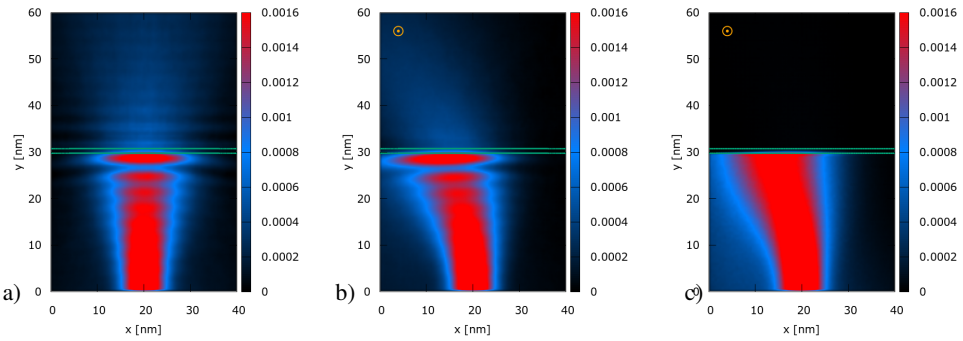

Figure 1: Electron evolution around a $0.2\,\mathrm{eV}$ potential barrier: a) quantum density (a.u.) for $\mathbf{B} = 0$, b) quantum density for $\mathbf{B} = 6\mathrm{T}$, c) classical density for $\mathbf{B} = 6\mathrm{T}$.

The SP concepts have been developed (for a recent review see [1]), by applying the numerical Monte Carlo theory to the integral form of the electrostatic ($\mathbf{B} = 0$) form of Equation 1. The corresponding Neumann series is convergent [2], but the kernel gives rise to a branching Markov chain with ± 1 weight factor of each branch. The stochastic process of construction of the numerical trajectories can be interpreted as a process of generation of positive and negative particles - the SPs, which evolve over fieldless Newtonian trajectories. The Wigner function in a phase space cell is given by the sum of the sign of the particles inside which corresponds to the opposite process of annihilation. A stochastic analysis shows that the numerical approach is generalized for $\mathbf{B} \neq 0$ by a SP evolution over

magnetic force governed Newtonian trajectories. Furthermore, apart from the processes of generation and annihilation, the stochastic evolution is the same as for the classical ballistic Boltzmann equation. The latter can thus be conveniently used as a reference frame to outline quantum processes. We note that magnetic field aware problems are utterly multidimensional and currently only the SP model allows multidimensional computations. As a generic application we demonstrate the effect of the magnetic field on the process of electron tunneling through a potential barrier. In the numerical experiment coherent electrons are injected from the bottom boundary towards the barrier marked by the green line in the middle of the simulation domain, Figure 1. The left picture shows the symmetry of the $\mathbf{B} = 0$ problem. Two important quantum properties are demonstrated: (i) interference effects reveal the wave nature of the evolution, in particular the finite density after the barrier is due to tunneling; (ii) the non-locality of the potential, which affects the electron density far before the barrier. In contrast, classical electrons with energies less than 0.2 eV (the here presented case) are back scattered locally. The magnetic field breaks the symmetry by bending the electron trajectory. Even if the electric field action is still non-local the coherence of the transport is affected. Fig. 1c) shows the density obtained by the solution of the corresponding Boltzmann equation under the action of the same magnetic field. In this case there is no wave-like transport and no tunneling as all particles are reflected back from the barrier. The SP approach has been recently applied also to the study of the quantum coherence effects induced by a single repulsive dopant in the center of a nanowire [3]. The physical setup is the same as in 1a), but the barrier is replaced by a dopant and the lateral boundary conditions are set to reflecting. Due to the reflection the shape of the current resembles a *tulip*, which is much more *closed* in the quantum case, Figure 2a). The reasons for the manifesting current density in the classically *shadowed* region - (i.e., the white area behind the dopant) on Fig. 2b), are twofold: (i) processes of tunneling, and (ii) nonlocal action of the potential, where reflected particles appear close to after the dopant due to the repulsion, occurring further before the dopant. These effects enhance the current as compared to the classical counterpart. *This talk highlights the role of the Monte Carlo SP approach as a powerful method for investigating quantum phenomena in nanoelectronics and physics.*

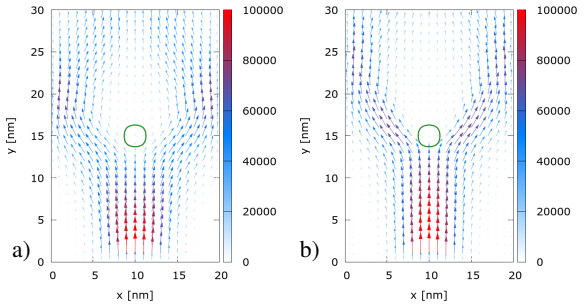

Figure 2: Quantum, (a) and classical (b), current density [a.u.] around a dopant indicated by a green 0.15 eV isoline.

References

[1] M. Nedjalkov, P. Ellinghaus, J. Weinbub, T. Sadi, A. Asenov, I. Dimov, and S. Selberherr, *Computer Physics Communications*, vol. 228, pp. 30–37, 2018, doi:10.1016/j.cpc.2018.03.010, and the references therein.

[2] I. Dimov, M. Nedjalkov, J. M. Sellier, and S. Selberherr, *Journal of Computational Electronics*, vol. 14, no. 4, pp. 859–863, 2015, doi:10.1007/s10825-015-0720-2.

[3] M. Ballicchia, J. Weinbub, and M. Nedjalkov, *Nanoscale*, 2018, doi:10.1039/c8nr06933.

Self-consistent Monte Carlo Solution of Wigner and Poisson Equations Using an Efficient Multigrid Approach

Majid Benam, Maciej Wołoszyn, Siegfried Selberherr

An accurate self-consistent solution of the coupled Wigner and Poisson equations is of high importance in the analysis of semiconductor devices. The solver proposed in this paper has two main components; a Wigner solver which treats the Wigner potential as a generating mechanism and is responsible for the generation and annihilation of signed particles, and a Poisson solver which uses an efficient multigrid approach to take the charge density distribution, and update the value of the potential in each time step.
As illustrated in Fig. 1, the Monte Carlo simulation starts with an initialization step in which geometrical aspects and physical quantities such as density and potential are fed to the simulator by input files or internal functions. Some other simulation parameters and the boundary conditions are set and the properties of the particles to be injected in the region are also decided. The Wigner potential is then calculated which in turn determines the statistics of generation mechanisms. The Poisson solver is called in each time step to use the current value of the charge density and update the value of the potential for the next time step. A charge redistribution scheme is then used to map charges in the neighboring cells in a more efficient way for the next round. The Monte Carlo evolution of particles is then performed using the Signed Particle Monte Carlo approach.

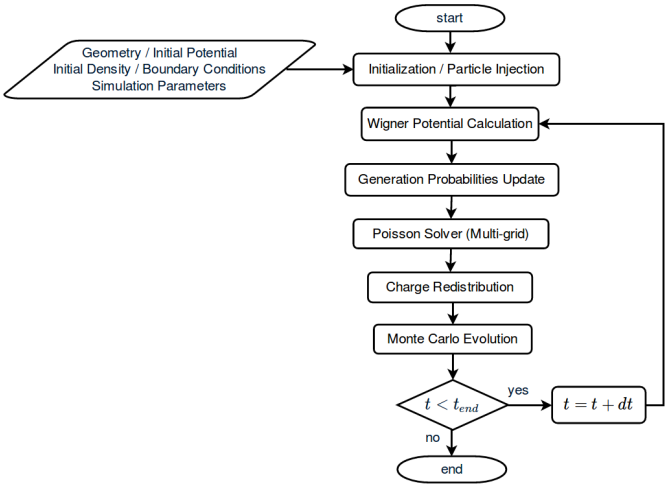

Figure 1: Flowchart for the self-consistent solution of Poisson and Wigner equations

The Poisson block receives the updated density in each time step and provides the updated potential which is then used to calculate the new Wigner potential, and hence the new statistics for the generation of new pairs of particles. Special considerations are taken into account in order to provide the solver with a compatible and consistent set of boundary constraints,

including Dirichlet and von Neumann conditions. Since the physical domain of interest is discretized in space, an efficient multigrid algorithm replaces the problem, which is on an initial fine grid, by an approximation on a coarser grid and uses the corresponding solution as a starting guess for the problem on the fine grid, which is then iteratively updated. The coarse grid problem is solved recursively, i.e. by using a still coarser grid approximation, etc. In this approach, efficiency depends on the coarse grid solution being a good approximation to the fine grid.
Results for density, potential and the electrostatic force calculated as the gradient of the potential energy are presented for a Cartesian xy-region which is not charged by any external doping or other sources of fixed charge in the beginning. However, wavepackets representing electrons are constantly injected from the bottom edge into the region every femtosecond, which results in a different distribution of charges in each time step. Fig. 2 shows the carrier density in two cases, namely, obtained without the application of the Poisson equation and with the Poisson equation, respectively, and illustrates the repulsion of wavepackets in the latter using the vectors of the force.

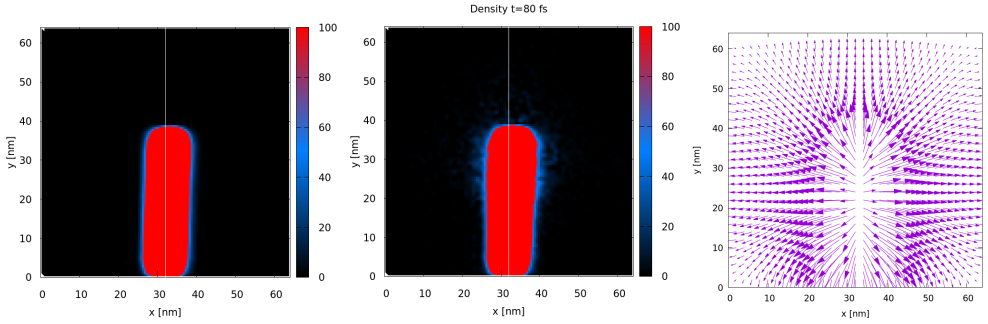

Figure 2: The carrier density without solving the Poisson equation (left), the carrier density with solving the Poisson equation (middle), and the force corresponding to the case with solving the Poisson equation (right) after 80 femtoseconds.

Note that the spread of the density is not due to the force acting on the particles, but entirely due to generation/annihilation of unaccelerated particles affected by the Wigner potential which is recalculated in every step based on the current position-dependent potential energy obtained from the solution of the Poisson equation. The Multigrid Poisson solver also allows for the selection of a position-dependent relative permittivity in the region in case one needs to model two or more materials next to each other in the same region.

Acknowledgements. This research is partially supported by the Austrian Science Fund through the project FWF-P29406-N30.

Maximizing the Biogas Production of a Fermentation Process Using Output Feedback with Discrete Time Delay

Milen K. Borisov, Neli S. Dimitrova, Mikhail I. Krastanov

The present study is devoted to the stabilization and control of a bioreactor model, describing an anaerobic fermentation process for biological degradation of organic wastes with biogas (methane) production. The model is presented by two nonlinear ordinary differential equations:

$$\begin{aligned} \frac{ds(t)}{dt} &= -k_1\mu(s(t))x(t) + u(s_{in} - s(t)) \\ \frac{dx(t)}{dt} &= (\mu(s(t)) - \alpha u(t))x(t) \end{aligned} \tag{1}$$

and one algebraic equation for the gaseous (methane) output:

$$Q(s(t), x(t)) = k_2\mu(s(t))x(t), \tag{2}$$

where x and s represent biomass and substrate concentration respectively, and the dilution rate u [day^{-1}] is considered as a control variable.

The feedback control of bioreactor (chemostat) models provides many advantages in operating a plant and is used to increase its efficiency and sustainable long-term energy production. We propose a feedback control law of the form $\kappa(s, x) = \beta k_2\mu(s)x$, where β is an auxiliary positive and properly chosen parameter. Obviously, the feedback is based on output measurements (i. e. biogas flow rate, see (2)), which are always on-line available. We assume the existence of a piecewise constant delay in this feedback, because there is always a time delay between output measurements and system's response in industrial applications.

The study is organized in the following way. First, we determine a nontrivial equilibrium point of the closed-loop system and investigate its asymptotic stability as well as the appearance of bifurcations with respect to the delay parameter. Second, we establish the existence of an attracting and invariant region around the equilibrium such that all trajectories enter this region in finite time for any value of the delay and remain there. Then based on the theoretical results, an iterative numerical extremum seeking algorithm is applied to the closed-loop system aimed to maximize the methane flow rate in real time. Numerical simulation are also presented to illustrate the efficiency of the extremum seeking algorithm.

Acknowledgements. The work of the first and the second author has been partially supported by the Bulgarian Academy of Sciences, the Program for Support of Young Scientists and Scholars, grant No. DFNP-17-25/25.07.2017. The work of the second and the third author has been partially supported by the Sofia University "St. K. Ohridski" under contract No. 80-10-133/25.04.2018.

Solidification process in 3D printing

St. Bushev

The Stefan's type problems in the theory of heat conduction are the mathematical basis of the basic processes of the material science, die-casting and heat treatment [1]. In Fig. 1 are presented the main steps of numerical simulation of drop solidification.

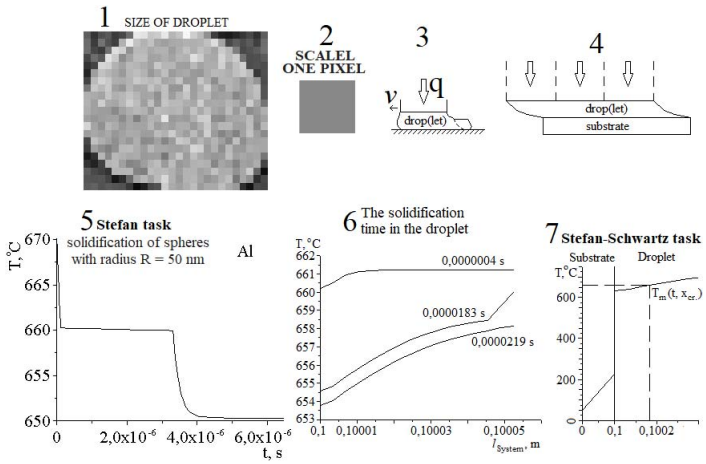

Figure 1. Spilled a drop in the printing process 3D Printer; digit scale is the size of one pixel; the geometric idea of solidification of a drop on substrate surface; and numerical results.

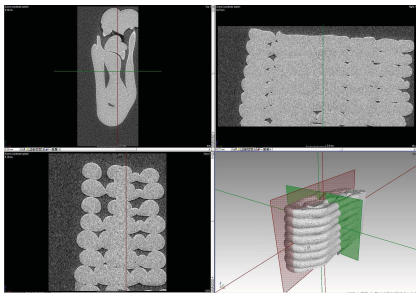

Figure 2. 3D visualization of 3D printed material.

References

[1] St. Bushev, I. Georgiev, Solidification on surface, International scientific journal mathematical modeling, year II, issue 1, 2018, p.33-36.

Modelled versus Satellite Retrieval Estimation of the Direct Normal Irradiance and the Sunshine Duration over Bulgaria

Hristo Chervenkov, Valery Spiridonov, Kiril Slavov

The incoming solar radiation is an essential climate variable that determines the Earth's energy cycle and climate. Its accurate assessment is also relevant for the correct sizing, design, and dynamic simulation of solar energy systems. The three main solar radiation components — global horizontal irradiance (GHI), direct normal irradiance (DNI) and diffuse horizontal irradiance (DHI) are usually not all available simultaneously as measured data. Thus, the missing components have to be obtained by means of the numerical modelling. Due to its physical core and good reputation among the expert community, the solar radiation model DISC, which is developed in the U.S. National Renewable Energy Laboratory (NREL) is a reasonable choice as a main simulation tool. The present article is dedicated on the evaluation of the simulation capabilities of DISC using satellite data as an input and as a reference.

Utilizing the expertise from the Member States, Satellite Application Facilities (SAFs) are dedicated centres of excellence for processing satellite data. They form an integral part of the distributed EUMETSAT Application Ground Segment. The EUMETSAT SAF on Climate Monitoring (CM SAF) develops, generates, archives and distributes high-quality satellite-derived products of the energy and water cycle in support of monitoring, understanding and adapting to climate variability and climate change. In the present work the DNI and, subsequently, the sunshine duration (SDU) are simulated using the surface irradiance (SIS) from the CM SAF SARAH2 product collection as the main input parameter GHI. The model set-up implements also information from the Bulgarian operative system ProData as an auxiliary data. This system is proved as a reliable source of consistent meteorological information with high spatial and temporal (1 hour) resolution and minimal latency from the input data acquisition time. The model has been coded in FORTRAN90/95 by the corresponding author and tested against the NREL examples. Computations on hourly basis for the year 2015 over domain, which covers Bulgaria with fine-spaced grid, have been performed. The results have been compared with their satellite counterparts from the same collection. The main conclusion is that the modelled results remarkably overestimate the satellite-derived estimations. The reason might be rooted in the fact, that the preliminary assumption that the CM SAF SARAH2 SIS can be used as proxy of DHI, is wrong.

Key words: DHI, DNI, SDU, CM SAF SARAH2 product, DISC model, ProData operative system

Blind Partial Key Exposure Attack on RSA Using 2-Dimensional Lattices

Miroslav Dimitrov

RSA is one of the first public-key cryptosystems and it is widely used by providing means of secure data transmission. It can be efficiently implemented on constrained devices such as smartcards. By using powerful attacks such as side-channel attacks, power analysis, timing attacks and others, an attacker can partially expose bits of the private exponent d or construct a hypothesis about the Hamming weight of consequent bits of d.

The concept of partial key exposure attacks on RSA was introduced in 1997 by Boneh, Durfee and Frankel in [1]. They showed that for low exponent RSA, a quarter of the list significant bits of d are sufficient for efficiently reconstructing d and obtained similar results for larger values of e as long as $e < \sqrt{N}$. These results demonstrate the danger of leaking part of the bits of d. Later, Blömer and May [2] extended their result with attacks for $e \in \left[N^{0.5}, N^{0.725}\right]$. Ernst, Jochemsz, May, and De Weger [3] have constructed flexible attacks including the cases where the private exponent d or the public exponent e is chosen to be small and both their attacks work up to full size exponents.

In [2, 3, 4, 5] lattice-based methods are used to perform a partial key exposure attack. The attacks using lattice-based methods are asymptotic, meaning that if one comes close to the maximal value for the unknown part of d for which an attack should work, the lattices involved are very large. This implies that the lattice reduction phase, for which the LLL-algorithm [6] is used, may take a prohibitively long time.

In [7] the authors explore the sizes of d for which one can mount an attack in a few seconds with a very simple method using a 2-dimensional lattice. More precisely, the attack can be applied when the private exponent d is chosen to be small, which can occur in practice. Although the attack does not achieve the theoretic bounds of known partial key exposure attacks using Coppersmith's method, it is much faster in its application range.

The current paper provide an automatic way of searching through possible choices of the private exponent d, under the condition that a sufficient length of consequent bits of the MSBs and/or LSBs of d has low Hamming weight. Moreover, even knowing only the public key, the attack can be used to blindly test different lengths d of the private exponent or to systematically search possible low Hamming weights of the first, the last or some combination of the first and the last $(2\beta - 1/2)n$ bits of d for $0 < \beta < \frac{1}{2}$. The search is blind because the hypothesis intervals for some expected values of d are not given as well as the possible Hamming weights for the corresponding part of d are not determined.

The implementation of the proposed attack was able to successfully solve one of the level III challenges published in "Mystery Twister C3" - the Crypto Challenge Contest [8]. The problems in this level represent current research topics that are believed to be very difficult

to solve. Thus, practical solutions may not even exist and ready-to-run tools almost certainly do not.

The particular challenge, which has been solved, is about reconstructing the private key which corresponds to a given public key, knowing that the bit length of d is 400 bits and the Hamming weight of the first 310 bits is 4. The blind RSA attack recovered the private key for less than 4 hours on a single computer using implementation written in SageMath. The current version of the software allows the user to apply successful attacks on RSA instances, even when the partial information is so limited, that directly applying the currently known state-of-the-art RSA attacks on the given RSA instance is not applicable.

Acknowledgments

This research was partially supported by the Bulgarian National Science Fund [Contract No. 12/8, 15.12.2017].

References

[1] Boneh, Dan, Glenn Durfee, and Yair Frankel. "An attack on RSA given a small fraction of the private key bits." International Conference on the Theory and Application of Cryptology and Information Security. Springer, Berlin, Heidelberg, 1998.

[2] Blömer, Johannes, and Alexander May. "New partial key exposure attacks on RSA." Annual International Cryptology Conference. Springer, Berlin, Heidelberg, 2003.

[3] Ernst, Matthias, et al. "Partial key exposure attacks on RSA up to full size exponents." Annual International Conference on the Theory and Applications of Cryptographic Techniques. Springer, Berlin, Heidelberg, 2005.

[4] Boneh, Dan, and Glenn Durfee. "Cryptanalysis of RSA with private key d less than N/sup 0.292." IEEE transactions on Information Theory 46.4 (2000): 1339-1349.

[5] May, Alexander. New RSA vulnerabilities using lattice reduction methods. Diss. University of Paderborn, 2003.

[6] Lenstra, Arjen Klaas, Hendrik Willem Lenstra, and László Lovász. "Factoring polynomials with rational coefficients." Mathematische Annalen 261.4 (1982): 515-534.

[7] Jochemsz, Ellen, and Benne De Weger. "A partial key exposure attack on RSA using a 2-dimensional lattice." International Conference on Information Security. Springer, Berlin, Heidelberg, 2006.

[8] "Finding Special Private RSA Keys", in *Mystery Twister C3* - the Crypto Challenge Contest, [Online]. Available: https://www.mysterytwisterc3.org/images/challenges/mtc3-kitrub-04-speciald-en.pdf.

Numerical Identification of the Time Dependent Vertical Diffusion Coefficient in a Model of Air Pollution

Ivan Dimov, Juri Kandilarov, Lubin Vulkov

The two dimensional non-stationary convection-diffusion equation

$$\frac{\partial c}{\partial t} - L(c,\varphi) = f, \quad L(c,\varphi) = a\frac{\partial^2 c}{\partial x^2} + \varphi(t)\frac{\partial}{\partial z}\left(b\frac{\partial c}{\partial z}\right) - u\frac{\partial c}{\partial x} - \omega\frac{\partial c}{\partial z} - kc, \quad (1)$$

$(x,z) \in (0,X)\times(0,Z),\ 0<t<T$ models the transport of air-borne pollutant in the atmosphere (and in water) at some simplification. Here c is the *concentration of pollutants*, (u,ω) are the components of the wind velocity,f is the power of source, $k = const. \geq 0$ is the transformation coefficient of the pollutants and a, b are the horizontal and vertical diffusion coefficients. For example, the Monin-Obukhov theory of the atmospheric boundary layer is applied and for the transversal eddy-diffusivity the expression is often used [1]

$$B(z,t) = \varphi(t)b(z) = \varphi(t)z(Z-z)\left(1-22z/L\right),$$

where $L<0$ is the Monin-Obukhov length and $\varphi(t)$ is *measured friction* velocity.
In some practical pollutant dispersion scenarios the function $\varphi(t)$ is defined by point measurements of the concentration or integral observations (domain-averaged concentrations), [1],

$$c(x^*,z^*,t) = \psi^*(t), \quad \int_0^X\int_0^Z c(x,z,t)\mathcal{X}(x,z)dxdz = \psi(t). \quad (2)$$

Define the time steps $\triangle t_j = t_j - t_{j-1},\ j = 1,2,\ldots,J,\ t_0 = 0,\ t_J = T$ and denote the values of the functions on the $(j+1)$-th level by $\widehat{c},\widehat{\varphi}$, etc. We propose the following decomposition algorithm of such defined *inverse problems*.
First, we perform a special form of Crank-Nicolson discretization in time, see e.g. [2],

$$(\widehat{c}-c)/\triangle t_{j+1} - \frac{1}{2}(L(\widehat{c},\varphi) + L(c,\widehat{\varphi})) = \frac{1}{2}(\widehat{f}+f). \quad (3)$$

Then we place the solution decomposition

$$\widehat{c} = \widehat{v} + \widehat{\varphi}\widehat{w} \quad (4)$$

in (3). As a result we obtain the following equations for the unknown functions $\widehat{w}$ and $\widehat{v}$:

$$(\widehat{v}-c)/\triangle t_{j+1} - \frac{1}{2}L(\widehat{v},\varphi) = \frac{1}{2}(\widehat{f}+f) + \frac{1}{2}L(c,\varphi) - \frac{1}{2}\varphi\frac{\partial}{\partial z}\left(b(z)\frac{\partial c}{\partial z}\right),$$

$$\widehat{w}/\triangle t_{j+1} - \frac{1}{2}L(\widehat{w},\varphi) = \frac{1}{2}\frac{\partial}{\partial z}\left(b(z)\frac{\partial c}{\partial z}\right).$$

To find $\widehat{\varphi}$, we substitute the representation (4) in the point measurement in (2), to obtain

$$\widehat{\varphi} = (\widehat{\psi}^* - \widehat{v}(x^*,z^*))/\widehat{w}(x^*,z^*).$$

For the integral observation case, we have

$$\widehat{\varphi} = \left(\int_0^X \int_0^Z \widehat{w} \mathcal{X} dx dz \right)^{-1} \left(\widehat{\psi} - \int_0^X \int_0^Z \widehat{v} \mathcal{X} dx dz \right).$$

Because the degeneration of the vertical diffusion $B(z,t)$ at $z = 0$ and $z = Z$ we employ the fitted finite volume method [3] for the numerical realization of the decomposition algorithm. Results of numerical experiments for inverse one- and two-dimensional model problems are discussed.

Acknowledgements The first author is supported by the Bulgarian National Fund of Science under Projects DN 12/5-2017 “Efficient Stochastic Methods and Algorithms for Large-Scale Computational Problems” and the second and third authors - by the Bulgarian National Science Fund under the Bilateral Project DNTS/Russia 02/12 "Development and investigation of finite-difference schemes of higher order of accuracy for solving applied problems of fluid and gas mechanics, and ecology" from 2018.

References

[1] J. M. Stokie, The mathematics of atmospheric dispersion modeling, SIAM, Review, **53**(2) (2011) 349-372

[2] P. N. Vabishchevich, M. V. Klibanov, Numerical identification of the leading coefficient of a parabolic equation, Differential Equations, **52**(7) (2016) 855–862

[3] S. Wang, A novel fitted finite volume method for the Black-Scholes equation governing option pricing, IMA J. of Numer. Anal., **24** (2004) 699-720.

The use of Wildfire Analyst in Bulgaria – a fire simulator to analyze fire progression in real-time. The Kresna case study(2017)

Nina Dobrinkova, Adrián Cardil

Currently, in Bulgaria, computer-based wildfire analysis tools are rarely used to support firefighters and incident commanders on field activities. Commonly, historical data is collected and used to reconstruct past fire events. Usually the work is limited to running fire simulations in scientific laboratories, but no further implementation is elaborated by operational teams. Some satellite images are usually used for the analysis of the fire perimeter and affected zones as well as input data to feed the fire spread models. Most of the cases simulated for past fire events have been done by PhD students in Bulgarian Academy of Sciences. This experiences and their descriptions started back in 2007 and nowadays is clear that the most difficult part in fire propagation simulator's usage in Bulgaria is the data. The data sets are in most cases paper documents and hardly ever available in digital formats.

In our article we will focus on a new tool called Wildfire Analyst (WFA) which is for first time applied for a Bulgarian test case. This software is a fire simulation framework that provides near real-time analysis of wildfire progression, fire behavior, suppression capabilities, and impact analysis for an incident. WFA has been developed to be used in fire operations by implementation of algorithms that allows doing the fire progression calculations in near-real time with a user friendly interface. It has ability to incorporate data from Geographic Information System's (GIS) layers and use it as direct inputs to the simulation with no need to preprocessing and creation of many other additional files. Assignment of Fire Behavior Fuel Models (FBFMs) is done directly in the attributive table of each GIS layer that has information of what is burning on the affected field. Meteorological data is extracted inside of the tool or if available as local collected data set, which can be used in table format for the simulation purposes. Wildfire Analyst is developed with the idea to simulate wildland fire in an efficient and fast way satisfying the operative necessities in real time. The the calculations of fire propagation have new simulation models, which makes this simulator as a step forward compared to what is available until now. The main purpose of WFA is to be able to offer realistic simulations in active fires and offer outputs to support in real time any suppression operations done in less than two minutes. Apart from its use in extinguishing operations, it is also used in analysis and planning preventive actions or post-fire analysis.

This tool is relatively young, but is used already in North and South America, as well as in Spain. Its first application as a wildland fire spread simulator is decided to be for a Bulgarian test case located in Kresna Gorge. The wildland fire of interest was active between 24-30 August 2017 and burned 1600 ha. forestry and around 2300 ha urban plus forested areas. The available data and satellite images for this fire have been preprocessed in a way to be directly included in the WFA as GIS layers. The preparation of the data and its initial outcomes will be described in this paper.

Keywords: Wildland fires, WFA, Simulations, Kresna Fire 2017.

Increase Speed of algorithm for Subtract of two 2D polygons. Comparing with commercial product and Genetic algorithm.

Georgi Evtimov

The Cutting Stock Problem (CSP) is an important industrial problem. In this article the polygons are only in 2D. I will suggest an approach for increasing of speed of algorithm for subtract of two polygons. The algorithm for subtract the polygons is based on geometrical computational methods. The basic methods are described in ESGI120'16, BGSIAM'16, BGSIAM'17, LSSC'17, NM&A'18. Generally we have to solve the subtraction between two polygons - the first is polygon to subtract from (Basic) and second is polygon to subtract (Knife). This function will repeat for each polygon (knife) and for each vertex of the knife polygon. This is a heavy calculation, witch means a lot of CPU time consuming. The main idea is to miss a vertex from Basic polygon witch is with angle less than angles from knife's polygon.

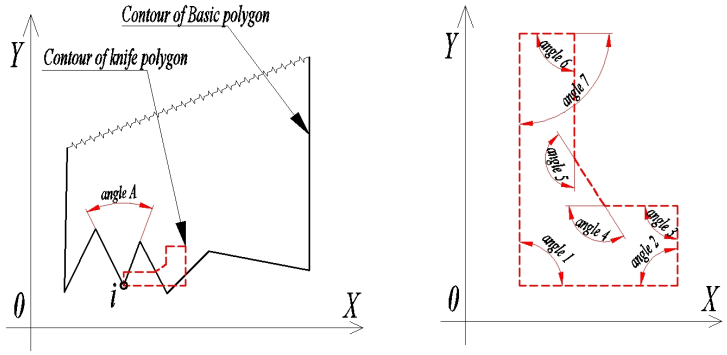

If the angle A is smaller than angles 1, 2 ... 7 than do not try to subtract the polygons.
The comparing will be for 107 polygons. Some of them are equals. All polygons are a simple with maximum number of the vertices are 8. The comparison between the methods is :

1. Genetic algorithm, authors Desislava Koleva, Maria Barova, Petar Tomov with issue "2D Optimal Packing with Population Based Algorithms", LSSC'17;

2. Commercial Software: FP_Opti2D v2.0/2 (Build 2) 30-Mar-2007, EMMEGISOFT S.r.l.

One polygons is a main (base) and the second polygon is the "knife" polygon. issue I will paper we focuse on the variant arasing in building construction, where a set of plates needs to be cut from rectangular stock, minimizing the waste. The CSP is known to be NP-hard combinatorial problem. The goal of this work is to propose an efficien way for subtracting of two polygons with some matching vertices.

Generalized Net Model for Flying Ant Colony Optimization

Stefka Fidanova, Krassimir Atanassov

Ant Colony Optimization (ACO) has been used successfully to solve hard combinatorial optimization problems. The method is inspired by the foraging behavior of real ant colonies, which manage to establish the shortest routes to feeding sources and back. In ACO the problem is represented as a graph and our artificial ants look for a shorter path taking in to account some constraints. The method is constructive. Every ant start to create its solution, starting from random node. It includes new node in the partial solution according probabilistic rule. In traditional ACO an ant can observe only the neighbor nodes and decides to include it or not in the partial solution.

In our previous work we try to improve ACO imitating flying ants. Thus the ant will receive more information about the search space. An ant make a decision about the direction to move (new added node), taking in to account the information from more than one step ahead. It observes the neighbors of the neighbors too and thus it can make better decision. The influence of the information depends of how far is the observed node. We use weights and the information from the neighbor nodes has the greatest weight and thus the greatest influence than the neighbors of the neighbors.

The Generalized Nets (GN) is a powerful tool for modeling real processes. GN are extension of ordinary Petry nets and other their extensions. GN are discrete tool for universal description of adaptable, structured and reusable models of complex systems with many different, non-homogeneous structure, usually involved in parallel, simultaneous activities. They can play a role of generator of new ideas for extending initial processes.

The structure of the GN is at the same time static and dynamic. The static structure consists of objects called *transitions*, which have input and output *places*. Two transitions can share a place, a place can be input of at most one transition and output of at most one transition.

The dynamic structure consists of tokens, which act as information carriers and can occupy a single place at every moment of GN execution. The tokens pass through he transitions from input to output places. The movement is governed by *predicates*, in the *predicate matrix*. The information carried by a token is contained in its *characteristics*.

The GN are expandable, every place can be replace with other GN. Thus a GN can be developed in depth, including more and more details. Therefore they are flexible and very appropriate for describing and modeling of great variety of processes, including algorithms.

In this work we apply GN for modeling Flying Ant Colony Optimization (FACO). Description of FACO by GN can give us new ideas for further development and improvement of the algorithm.

The braided group of a square-free solution of the Yang-Baxter equation

Tatiana Gateva-Ivanova

Set-theoretic solutions of the Yang–Baxter equation (YBE) form a meeting-ground of mathematical physics, algebra and combinatorics. Such a solution (X, r) consists of a non-empty set X and a bijective map $r : X \times X \to X \times X$ which satisfies the braid relation

$$r^{12}r^{23}r^{12} = r^{23}r^{12}r^{23}$$

in $X \times X \times X$, where $r^{12} = r \times id_X$, $r^{23} = id_X \times r$. In this case (X, r) is called *a braided set*. A braided set (X, r) with r involutive is called *a symmetric set*. (X, r) is said to be *square-free* if $r(x, x) = (x, x)$ for all $x \in X$. The question of studying set-theoretic solutions of YBE was posed by Drinfeld, [1] and since then they are objects of active investigation.
Set theoretic solutions extend to special linear solutions, but it is more interesting that they also lead to a great deal of combinatorics, group action on X, cyclic conditions; matched pairs of groups, matched pairs of monoids, braided groups and braided monoids; semigroups of I type with a structure of distributive lattice; special graphs; quadratic algebras with very nice algebraic and homological properties such as being: (i) Artin-Schelter regular algebras; (ii) Koszul algebras; (iii) Noetherian domains with a **k**-basis of Poincaré-Birkhoff-Witt type; (iv) with good computational properties -the theory of noncommutative Groebner bases is applicable. Each set-theoretic solution of YBE induces naturally a solution to the (general) Yang-Baxter equation and the Quantum Yang-Baxter equation.
Associated to each set-theoretic solution are several algebraic constructions: the structure group $G(X, r)$, the semigroup $S(X, r)$, the quadratic algebra $A(k, X, r) \cong \mathbf{k}S(X, r)$, each of these structures is generated by X and has quadratic relations $xy = \cdot r(x, y)$, where "$\cdot$" denotes product in the free semigroup, resp. free group. The permutation group $\mathbf{g}(X, r) \subset Sym\ (X)$ is defined by the corresponding left translations $y \mapsto {}^x y$ for $x \in X$, where $r(x, y) = ({}^x y, y^x)$.
In this work we study the structure group $G = G(X, r)$ in the special case when (X, r) is *a non-degenerate square-free solution of finite order* $|X| = n$.
It is known, see [4], that if (X, r) is a finite square-free solution then the set X can be ordered

$$X = \{x_1 < x_2 < \cdots < x_n\},$$

so that the quadratic **k**-algebra $A = A(\mathbf{k}, X, r) = \mathbf{k}\langle X \mid R\rangle$ over arbitrary field **k**, is *a binomial skew-polynomial rings* in the sense of [2]. The set of quadratic defining relations of A, denoted $R_0 = R_0(r)$, is a Groebner basis w.r.t. degree-lexicographic order on $\langle X\rangle$. The set R_0 consists of exactly $\frac{n(n-1)}{2}$ binomial relations which satisfy the following condition.
For every pair $x, y \in X$, with $x > y$, the equality $r(x, y) = ({}^x y, x^y)$ implies

$$xy - ({}^x y)(x^y) \in R_0, \quad {}^x y < x^y, \quad {}^x y < x, \quad y < x^y.$$

Equivalently, $A = \mathbf{k}\langle x_1, \cdots, x_n\rangle/(R_0)$ is a quadratic algebra with a **k**-basis **N** of Poincaré-Birkhoff-Witt type:

$$\mathbf{N} = \{x_1^{\alpha_1} \cdots x_n^{\alpha_n} \mid \alpha_i \geq 0,\ 1 \leq i \leq n\}.$$

Recall from Groebner bases theory that **N** is the set of *normal monomials*, and each monomial $u \in S = S(X, r)$ has unique normal form $u_0 \in \mathbf{N}$. So the monoid S (considered as a set) can be identified with the set **N**. Conversely, every X-generated binomial skew-polynomial ring A defines a square-free solution (X, r), see [3]. In this case the map r is defined canonically via the set of quadratic defining relations of A. Algebraic and homological properties of binomial skew polynomial rings and their close relation to YBE were studied in [2, 3, 5], et al. It was also proven that the map r extends to a braiding operator r_G on G so that (G, r_G) is *a braided group* (a group analogue of braided sets), similarly (S, r_S) is *a braided monoid*.

Notation-Convention. We fix the enumeration $X = \{x_1 < x_2 < \cdots < x_n\}$, described above. Let p *be the least common multiple of all orders of permutations* $L_x \in \mathbf{g}$, where $x \in X$. Clearly, $(L_x)^p = id_X$ for all $x \in X$. We shall work with the sets

$$Y := \{x_1^{\alpha_1} \cdots x_n^{\alpha_n} \mid 0 \leq \alpha_1 \leq p-1\} \subset \mathbf{N}; \qquad X_p := \{x_1^p, x_2^p, \cdots, x_n^p\}.$$

Theorem. *Let (X, r) be a square-free symmetric set of finite order $|X| = n$, $G = G(X, r)$, $S = S(X, r)$, notation and conventions as above. Let $\mathbf{F} = {}_{gr}[X_p] \leq G$ be the subgroup of G generated by X_p, and let $\boldsymbol{N}_p := [X_p]$ be the submonoid of S generated by X_p. Then the following conditions hold. (1) The group $\mathbf{F}$ is isomorphic to the free abelian group in n generators. (2) One has $\mathbf{F} \subset \boldsymbol{K}$, where $\boldsymbol{K}$ is the kernel of the left action of G upon itself. The monoid $\boldsymbol{N}_p$ and the group $\mathbf{F}$ are G-invariant with respect to the left and the right actions of G upon itself. (3) Every element $u \in G$ can be presented as $u = yW$, where $y \in Y$, $W \in \mathbf{F}$, and the pair y, W in this presentation is unique. (4) $\mathbf{F}$ is a normal subgroup of G of index $[G : \mathbf{F}] = p^n$. More precisely, the set of (left) cosets of $\mathbf{F}$ in G is $G/\mathbf{F} = \{y\mathbf{F} \mid y \in Y\}$. (5) The order of the retract $|Ret(G, r_G)| = |\boldsymbol{g}|$ divides p^n. Moreover, if p is a prime number, then the permutation group $\boldsymbol{g}(X, r)$ is a p-group.*

References

[1] Drinfeld, V., *On some unsolved problems in quantum group theory*, Lecture Notes in Mathematics **1510** (1992), 1–8.

[2] Gateva-Ivanova, T., *Skew polynomial rings with binomial relations*, J. Algebra **185** (1996), 710–753.

[3] Gateva-Ivanova, T. and Van den Bergh, M., *Semigroups of I-type*, J. Algebra **206** (1998), 97–112.

[4] Gateva-Ivanova, T., *A combinatorial approach to the set-theoretic solutions of the Yang-Baxter equation*, J.Math.Phys. **45** (2004), 3828–3858.

[5] Gateva-Ivanova, T., *Quadratic algebras, Yang-Baxter equation, and Artin- Schelter regularity*, Adv. in Math. **230** (2012), 2152–2175.

[6] Gateva–Ivanova, T., *Set–theoretic solutions of the Yang–Baxter equation, Braces and Symmetric groups*, Adv. in Math. **338** (2018), 649–701.

On Some Sources of Inaccuracy in Classical Molecular Dynamics Simulations

Jordan Genoff

Computer simulated classical molecular dynamics is a major methodology in the modern molecular biology and many other nanoscale studies. The goal is to evolve the spatial trajectory of each atom in a given formation, over a given time interval, starting from a given initial configuration and utilizing the Newtonian mechanics.

The simulation engine performs numerical solution of the equations of motion in discrete time steps. At each step, each particle: 1) has its spatial coordinates and its velocity vector, and 2) interacts with each other through force vectors that are derived from an interatomic potential function or force field. Interaction forces participate in a system of coupled ordinary differential equations. The latter are solved by numerical integration and give the particle's spatial coordinates and velocity vector for the next time step. In addition, different kinds of conservation constraints apply throughout the process.

Although this brief explanation may seem simple, in reality things are very complicated by many unavoidable circumstances and details. A short list of them: even the most modest adequate simulation is performed on at least several tens of thousands of particles; the integration time step should be very small, e.g. under one femtosecond; a meaningful simulation usually requires an insanely long time interval, relative to the integration step, which leads to enormous number of steps, e.g. tens of millions; these three so far turn the task into a large-scale one; the underlying math is complex enough even in the simplest cases of force fields and integration algorithms, which leads to significant computation error; the system under simulation is in fact a chaotic one, which may turn the error and its accumulation into a nightmare.

There are, in both theory and practice, many approaches that attempt to solve or at least to minimize the effects of the above stated and other problems. Perhaps the most important of them are: the simulation takes place in a bounded subspace – a box, which immediately introduces a set of boundary conditions that are eliminated by box periodic replication; each particle's neighborhood is split into a short-range part and a long-range part, with distinct interaction potential functions; different integration algorithms are adopted; etc.

The research presented here investigates in great detail the impact of four factors on the simulation result accuracy: the computational precision; the integration step; the extension of the short-range neighborhood beyond the theoretic rationale; and the size of the bounding box in relation to the size of a smaller "significant" sub-box, where the most important part of the simulated atomic formation is located, while the rest of the volume is filled with an "insignificant" substance, e.g. explicit solvent.

Naturally and first of all, a concept of an accurate simulation result is needed. Unfortunately, there is no such one that covers all simulation aspects. The reason is that except the statistical quantities, like temperature, nothing more sophisticated, like a single particle trajectory or a single pair of particles interaction, can be checked and proven by real physical experiment. In the scope of this research, the solution is to perform a comparative analysis of the simulation and its result, when done in different conditions, caused by the influence factors listed above.

Besides, the chaotic nature of the simulated system amplifies its sensitivity to the said factors. Thus, a simulation run is considered accurate, with respect to a certain factor, until it gives exactly the same intermediate result as a simulation run, which is executed with only a slightly changed value of the factor, and nothing else changed. Once the intermediate results begin to diverge, both runs are considered inaccurate.

Second, a measure of simulation accuracy must be formulated. The above definition of accuracy leads to a comparative measure of dissimilarity or divergence of the simulation result (intermediate or final), produced in different conditions. Actually, not a single one, but a set of measures are formulated: one estimates the simple dissimilarity between two vector sets as an average distance; others are more complex and estimate the degrees of distance preservation and angle preservation between two vector sets; another one estimates the individual particle trajectories divergence. All of them, when taken together, give a clear view of what is happening during a simulation run and until when it may be considered accurate.

In order to assure the real life pragmatic value of the research, all of the experimentation is conducted using three popular and widely adopted molecular dynamics simulation open-source software packages.

Experiments show strikingly surprising results about the extreme requirements on the considered factors.

Digital Cranial Suture Analysis with Application in Age Estimation

Ivan Georgiev, Andrey Gizdov, Stanislav Harizanov, Silviya Nikolova, Diana Toneva

The neurocranium is composed of flat bones fastened together by calvarial sutures, which represent bands of fibrous connective tissue. The sutures allow no active motions, but act as flexible joints and permit adjustive overlap of the calvarial bones as the head becomes compressed during the childbirth. When the brain reaches its optimal shape and size during the early adulthood, the process of suture maturation usually begins with a series of morphological changes. The reorganization in the micro-structural finally leads to complete remodeling and obliteration of the sutural area.

Until now, the correlation between suture closure and age-at-death has been examined by conventional quantifying methods based on a superficial subjective assessment of the suture patency on the endo- and exo-cranial surfaces together or individually, using descriptive rank-ordered scoring scales of various grades.

Nowadays, technology like Computed Tomography (CT) allows an inside view cross-sectional observation of the suture morphology. This type of in-depth analysis of a suture is a new approach, and only few studies have been made on the topic. In two of the studies a human is responsible for evaluating the level of bone fusion along the suture, which is time consuming, subjective and thus, sometimes inaccurate. There has been an attempt to automatize this process with the use of a simple algorithm, but the results are not promising, as the algorithm lacks the ability to consider enough factors in the suture image and the output is only binary: either "closed" or "open". On the other hand, how far the bones are from complete fusion directly depends on the gray-scale intensities of the suture pixels. Computationally, this is relatively easy to calculate but it can hardly be done manually along the whole length of the suture. Those bits of extra information are neglected by all currently known techniques for age estimation. Taking them into account can be a key to improving the accuracy of age estimation based on cranial sutures, with real world applications in multiple fields including forensic anthropology and bioarchaeology.

This study, is aimed to develop an algorithm for objective automatic assessment of the suture closure degree in cross-section and to assess its relation to aging. For this purpose volumetric images (.TIFF series) of dry skulls of adult males with known age-at-death generated by industrial μCT are processed. The obtained spatial resolution (voxel size of 97.5 μm) is high enough to allow precise detection of the contact between the adjacent calvarial bones in each of the three bone layers: internal table, *diploë* and external table. Thus, such a setup is perfect for the validation of our approach. With the use of different algorithms and deep learning, the purpose is to achieve a better cross-sectional view of sutures from a skull CT scan, and to create an automatically executed metric system for estimating the age of an individual, based on this cross-sectional view.

The execution of the algorithm contains several stages. The first one is the 3D image generation, which is done in Matlab. A downscaled, triangulated version of the full volumetric data, centered around a particular skull suture is used. The user manually defines a set of points

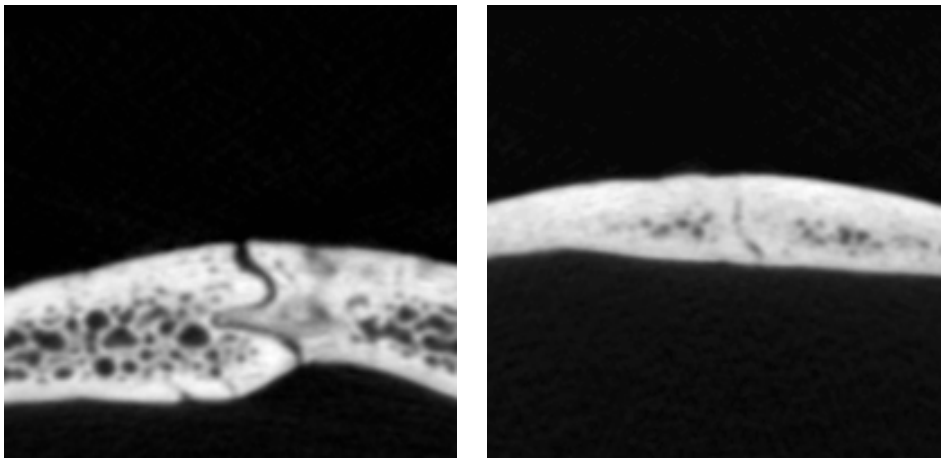

"Open" suture "Closed" suture

Figure 1: Cross-sectional tomograms, generated by μCT

on the suture and those points are joined in a "smallest cost path" with respect to a given criteria. Next, the normal vector to the skull surface at each marking point is calculated and the local cross-sectional image is oriented in the tangential plane. Data processing consists of measuring a number of quantifying characteristics for the detected suture region, such as the width of the suture on a number of equidistant locations and the gray-scale intensity of the selected pixels. Based on the results, an overall age estimation is produced.

A characteristic feature of μCT systems, is the very high quality of the generated images. This makes the data extraction relatively easy, and does not require the necessity of any additional image processing to improve the quality of the under laying data (see Fig. 1). On the other hand, medical CT gives rise to low-resolution data, that have been already pre-processed. For a good cranial suture analysis, however, it is important to have a clear view of the edges and a measurable distance between the two ends of the suture. This can be very hard to achieve even by a trained professional, given such a poor quality, blurred image. Thus, the study also aims to apply theoretical and experimental scientific techniques to artificially improve the data quality and adapt the degraded CT data to the described above functionality for automatic suture assessment.

Acknowledgement: This research is partially supported by the Bulgarian National Science Fund under grant No. BNSF-DN01/15 from 20.12.2016.

Numerical Homogenization of Porous Materials Based on Micro CT Data

I. Georgiev, S. Margenov, J. Stary, and S. Zolotarev

The talk concerns linear micromechanics exploiting Industrial Computed Tomography (micro-CT) data for determination of microstructure and numerical homogenization with a focus on analysis of fiber-reinforced silicate composites. The analysis includes an identification problem and stochastic uncertainty, which bring new dimensions and enhance the need for fast solvers and High Performance Computing [1]. Fiber-reinforced composites has many applications in industry, civil and geotechnical engineering. The shape, dimension, and length of the fiber together with fiber volume amount and distribution are important parameters influencing the tensile strength of the composite. The analysis includes an assessment of tensile stiffness for several samples of composite material, which differ in amount and distribution of fibers. These samples are scanned by micro-CT and analyzed with provided elastic parameters for fibers and matrix. The detailed scan of a sample leads to solving of linear elasticity problems with more than 200 million degrees of freedom. If the global response of the samples can be tested on a loading frame, then the output allows solving an inverse material identification procedure to determine the elastic properties of the matrix. In this way, we can both determine the properties of concrete matrix, which can also be variable to some extent, as well as assess if some discrepancy can be explained by imperfect bonding of fibers. The main goal of the study is solving a microscale problem for homogenization within the range of linear material behavior. This basic problem can be extended in the direction to the solution of the inverse problem of identification of local material parameters or some level of deboning of the matrix and fibers. This problem is solved by an optimization procedure which requires repeated solution of the basic problem. The computational demand may increase about hundred times. Another possible extension is in solving not only selected and scanned samples of the concrete, but stochastic generation of a set of such samples and evaluation of the mean properties by Monte Carlo or multi-level Monte Carlo methods.

References

[1] R. Blaheta, I. Georgiev, K. Georgiev, O. Jakl, R. Kohut, S. Margenov, J. StarÃ½, High Performance Computing in Micromechanics with an Application, Cybernetics and Information Technologies, 17(5) (2017), 5-16

Numerical Determination of Time-Dependent Implied Volatility by Point and Integral Observations

Slavi G. Georgiev, Lubin G. Vulkov

Volatility has become widely used in the risk management, portfolio hedging and option pricing measuring the amount the randomness since volatility is the only unobservable parameter from the financial market, in general, which can be estimated from the observed market option prices. So, the *calibration* of the volatility from observed market data seems to be of high interest, see e. g. [1].
The European *call option* premium $C = C(S,t;K,T)$ satisfies the following generalized Black-Scholes equation

$$\frac{\partial C}{\partial t} + \frac{1}{2}\sigma^2(t)S^2\frac{\partial^2 C}{\partial S^2} + (r(t) - d(S,t))S\frac{\partial C}{\partial S} - r(t)C, \quad (S,t) \in R^+ \times [0,T), \tag{1}$$

where S is underlying asset, r is the risk-free rate of interest, d is the stock dividend and σ is the volatility function. We will solve the equation (1) at Dirichlet boundary conditions and the terminal condition

$$C(S,T) = \max(S-K,0) \equiv (S-K)^+, \tag{2}$$

where T is the maturity, K is the strike. For constant coefficients we take the Black-Scholes formula for a call and substitute the interest rate r, the strike price K, the maturity T and today's asset price S_0 into the formula. Then we find the constant volatility σ for which the result coincide with the the observed option price in the market. This volatility, derived from the quoted price for a single option, is called the *implied volatility*, i. e.
$C^{obs} = C^{BS}(S_0, t_0; K, T, r, d, \sigma^{imp})$.
We consider two kinds of problems for the time-dependent implied volatility.
Problem 1 Let $C(S,t)$ be the option price which satisfies (1), (2) on localized domain $(0, S_{max})$.

$$\text{Assume that when } 0 < S^\star < S_{max}, \quad C(S^\star,t) = C^\star(t), \quad 0 < t < T \tag{3}$$

and $C^\star(t)$ is given function . *Determine C and σ^2 with extracondition (3).*
Problem 2 Let $C(S,t)$ be the option price which satisfies (1) - (2).

$$\text{Assume that} \quad \frac{1}{S_{max}}\int_0^{S_{max}} C(S,t)dS = C^\star(t), \quad 0 < t < T, \tag{4}$$

where $C^\star(t)$ is given function of t. *Determine C and σ^2 with extracondition (4).*
Let $\tau = T - t$ and $\overset{o}{D}, D, D^2$ be the usual difference operators . Write for (1), (2) the implicit difference scheme

$$\frac{c_i^{j+1} - c_i^j}{\triangle\tau} = (\sigma^{j+1})^2 S_i^2 \, \mathrm{D}^2 c_i^{j+1} + (r^{j+1} - d^{j+1})S_i \left\{ \begin{array}{l} \overset{\circ}{\mathrm{D}}\, c_i^{j+1}, \\ \mathrm{D}\, c_i^{j+1} \end{array} \right\} \tag{5}$$

$$-rc_i^{j+1},\ \ (1 \le i \le I),\ \ c_{I+1}^{j+1} = \left(S_{I+1} - Ke^{-r(j+1)\triangle\tau}\right),\ \ (0 \le j < J,\ T = J\triangle\tau).$$

The *discrete inverse problem*, which requires the determination of the pair $\left\{c_i^{j+1}\right\}_{i=1}^{I+1}$, $(\sigma^{j+1})^2$, is nonlinear. The algorithm we propose is based on the approximation of the product $p(\tau)q(\tau)$ at the point $\tau^{j+1/2} = (j+1/2)/\triangle\tau$:

$$p(\tau^{j+1/2})q(\tau^{j+1/2}) = \frac{1}{2}p(\tau^{j+1})q(\tau^j) + \frac{1}{2}p(\tau^j)q(\tau^{j+1}) + \mathcal{O}(\triangle\tau^2).$$

To find an approximate solution $(\sigma^{j+1})^2$ at the new time level, we insert the decomposition $c_i^{j+1} = z_i^{j+1} + (\sigma^{j+1})^2.w_i^{j+1}$ in (5) to obtain separate discrete problems for z_i^{j+1} and w_i^{j+1}. Then, we perform the **algorithm**:
Step 1 Solve the discrete problem for z_i^{j+1} .
Step 2 Solve the discrete problem for w_i^{j+1}.
Step 3 From discrete version of (4) (or (3)) we find

$$(\sigma^{j+1})^2 = \left(C^\star(\tau^{j+1}) - \frac{1}{S_{max}}\sum_{i=1}^{I+1} z_i^{j+1}\triangle S_i\right) \Big/ \left(\frac{1}{S_{max}}\sum_{i=1}^{I+1} w_i^{j+1}\triangle S_i\right).$$

Numerical experiments using synthetic data and real data are analyzed.
We also solve the corresponding inverse problems for the two-asset time-dependent volatility Black-Scholes equation

$$\frac{\partial V}{\partial t} + \frac{1}{2}\sigma_1^2(t)S_1^2\frac{\partial^2 V}{\partial S_1^2} + \rho\sigma_1(t)\sigma_2(t)S_1S_2\frac{\partial^2 V}{\partial S_1\partial S_2} + \frac{1}{2}\sigma_2^2(t)S_2^2\frac{\partial^2 V}{\partial S_2^2}$$

$$+(r(t) - d_1(t))S_1\frac{\partial V}{\partial S_1} + (r(t) - d_2(t))S_2\frac{\partial V}{\partial S_2} - r(t)V = 0.$$

Acknowledgments. The authors are supported by the Bulgarian National Science Fund under Project DN 12/4 "Advanced analytical and numerical methods for nonlinear differential equations with applications in finance and environmental pollution", 2017.

References

[1] Saporito Y. F., Yang X., Zubelli J. P., The Calibration of Stochastic-Local Volatility Models – An Inverse Problems Perspective, arXiv:1711.03023 [q-fin.CP], 2017

Homotopy analysis method to solve two-dimensional nonlinear Volterra-Fredholm fuzzy integral equations

Atanaska Georgieva, Albena Pavlova, Lozanka Trenkova

The integral equations arise in many industrial fields, such as: electromagnetic fields and thermal problems. We know that solving fuzzy integral equations requires appropriate and applicable definitions of fuzzy function and fuzzy integral of a fuzzy function. The fuzzy mapping function was introduced by Chang and Zadeh [1]. Later, Dubois and Prade [3] presented an elementary fuzzy calculus based on the extension principle.

In 1992, Liao [4] employed the basic idea of the homotopy in topology to propose a general analytic method for nonlinear problems, namely "homotopy analysis method" (HAM), [5, 6]. The HAM always provides us with a family of solution expressions in the auxiliary parameter h, the convergence region and rate of each solution might be determined conveniently by the auxiliary parameter h. This method has been successfully applied to solve many types of nonlinear problems [1, 2, 3, 6, 7].

The work [2] shows the application of the HAM for solving a given type of linear and nonlinear integral equations, the special case of which is the Volterra-Fredholm integral equation. The authors also provide some theoretical results about the convergence of the HAM and the error estimation.

In this paper, we consider the following nonlinear Volterra-Fredholm fuzzy integral equation in two variables

$$u(s,t) = g(s,t) \oplus (FR) \int_c^t k_1(t,\tau) \odot G_1(u(s,\tau))d\tau \oplus (FR) \int_a^b k_2(s,\xi) \odot G_2(u(\xi,t))d\xi,$$

where $g,\ u : A = [a,b] \times [c,d] \to E^1$ are continuous fuzzy-number valued functions, $k_1 : [c,d] \times [c,d] \to R_+,\quad k_2 : [a,b] \times [a,b] \to R_+$ are continuous functions and $G_1,\ G_2 : E^1 \to E^1$ are continuous functions on E^1. The set E^1 is the set of all fuzzy numbers.

This equation is called Fredholm integral equation with respect to the position and Volterra with respect to the time. This type of equation appears in many problems of mathematical physics, theory of elasticity, contact problems and mixed problems of mechanics of continuous media.

The aim of this paper is to apply, the HAM to obtain approximate solutions of the two-dimensional nonlinear Volterra-Fredholm fuzzy integral equation. We convert fuzzy Volterra-Fredholm integral equation to a system of Volterra-Fredholm integral equation in crisp case. The approximated methods using to find the approximate solutions of this system and hence obtain an approximation for the fuzzy solution of the fuzzy Volterra-Fredholm integral equation. We give the convergence of the proposed method and error estimation between the exact and the approximate solution. Also, some numerical example is included to demonstrate the validity and applicability of the proposed technique.

References

1. Chang S., Zadeh L.: On fuzzy mapping and control, IEEE Transactions on Systems, Man, and Cybernetics, **1**, 30–34, (1972).

2. Hetmaniok E. , Nowak I. ,Slota D., Witula R.: Convergence and error estimation of homotopy analysis method for some type of nonlinear and linear integral equations, Journal Numer. Math., **23**, 331–344, (2015).
3. Dubois D. and Prade H.: Towards fuzzy differential calculus part 3: Differentiation, Fuzzy Sets and Systems, **8**, 1-17, 106-111, 225-233, (1982).
4. Liao S. J.: The proposed homotopy analysis technique for the solution of nonlinear problems, Ph.D. Thesis, Shanghai Jiao Tong University, (1992).
5. Liao S.J.: Beyond perturbation: introduction to the homotopy analysis method. Boca Raton: Chapman and Hall, CRC Press, (2003).
6. Liao S.J.: On the homotopy analysis method for nonlinear problem, Applied Mathematics and Computation, **147**, 499–513, (2004).
7. Liao S.J.: Series solution of nonlinear eigenvalue problems by means of the homotopy analysis method, Nonlinear Analysis: Real World Applications, **10**, 2455–2470, (2009).

Spectral Fractional Laplacian with Inhomogeneous Dirichlet Data: Questions, Problems, Solutions

S. Harizanov, R. Lazarov, S. Margenov, N. Popivanov

In this talk we shall discuss the topic of correct setting for the equation $(-\Delta)^s u = f$, with $0 < s < 1$. The definition of the fractional Laplacian on the whole space R^d, $d = 1, 2, 3$ is understood through the Fourier transform, see, e.g. [1]. The real challenge however represents the case when this equation is posed in a bounded domain Ω and proper boundary conditions are needed for the correctness of the corresponding problem.

In the last decade this equation has been used as a mathematical model in various applications, which resulted in intensification of both, theoretical and numerical studies of boundary value problems for the fractional Laplacian, (see for example [1, 2, 3, 4, 5, 6]). However, the case of non-homogeneous boundary data has been avoided up to the last years. The reason is that imposing nonzero boundary conditions in a nonlocal setting is highly nontrivial. Discussion of this fact is one of our goals in this talk.

There are at least three different definition of the fractional Laplacian that are in the framework of fractional Sobolev spaces (for example, see [7]). Under each definition even the classical problem with homogeneous Dirichlet data has different kind of solutions even for smooth right hand side (for example, $f(x) = 1$). As a result, the situation with the boundary conditions is very sensitive and its study must be handled with extreme care. We would like to mention that even the very interesting and fundamental paper of 85 pages, [1] written by experts in this area, has a number of misprints and mistakes.

The focus of our study is a new characterization of the spectral fractional Laplacian. This is tailored to the aim of incorporating non-homogeneous Dirichlet boundary data in a bounded, quasi-convex domain with Lipschitz boundary. The classical problems of homogeneous Dirichlet boundary data arise as a special case. We treat the fractional Laplacian with nonzero Dirichlet (or Neumann) boundary data though a construction of a fractional harmonic extensions of the boundary data. The other fractional elliptic problems (with homogeneous boundary data) can be realized using the existing techniques.

Finally, we shall apply such a technique even to the case of non-convex domains, where additional difficulties arise even for the problem involving the classical Laplacian (see [8]).

References

[1] A. Lischke, G. Pang, M. Gulian, F. Song, C. Glusa, X. Zheng, Z. Mao, Wei Cai, M. M. Meerschaert, M. Ainsworth, G. E. Karniadakis, What Is the Fractional Laplacian?, arXiv:1801.09767v2 [math.NA], 12 Nov 2018.

[2] N. Cusimano, F. del Teso, L. Gerardo-Giorda, G. Pagnini, Discretizations of the Spectral Fractional Laplacian on General Domains with Dirichlet, Neumann, and Robin Boundary Conditions, SIAM Journal on Numerical Analysis, 56 (3), (2018), 1243-1272

[3] H. Antil, J. Pfefferer, S. Rogovs, Fractional Operators with Inhomogeneous Boundary Conditions: Analysis, Control, and Discretization, arXiv: 1703.05256v2 [math.NA] 11 Sep 2017

[4] C. Bucur, Some Observations on the Green Function for the Ball in the Fractional Laplace Framework, Communications on Pure and Applied Analysis, 15 (2), (2016), 657-699

[5] C. Bucur, E. Valdinoci, Nonlocal diffusion and applications, Springer 20, xii-155, 2016/4/8

[6] G. Acosta, J. P. Borthagaray, N. Heuer, Finite Element Approximations of the Nonhomogeneous Fractional Dirichlet Problem, arXiv:1709.06592v1 [math.NA] 19 Sep 2017

[7] E. Di Nezza, G. Palatucci, E. Valdinoci, Hitchhiker's guide to the fractional Sobolev spaces, Bull. Sci. Math., 136 (2012), 521-573

[8] T. Apel, S. Nicaise, J. Pfefferer, Adapted numerical methods for the numerical solution of the Poisson equation with L^2 boundary data in non-convex domains, SIAM J. Numer. Anal., 55 (4), (2017), 1937-1957

High-Resolution Digital Image Processing

Stanislav Harizanov, Yavor Vutov

Image processing is a modern and extremely active scientific field, that combines mathematical and computer science research techniques. The quality and the practical value of the image are in direct correlation with the image resolution, thus the scientific progress here is everlasting and always significant. Every year new data acquisition devices with higher and higher resolution appear on the market. Increasing the resolution gives rise to the generation of large-scale images, the processing of which requires serious computer resources with respect to both memory and time.

The main goal of this study is the development of fast and efficient algorithms for denoising, reconstruction, feature extraction, and segmentation of high-resolution images. The considered mathematical models are based on constrained convex optimization. The proposed and analysed algorithms are within the class of Primal-Dual algorithms, which is the modern approach towards solving such problems. Those algorithms are iterative in nature and theoretically convergent, provided their free parameters are chosen within an a priori fixed range. Their execution time depends on the execution time of a single iteration, as well as on the total number of executed iterations. To decrease the former, we develop algorithms for which the correlation between the different pixel data is as small as possible. Such algorithms allow for parallel computer implementation and significant acceleration of the execution time when they are run on multiprocessing operating systems. To decrease the latter, we offer detailed theoretical and experimental analysis of each of the algorithmic steps and analysis of the role of the free parameters on the rate of convergence. As a result, we have developed improved, modified versions of the basic Primal-Dual algorithms, which are adapted to the specifics of the concrete mathematical model we use. The model itself is also a subject of thorough analysis and additional refinements of it are considered, in order for optimal alignment to be achieved between model and algorithm.

Acknowledgement: This research is partially supported by the Bulgarian National Science Fund under grant No. BNSF-DM02/2.

Lipschitz stability of neural networks with non-instantaneous impulses

Snezhana Hristova, Radoslava Terzieva

In this paper we consider the Hopfield's graded response neural network in the case when the neurons are subject to a certain impulsive state displacement at fixed moments and the duration of this displacement is not negligible small (they are known as non-instantaneous impulses). We examine the stability of the equilibrium of the model. One type of stability, very useful in real world problems, is so called Lipschitz stability. Dannan and Elaydi [2] introduced the notion of Lipschitz stability for ordinary differential equations. As it is mentioned in [2] this type of stability is important only for nonlinear problems, since it coincides with uniform stability in linear systems. In this paper sufficient conditions for Lipschitz stability of equilibrium of neural networks with We study the general case when

- the self-regulating parameters of all units are variable in time (usually, in the literature only constants are studied, see for example [3]);
- the functions of the connection between two neurons in the network are variable in time bounded functions;
- the activation function are non-Lipschitz (usually in the literature only the case of Lipschitz activation functions is studied).

The investigation is based on applying the Lyapunov approach and various types of Lyapunov functions are used. These piecewise continuous Lyapunov functions are used as an apparatus to study stability properties of the considered neural networks with non-instantaneous impulses for different types of activation functions. Many examples with different types of activation functions such as $\cos$ function, Logit function, continuous Tan-Sigmoid function, are provided to illustrate the practical application of the sufficient conditions obtained.
Note that in the literature the instantaneous impulsive neural networks are studied in [4] - [10].

Acknowledgements

Research was partially supported by Fund FP17-FMI-008, University of Plovdiv "Paisii Hilendarski".

References

[1] R. Agarwal, S. Hristova, D. O'Regan, *Non-Instantaneous Impulses in Differential Equations*, Springer, 2017.

[2] F. M. Dannan and S. Elaydi, Lipschitz stability of nonlinear systems of differential equations,*J. Math. Anal. Appl.*, **113**(1986), 562–577.

[3] K. Gopalsamy, Stability of artificial neural networks with impulses, *Appl. Math. Comput.*, **154**, (2004) 783-813.

[4] K. Guan, Global power stability of neural networks with impulses and proportional delays, *Bull. Malays. Math. Sci. Soc.* , (2018) , 1-28.

[5] Y. Liu, R, Yang, J. Lu, B. Wu, X. Cai, Stability analysis of high-order Hopfield - type neural networks based on a new impulsive differential inequality, *Int. J. Appl. Math. Comput. Sci.*, **23**, 1, (2013), 201-211.

[6] R. Rakkiyappan, P. Balasubramaiam, J. Cao, Global exponential stability of neutral-type impulsive neural networks, *Nonlinear Anal. Real World Appl.*, **11**, (2010), 122-130.

[7] X. Song, P. Zhao, Z. Xing, J. Peng, Global asymptotic stability of CNNs with impulses and multi-proportional delays, *Math. Methods Appl. Sci.*,**39**, (2016), 722-733.

[8] Z. Yang, D. Xu, Stability analysis of delay neural networks with impulsive effects, *IEEE Transactions on Circuits and Systems II: Express Briefs* , **52**, 8, (2015), 517-521.

[9] Z. Wu, C. Li, Exponential stability analysis of delayed neural networks with impulsive time window, *Advanced Computational Intelligence (ICACI)*, 2017 Ninth International Conference on on Advanced Computational Intelligence (ICACI), 2017, 37-42.

[10] Q. Zhou, Global exponential stability of BAM neural networks with distributed delays and impulses, *Nonlinear Anal. Real World Appl.*, **10**, (2009), 144-153.

Tracing point-mutation implications in human interferon-gamma variants

Nevena Ilieva, Elena Lilkova, Peicho Petkov, Leandar Litov

Even isolated single-point mutations in key structural/functional domains of biomolecules may lead to conformational changes whose consequences for the functional integrity of the affected molecule might be distinct or less pronounced and might affect functional aspects like binding affinity or biological activity. When spontaneous, such mutations are in most cases unfavorable for the affected biosystem. However, in biomedical engineering and drug design they often provide the targeted solution, when inactive mutated forms with preserved conformational identity or still active variants with slightly deformed geometry are sought. Purely experimental approaches for achieving such goals, though possible, are extremely time- and resources consuming. Mathematical modelling and computer simulations step forward as a key element of the research program.

In computational studies of such objects, it is of primary importance to identify measurable macroscopic parameters, which substantiate these transformations and allow for their prediction in absence of experimental data. In an earlier paper, we discussed the application of the spatio-temporal multistage consensus clustering method (SMCC) for studying single-point mutations in the molecule of the native human interferon-gamma (hIFNγ). We could develop a reliable protocol (clusterization procedure & parameter set & structure domain identification), providing excellent agreement with the experimental data.

Table 1: Amino acid substitutions in the double-mutated hIFNγ variants

position	...	27	...	44	...	88	...
hIFNγ	...	Thr	...	Asp	...	Lys	...
K88Q_D41N	...	Thr	...	Asn	...	Gln	...
K88Q_T27Y	...	Tyr	...	Asp	...	Gln	...

Further laboratory work revealed the necessity for stabilization of the mutated-forms behavior, intended to be achieved by additional point mutations at appropriate locations in the cytokine molecule, introduced in the regions, which are responsible for the binding to its extracellular receptor and for its biological activity, Table 1.

As a starting structure for the native cytokine in the conducted *in silico* studies we used the earlier developed by us model of the folded full-length hIFNγ dimer. The two mutated forms (Fig. 1) were modelled with the help of the Mutator Plug-in of the molecular visualization and manipulation program VMD. All three proteins were subjected to 200 ns long molecular-dynamics simulations along the protocol from the justification studies of the SMCC method. We observe essential differences in the cluster positions, sizes and content before and after the exclusion of the highly-volatile C-termini of the cytokine from the procedure (Fig. 2). According to our results, the K88Q_T27Y variant exhibits a much higher resemblance to the wild-type cytokine and a more pronounced summetry between the two monomers. In the same time, in the K88Q_D41N variant part of the chain A residues from the receptor-binding

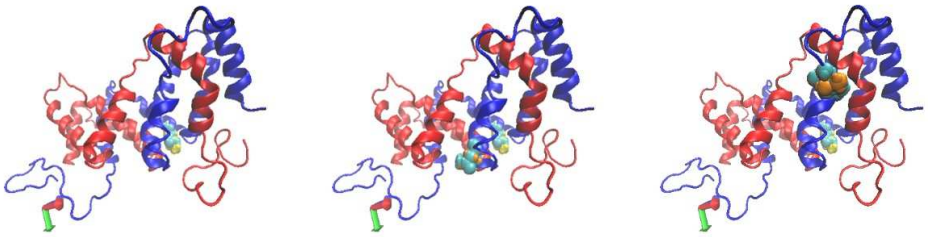

Figure 1: hIFNγ with the mutated residue at position 88 (the single-point variant K88Q)(left); K88Q_D41N variant, with a second mutation at position 41 (middle); K88Q_T27Y variant, with a second mutation at position 27 (right), all mutation cites indicated on top of the secondary structure representation by Van der Waals spheres in cyan. The underlying native structure at these positions (88, 41 and 27, resp.) is shown with Van der Waals spheres in yellow (position 88), resp. ochre (positions 27 and 41)

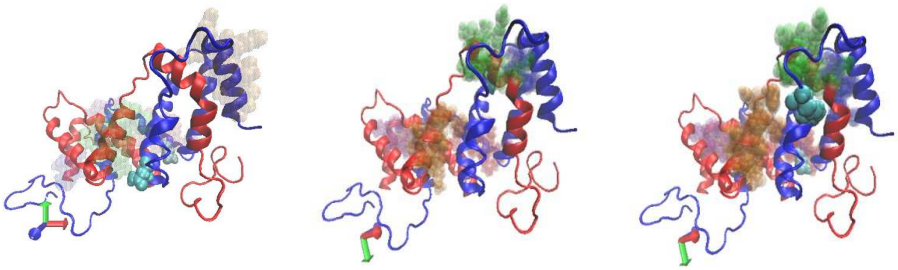

Figure 2: Clusters in K88Q_D41N variant (left), native hIFNγ (middle) and K88Q_T27Y variant (right), based on the globular-part trajectories. The cluster ranking by size is color-coded in descending order as red–orange–green–lila.

site enter the largest semi-rigid domain of the molecule. This might be an indication for a stronger binding affinity conjugated with a lower biological activity. We further explore these behaviour patterns by comparing the contact map for each of the double-mutated variants with the one of the wild type protein.
We discuss the clustering results to provide a basis for a quantitative assessment of the suitability of the two double-mutated forms of hIFNγ for the purposes of an innovative replacement therapy of deceases associated with its pathological over-expression.

Acknowledgements This research was supported in part by the Bulgarian Science Fund under grants DNTS-Austria-01/2/2013 and DN-11/20/2017. The simulations were performed on the supercomputer Avitohol@BAS (http://www.hpc.acad.bg/system-1/) and on the HPC Cluster at the Faculty of Physics of Sofia University "St. Kl. Ohridski". We acknowledge the experimental insight and the discussions with G. Nacheva and E. Krachmarova, also part of the project team under grant DN-11/20/2017.

Programming Techniques for Energy-efficient Software

Vesselin Iossifov

Software is becoming a central issue in decreasing the power consumption in lowpower programmable computer systems. In such systems the amount of energy consumption caused by software has several impact of the systems costs. Minimizing power consumption is one of the primary challenges that applications developers faces due to lack of the running cost (x86 based server or HPC) or the instrumentation functionality (Embedded Applications) of the system. This lecture will cover different prospect of energy usage and energy aware software design in computer systems ranging from Embedded Systems to x86 based server or HPC. This lecture will present some examples of the role of programming techniques to rise the system energy efficiency, quantify the impact and fix the issues in applications to minimize the power consumption.
Keywords: Energy aware computing, software design for power optimization, Embedded Applications, IoT, x86 based server and HPC.

I. INTRODUCTION

Power consumption is a key element for different form factors of computer systems. The lecture will focus on the important role of application software for x86 servers an HPC and Embedded Systems. Such systems are placed on both ends of computer's performance range. Applications can extend or remove advantages of low power designed hardware. As the hardware becomes more sensitive for several energy states in the last 20 years, algorithms and resulting codes must be well behaved to use the opportunity of many energy states [1] to [3] to exploit hardware components to have minimal power impact during active processor workload state. This lecture describes several case studies that show how application algorithms can be codded with low-power techniques to implement the opportunities of low power designed hardware. Several methodologies for both x86 and Embedded processors to optimize the applications for power are described. Possible power savings by implementing the optimization on Parallel Assembly Level (x86) and the use of Interrupt techniques (Embedded) for typical applications will be presented.

II. OVERIVEW OF POWER METRICS

Power Metrics gives the behavior of the system and how we quantify an application if it is sub optimal or optimal written for the power profile. Power metrics which are presented in this lecture are number of processor clocks and programmed processor power states and interrupts to become one optimal mixture of it to minimize the system power consumed for given application. Power management is categorized into following important goals [1] to [3]:

A. Minimize number of CPU Clocks Consumed power by a running code in a digital system is described by the formula:

$$P = \Delta T \times F \times U \times I$$

where F is the frequency clocking the digital components, ΔT the code run time and U and I are voltage value and current rating. Minimizing the average F is discussed at point **B**. Minimizing ΔT means to cut the number of clocks at the average F using programming techniques on the HLL or use Parallel Assembly instructions for integer or float data types (**x86**).

B. Use Processor power management technologies [2], [3]

*** Processor idle sleep states (x86)** CPU supports several levels of core and package idle states. Idle states are also known at C-states. Deeper the C-states and more time spent in deep C-states by an application, more power is saved. C-state transitions have direct impact on power consumption and response time.

*** Power performance states (x86)** P-States is an operational state, also can be called as part of C0-State. P-States provide a way to scale the frequency and voltage at which the processor runs to reduce power consumption. Processor in active P-states consumes maximum power called in Thermal Design Power (TDP) specs.

Embedded CPUs (**MSP430FR5969**, Texas Instruments, [3]) use as x86 as well also four power states – **Low Power Management States** (LPM) 1 to 4.

C. Application specific use of Interrupts to minimize power consumed [3]

Using Interrupts in Embedded Systems waiting on process responds gives the possibility to bring CPU and other components in to the idle mode (LPM 1 to 4) and to rise down the clock frequency for them. This and other programming techniques in HLL, assembly language and Fixed Point Math Libraries instead of float data types and functions will be presented and measured for **MSP430** code.

III. SUMMARY AND CONCLUSION

Software power optimization makes a huge impact on overall CPU platforms. Power awareness is a critical step in minimizing power costs for x86 servers and HPC or to make Embedded applications (IoT, Wireless Sensor networks) in a energy harvesting environment possible. There are many steps that developers can follow to reduce their application power consumption. This lecture gives overview on how to analyze, use handful of tools and optimize applications to create energy aware applications (x86 and Embedded).

IV. REFERENCES

[1] Hewlett-Packard Co.,Intel Co., Microsoft Co., Phoenix Technologies Ltd., and Toshiba Co. Advanced Configuration and Power Interface Specification, November 13, 2013.
http://www.acpi.info/spec.htm

[2] Microsoft Co., CPU Power Management, Hewlett-Packard Co., Intel Co., Microsoft Co., Phoenix Technologies Ltd., Toshiba Co., 31.05.2018,
https://docs.microsoft.com/de-de/previous-versions/windows/desktop/xperf/cpu-power-management

[3] Texas Instruments, MSP430™Advanced Power Optimizations: ULPAdvisor™Software and EnergyTrace™Technology, June 2014,
http://www.ti.com/lit/an/slaa603/slaa603.pdf

Modelling Human Biometeorological Conditions Using Meteorological Data from Reanalysis and Objective Analysis — Preliminary Results

Vladimir Ivanov and Hristo Chervenkov

The influence of the environment on the human beings in the aspect of different weather conditions is one of the main problems in the modern science. The degree of sultriness and coldness are decisive for the regular and stable work of the human thermoregulatory system. That affects the ability of the human beings to doing their work and everyday activities, and more important to the possible advent of different heat and cold related diseases. The weather influence is manifested in different ways, but the most notable one is the sensation to the thermal properties of the environment. That means how cold or how hot the human individual feels it is. For the consistent assessment of the thermal influence of the environment on the human body the integrated effects of all thermal parameters have to be taken into account. This leads us to the necessity of modelling the human heat balance. In this sense, empirical thermal indices, like the discomfort index, apparent temperature, wind-chill index or similar ones considering only some of the relevant meteorological parameters and not accounting for thermal physiology, have to be regarded as not being "state of the art" — yet they are used very often. They might be helpful in very specific situations as they can be calculated easily but they have many limitations.

In the last decades, heat-balance models of the human body with different degree of complexity have gained more and more acceptance in the assessment of thermal comfort. The basis for all of these models is the heat-balance equation for the human body. Various input indicators, concerning, in particular, the personal physiology and clothing are needed for the correct execution of such simulation, but the meteorological parameters have primary importance. The output of such models consists of so-called biometeorological indices (BI), which are synthetic indicators, quantifying the human thermal comfort.

The research works in that field reveal that the extreme weather conditions have significant adverse effect on the human illness and mortality. The heat conditions in Southern Europe are more heat stressful than the other parts of the continent. The predictions of many global climate models show that the summer heat stress will worsen in the future. The long-term observations from different European cities show similar results. Therefore, it is important to study not only heat, but also the cold stress conditions in Bulgaria.

Our research is focused on the calculation of three BIs — "Predicted Mean Vote" (PMV) "Physiological Equivalent Temperature" (PET) and "Universal Thermal Climate Index" (UTCI). The RayMan model, which simulates the short- and long-wave radiation flux densities from the three-dimensional surroundings in simple and complex environments, is adapted and tested. The Rayman model is used also for calculation of the three considered BIs. The meteorological input parameters, except the albedo and surface temperature, are taken on hourly basis from the Bulgarian operative system ProData. ProData assimilates in situ measurements and satellite retrievals and produces estimates of 10 near-surface meteorological parameters. The system is proved as reliable source of consistent meteorological

information with high spatial and temporal (1 hour) resolution with minimal latency from the input data acquisition time. The albedo and the surface temperature are taken from the newest reanalysis of the European Centre for Medium-Range Weather Forecasts ERA5. All computations are performed on hourly basis in grid with spacing of approximately 4×4 km, which covers entirely Bulgaria. The preliminary simulations are performed for January, April, July and October 2017, which are considered as representative for the four seasons correspondingly.

Our calculations for the winter month suggest more stressful situations in West Bulgaria. On average, the minimum and maximum daily values of PET are in the extreme cold stress interval. The average minimum values of the PMV suggest cold and very cold conditions. On the other side, its average maximum show cool conditions in almost all parts of the domain. Concerning the UTCI index, its average minimum is in the range from moderate to very strong cold stress, and its average maximum values reach to slightly cold stress especially in the lowlands of the southern part of the domain.

The conditions in July 2017 go down to cold and very cold PMV, to very cold, cold and cool PET. The average of the daily minimum of UTCI suggest conditions from slight cold stress to no thermal stress. The average daily maximum values suggest from slightly cool to hot PMV, from no thermal stress to strong heat stress PET, and for UTCI from no thermal stress to very strong heat stress. The differences in stress are reflected particularly between the lowlands and the mountain areas.

The April and October 2017 show a kind of mixed conditions between the winter and summer month. The coldest daily values of PMV in April 2017 suggest conditions from cold to slightly cool. On the other side, the warmest daily values are from neutral to warm perception. The PET in April suggest that the coldest conditions are from cold to slightly warm feeling, and from comfortable to hot situations for the average of the maximum daily values. The average of the minimum UTCI show slightly cold stress and no thermal stress throughout of the domain. The warmest UTCI are from no thermal stress to moderate heat stress. The main difference between the October and the April is the bigger areas with comfort and heat stress.

As conclusion can be outlined, that the spatial distributions of the heat and the cold stress conditions in Bulgaria vary in extent enough to bring our interest to studying them more carefully.

Key words: thermal comfort, heat balance, Rayman model, biometeorological indices, ERA5, ProData

Theoretical Properties Of Exploration and Exploitation of the Neighborhood-based Widening Approaches

Violeta N. Ivanova-Rohling

In contrast to most current directions in the field of Machine Learning, where parallel compute resources are used to improve the efficiency of algorithms, our research focuses on investing parallel resources to obtain a solution of higher quality. We present parallel strategies for a better exploration of the search space. We achieve this by *widening* the search, where instead of pursuing only one solution at each step, we consider several solution candidates. We investigate approaches that do not require communication between the parallel workers [1, 2]. A greedy data mining heuristic can be represented as a search through the space of models. The greedy search can be formalized as an iterative application of two operators: *refinement* r and *selection* s. The refinement operator generates a set of more specific models (*refinements*): $r(m) = M^r$. The *selection* operator s uses a model evaluation function ψ to choose the locally best model from the set of all possible refinements M^r. In Widening, at each step the selection operator s considers the refinements of a set M with cardinality k of original models and returns a new set M' of k refined models for further investigation. The cardinality k of the considered sets of models, we will call the *width* of the widened search. One way to achieve communication-less Widening is to use a local approach: given a set of refinements $M^r = r(m)$, we can directly force each individualized selection operator to pick a different refinement.

Definition 1. *Given a model m, a selection operator s, a refinement operator r, and a distance measure d, the k-**neighborhood** of $m' = s(r(m))$ is the ordered set $N_k(m') = (m', m'_1, \ldots, m'_{k-1}) \subseteq r(m)$ where $\forall i \in \{1, k-2\} : d(m'_i, m') < d(m'_{i+1}, m')$ and $\nexists m'' \in r(m) \setminus N_k(m') : d(m', m'') < d(m', m'_{k-1})$.*

In other words, a k-neighborhood of m', which is a refinement of model m, consists of the top k refinements of model m (including m'), which are closest to m' according to some distance d. Using the definition of k-neighborhood above, we can define the set of individualized selection operators for the parallel workers $w_1, \ldots, w_k$, $\{s_1^{\mathrm{N}}, \ldots, s_k^{\mathrm{N}}\}$, and these individualized selection operators perform *Widening via k-neighborhoods*. We will denote this Widening as N_k. Based on the distance function d, different types of neighborhoods can be defined. For example, a **optimality k-neighborhood** is a k-neighborhood, in which d is the original model evaluation function ψ. In a optimality k-neighborhood the neighbor models are of similar quality. We will refer to Widening via optimality neighborhoods as N_k^o. Choosing models similar to the greedy choice, based on some properties is useful for similarity searches, or for *exploitation* of promising regions. We will denote such Widening as N_k^s. Additionally, in order to perform *exploration* of the search space, diversity can be incorporated within optimality k-neighborhoods. We will denote Widening via diverse neighborhoods as N_k^d.

Definition 2. *We define* randomized k-neighborhood *as a k-neighborhood, for which each of the k models is assigned to a parallel worker w_i with a probability p_i from a probability distribution $P(x)$.*

Let $\mathcal{M}$ be a family of models, X be the set of model fragments in $\mathcal{M}$, r be a refinement operator over $\mathcal{M}$. We can use $\mathcal{M}$ and the refinement operation $r(\cdot)$ to define a graph $G_{\mathcal{M}}(V, E)$, where V is the set of vertices, and E is the set of edges, defined as follows: $v \in V \Leftrightarrow v \in \mathcal{M}$ and $\forall m, m' \in \mathcal{M}, m' \in r(m) \exists e(m, m') \in E$. $G_{\mathcal{M}}(V, E)$ is a DAG and we will use it in investigating the properties of different neighborhood-based Widening approaches. Widening via randomized k-neighborhoods can be presented as a random walk on a graph.

1 Properties of Widening via Similarity and Diversity Neighborhoods

Widening via similarity neighborhoods is a parallel search that is focused on a particular area of the space of models $\mathcal{M}$. Based on the number of parallel workers, how far away will the solutions be from the optimal solution within the area of exploration? Using the assumption that similar models have similar performance and similar optimal refinements, we evaluate the size of the explored area as well as the distribution of the search paths of the independent parallel workers in this area. Given that each model neighborhood of size δ has distribution $f(x)$ of models, then at level l the probability distribution of models will be characterized by the convolution, $P^l(x) = (P^{l-1} \circledast f)(x)$. We calculate the number of workers needed to be ϵ from the best model within the investigated area for $f(x)$ uniform or Gaussian.
We investigate the effect of using diverse neighborhoods without communication on the refinement graph structure, and whether diversity affects the structure of the graph in a positive way. Namely, we investigate the effect of diversity applied locally in building diverse neighborhoods on the global properties of the graph: distribution of the number of paths to each node and the maximal distance between the models-nodes at refinement level l. Generally speaking, we claim that using diversity will lead to fewer intersections between neighborhoods and the distribution of paths in $G_{FullN_k^d}$ will be closer to a uniform distribution compared to simply using optimality neighborhoods without diversity in graph G_{FT-k}. The theoretical results are confirmed by practical experiments using Widening of the greedy algorithm for the set covering problem.

References

[1] Akbar, Z., Ivanova, V.N., Berthold, M.R.: Parallel data mining revisited. Better, not faster. In: IDA. (2012)

[2] Ivanova, V., Berthold, M.R.: Diversity-driven widening. In: Proceedings of the 12th International Symposium on Intelligent Data Analysis(IDA 2013). (2013)

Exploring Applicability of InterCriteria Analysis on the Performance of MOE and GOLD Scoring Functions

Dessislava Jereva, Tania Pencheva, Ivanka Tsakovska, Petko Alov, Ilza Pajeva

Drug design is a time-consuming and costly process that motivates the intensive development and use of approaches that help in its optimization such as computer-aided (*in silico*) ones. Molecular docking is the most commonly used technique in the structure-based approaches to *in silico* drug design. A key element in the algorithms for docking of bioactive molecules is the scoring function, which purpose is to calculate quickly and accurately the energy of the interaction in protein-ligand complexes and to allow for selection of appropriate ligand poses in the binding pocket.

Despite the large number of comparative studies of various scoring functions, the question of which docking programs and protocols are performing better is still unresolved and the results are often contradictory. InterCriteria analysis (ICrA), developed as a multi-criterion decision-making approach, has the prerequisites to assist in selecting the most appropriate scoring functions for outlining drug candidates. ICrA has been elaborated to discern possible similarities in the behaviour of pairs of criteria when multiple objects are considered [1]. ICrA is based on two mathematical formalisms, namely intuitionistic fuzzy sets and index matrices, thus relying on methodology different from the classical correlation analysis.

This study is focused on two of the widely used software packages for docking, Molecular Operating Environment (MOE) [2] and Genetic Optimization for Ligand Docking (GOLD) [3]. Eighty eight benzamidine-type protease inhibitors [4] were subjected to docking in two target proteins, thrombin and trypsin. The performance of the mostly used scoring functions available in both software packages, London dG (in MOE) and GoldScore (in GOLD), was explored based on the binding energies and the experimental binding affinities of the compounds in the protein-ligand complexes. The obtained results were subjected to ICrA and subsequently analyzed.

No one of the studied scoring functions appeared as a good predictor of the compounds' binding affinities for the two considered targets, thrombin and trypsin. The docking scores recorded for trypsin, however, are closer to the experimental data than those recorded for thrombin. In addition, there is no significant correlation between the two considered scoring functions, London dG in MOE and GoldScore in GOLD. Further, the potential of ICrA was explored on different docking speed selections in GOLD: slow, medium or fast. While for thrombin the three running modes were mostly in a positive consonance, for trypsin the fast mode was in a dissonance with the slow and medium mode in almost all cases.

Our results suggest that London dG and GoldScore scoring functions do not produce equivalent results and can be combined in consensus docking studies. Additionally, the results obtained using the medium docking speed in GOLD appears to be closer to the more precise

slow speed setting than to the fast one for the particular dataset.

Acknowledgements: The work is supported by the National Science Fund of Bulgaria, grant No DN-17/6 “A New Approach, Based on an Intercriteria Data Analysis, to Support Decision Making in *in silico* Studies of Complex Biomolecular System".

References

[1] Atanassov K., D. Mavrov, V. Atanassova, Intercriteria Decision Making: A New Approach for Multicriteria Decision Making, Based on Index Matrices and Intuitionistic Fuzzy Sets, Issues in Intuitionistic Fuzzy Sets and Generalized Nets, 2014, 11, 1-8.

[2] Molecular Operating Environment, The Chemical Computing Group, v. 2016.08, http://www.chemcomp.com.

[3] Genetic Optimization for Ligand Docking, The Cambridge Crystallographic Data Centre, v. 5.6.3, https://www.ccdc.cam.ac.uk/solutions/csd-discovery/components/gold/.

[4] Boehm M., J. Stuerzebecher, G. Klebe, Three-Dimensional Quantitative Structure-Activity Relationship Analyses Using Comparative Molecular Field Analysis and Comparative Molecular Similarity Indices Analysis To Elucidate Selectivity Differences of Inhibitors Binding to Trypsin, Thrombin, and Factor Xa, Journal of Medicinal Chemistry, 1999, 42(3), 458-477.

Recent advances in numerical methods for fractional differential equations with non-smooth data: a concise overview

Bangti Jin, Raytcho Lazarov, Joseph Pasciak, and Zhi Zhou

Introduction. We shall survey some resent results in numerical treatment of initial and boundary value problems for time fractional differential equations involving both Riemann-Liouville and Caputo fractional derivatives. Examples of such problems include fractional time dependent diffusion equation, convection-diffusion problems, and multi-term transient diffusion equation.

Problem formulation. We shall survey the latest development in numerical methods for solving initial and boundary valued problems for fractional differential equations. Our focus will be the following time fractional diffusion and diffusion-wave equations:

$$\partial_t^\alpha u(x,t) - \Delta u(x,t) = f(x,t) \quad x \in \Omega,\ t \in (0,T). \tag{1}$$

Here $\partial_t^\alpha u$ denotes the Caputo fractional derivative with respect to t and $\Omega \subset \mathcal{R}^d$ ($d = 1, 2, 3$) is a bounded convex polygonal domain with a boundary $\partial\Omega$. We assume that problem (1) is subject to the following initial and boundary value conditions

$$\begin{aligned} &u(x,t) = 0, \quad (x,t) \in \partial\Omega \times (0,T), \\ &u(x,0) = v(x), \quad x \in \Omega, \quad (\text{and } \partial_t u(x,0) = w(x) \quad x \in \Omega, \text{ if } 1 < \alpha < 2). \end{aligned}$$

Here $f(x,t),\ v(x)$, and $w(x)$ are given functions.
We shall also briefly discuss the steady-state sub-diffusion convection-reaction problem

$$-\partial_x^\alpha u(x) + b(x)u'(x) + q(x)u(x) = f(x), \quad x \in D = (0,1), u(0) = u(1) = 0, \tag{2}$$

where the source term f belongs to $L^2(D)$ or suitable subspace, and $\partial_x^\alpha u$ denotes either the left-sided Riemann-Liouville or Caputo fractional derivative of order $\alpha \in (3/2, 2)$. We assume a convection coefficient $b \in W^{1,\infty}(0,1)$ and a potential coefficient $q \in L^\infty(0,1)$. When $\alpha = 2$, the problem recovers the canonical one-dimensional steady-state convection diffusion-reaction equation.

Main topics to be discussed. It is impossible to survey all important and relevant works in a short talk. Instead, we aim at only reviewing relevant works on the numerical methods for the sub-diffusion model (1) with non-smooth problem data. This means that the initial data v belongs only to $L^2(\Omega)$ or the source term f is not compatible with the initial data or/and boundary condition. First, this choice allows us to highlight some distinct features common to many nonlocal models, especially how the smoothness of the problem data influences the solution and the corresponding numerical methods. These are the features that pose substantial new mathematical and computational challenges when compared with standard parabolic

problems – and extra care has to be taken when developing and analyzing relevant numerical methods. In particular, since the solution operators of the fractional model have limited smoothing property, a numerical method that requires high regularity of the exact solution will impose severe restrictions (compatibility conditions) on the data and generally does not work well. Schemes that are constructed and analyzed under high regularity assumptions on the solution, substantially limit their potential applications. For example, non-smooth data analysis is fundamental to the rigorous error analysis of various applications in optimal control, inverse problems, and stochastic fractional diffusion. For relevant discussion on this important topic we refer to recent paper [1]. We shall review briefly the following four topics and give some representative results:

(i) Importance of the regularity theory in Sobolev spaces;

(ii) Spatial discretization via Galerkin finite element and finite volume element methods;

(iii) Temporal discretization via time-stepping schemes;

(iv) Space-time formulations (Galerkin or Petrov-Galerkin type).

The talk is based on our resent works in this area [2, 3, 6, 4, 5, 7].

References

[1] M. Stynes, *Too much regularity may force too much uniqueness*, Fractional Calculus and Applied Analysis, 19 (6) (2016), 1554 –1562

[2] B. Jin, R. Lazarov, and Z. Zhou, *Error estimates for a semi-discrete FEM for fractional order parabolic equations*, SIAM J. Numerical Analysis, **51 (1)** (2013), 445 – 466.

[3] B. Jin, R. Lazarov, J. Pasciak, and Z. Zhou, *Error analysis of a finite element method for a space-fractional parabolic equation*, SIAM J. Numerical Analysis, **52** (2014), 2272 – 2294.

[4] B. Jin, R. Lazarov, J. Pasciak, and Z. Zhou, *Error analysis of semidiscrete FEM for inhomogeneous time-fractional diffusion*, IMA J. Numererical Analysis, **35 (2)** (2015), 561 – 582.

[5] B. Jin, R. Lazarov, and Z. Zhou, *A Petrov-Galerkin FEM for fractional convection-diffusion equations* , SIAM J. Numerical Analysis, **54 (1)**, (2016), 481– 503.

[6] B. Jin, R. Lazarov, J. Pasciak, and W. Rundell, *Variational formulation of problems involving fractional order differential operators*, Mathematics of Computation, **86 (307)**, (2017), 2239 – 2260.

[7] B. Jin, R. Lazarov, and Z. Zhou, *Numerical methods for time-fractional evolution equations with non-smooth data: a concise overview*, preprint arXiv:1805.11309, (2018).

Comparative Study of Social Network Interactions in Unexpected Event: the Cases of Journalists Jan Kuciak and Viktoria Marinova

Kristina G. Kapanova, Velislava Stoykova

Current interdisciplinary research interests often involve how platforms such as Twitter and Facebook are utilized in the benefit of social and political movements. One of the great advantages of social media platforms is the substantial amount of user-generated materials such as photos, textual content, hyper-links, videos, they host on a variety of real-world events. In our research, we offer interpretation and analysis of communication patterns of social media activists' behavior resulting in common responsive reaction to an unexpected event. We present a comparative study of interaction activity, communication behavior and attitude of network users and their responsive reactions to two unexpected events – the murder of journalist Jan Kuciak (21 February 2018 in Slovakia) and the murder of journalist Viktoria Marinova (6 October 2018 in Bulgaria). In studying the two social activist cases in Slovakia and Bulgaria, we use methods from the field of networks analysis and machine learning to investigate the thematic and temporal structure in those multilingual and multicultural online communications. We analyze the type of activists' communication with respect to its expansion, globality, timeline and the linguistic tags used, with the aim to evaluate the level of interactivity and the way the type of communication is resulting in common reaction and organizational response. We furthermore explore several techniques for learning multi-feature similarity metrics.

The collected data from Twitter for the Jan Kuciak case consist of 4611 tweets from the time period $28-02-2018$ until $28-07-2018$. The second case (Viktoria Marinova), involves data gathered for the time period $07-10-2018$ until $15-10-2018$ and consisting of 4058 tweets.

Our aim with this study contains two fold. First, we attempt to reveal the underlying properties of social media communication content and how they reflect specific bursting events through the exploration of rich context consisting of both textual and non-textual features and encompassing several different European languages. As structural markers, the hashtags used in those two events are important to analyse the role of the linguistic patters in the flow of information and the emergence and magnitute of message virality. We argue, that hashtags as a important "attention mobilizer" for one events are carried out in the second, bringing specific semantic and linguistic overtones. Secondly, we are interested in the methodologies to apply and adapt network analysis techniques with machine learning to the analysis of such data in order to obtain information relevant to social activist events.

Multicriteria Approach for Solving Engineering Robust Design Problems

Leoneed Kirilov, Petar Georgiev

Robust design has been the focus of researchers for more than three decades. The beginning was set by a Japanese engineer and a statistician Genichi Taguchi. The Robust Parameter Design (RPD) proposed by Taguchi consists of finding the optimal setting of the controllable factors that minimizes the response variance while keeping the mean output on a predefined target value. Controllable factors are design variables that can easily be controlled or manipulated by a designer while the response variance is due to the noise factors, i.e. inputs that are beyond the control of a designer, and are typically decided by the operating environment. Despite some criticism concerning the statistical design and analysis in Taguchi's approach his philosophy for RPD is widely used.

The robust design is classified into three methods: 1) the Taguchi method, 2) robust optimization, and 3) robust design with the axiomatic approach. The main drawbacks of Taguchi method are relatively higher number of experiments, using only a single characteristic function and the inability to include constraints to the engineering problem. The robust optimization is based on the Response Surface Methodology (RSM). This is a collection of statistical and mathematical techniques used for developing an approximate relationship between a response of interest and a number of input variables.

The task for optimizing conflicting parameters arises very often when solving design problems. Therefore including new approaches resolving these cases is a live question.

In this paper we present an approach for Engineering Robust Design Problems based on multi objective optimization in the solution phase. One of the advantages of multicriteria approach is that it allows simultaneously research of several conflicting parameters/objectives. The model constraints define the feasible set. The efficiency of the proposed approach is demonstrated by solving the real task of designing the main dimensions of a bulk carrier. The goal is to find the set of main particulars of the ship that minimize together the Required Freight Rate (RFR) and standard deviation due to uncontrollable parameters. The design variables are the main dimensions of the ship – length, breadth, depth and draught and block coefficient. The uncontrollable parameters are the price of a ton hull structures and fuel. The objective functions are obtained by computer experiments based on Response Surface Methodology.

Iterative Implicit Schemes for Compaction-Driven Darcy Flow Viscoelastic Rock Magma

Miglena N. Koleva, Lubin G. Vulkov

The model equations of compaction-driven Darcy flow in viscoelastic rock are derived in [1]. The corresponding 1D motion of magma is described by the integro-differential system [2]

$$\frac{\partial}{\partial t}\left(a(\phi)\rho\right) - \frac{\partial}{\partial x}\left(K(\phi)b(\rho)\frac{\partial \rho}{\partial x}\right) = 0, \quad x \in (0,1), \quad 0 < t < T, \tag{1}$$

$$\frac{\partial G(\phi)}{\partial t} = p(\rho) - p^0(t), \quad p^0(t) = \int_0^1 A_1(\phi)p(\rho)dx \left[\int_0^1 A_1(\phi)dx\right]^{-1}, \quad A_1(\phi) = \frac{a_1(\phi)}{1-\phi}, \tag{2}$$

where ρ is the density and ϕ is the porosity. Here, $a_1(\phi) = 1/\xi(\phi)$, the function $G(\phi)$ is defined by $G'(\phi) = (1-\phi)^{-1}a_1^{-1}(\phi)$ and

$$a(\phi) = \phi(1-\phi)^{-1}, \quad K(\phi) = k(\phi)(1-\phi), \quad b(\rho) = \rho p'(\rho). \tag{3}$$

We solve the system (1) - (3) subjected with initial and boundary conditions

$$\rho(x,0) = \rho_0(x), \quad \phi(x,0) = \phi_0(x); \quad \frac{\partial \rho}{\partial x}(0,t) = \frac{\partial \rho}{\partial x}(1,t) = 0.$$

Moreover, from physical motivation $0 < \phi < 1$ and $\rho > 0$. Define the time step $\tau_j = t_j - t_{j-1}$, $j = 1, 2, \ldots, J$, $t_0 = 0$, $t_J = T$ and denote the values of the functions on the $(j+1)$-th level by $\widehat{\rho}, \widehat{\phi}$. The backward Euler time discretization is applied to (1), (2):

$$\frac{a(\widehat{\phi})\widehat{\rho} - a(\phi)\rho}{\tau_j} = \frac{\partial}{\partial x}\left(K(\widehat{\phi})b(\widehat{\rho})\frac{\partial \widehat{\rho}}{\partial x}\right), \quad \frac{G(\widehat{\phi}) - G(\phi)}{\tau_j} = p(\widehat{\rho}) - p^0(\widehat{\rho}, \widehat{\phi}),$$

$$p^0(\widehat{\rho}, \widehat{\phi}) = \int_0^1 A_1(\widehat{\phi})p(\widehat{\rho})dx \left[\int_0^1 A_1(\widehat{\phi})dx\right]^{-1}.$$

We develop two iteration schemes by using *Jacobi linearization*.

Scheme 1. Given the m-th iterative solution $(\hat{\rho}^m, \hat{\rho}^m)$, find $(\widehat{\phi}^{m+1}, \widehat{\phi}^{m+1})$,

$$\frac{a(\widehat{\phi}^m)\widehat{\rho}^{m+1} - a(\phi)\rho}{\tau_j} = \frac{\partial}{\partial x}\left(K(\hat{\phi}^m)b(\hat{\rho}^m)\frac{\partial}{\partial x}\hat{\rho}^{m+1}\right),$$

$$\frac{G(\phi^{m+1}) - G(\phi)}{\tau_j} = p(\widehat{\rho}^m) - p^0(\widehat{\rho}^{m+1}, \widehat{\phi}^m).$$

The realization of a spatial discretization requires solving threediagonal linear systems of algebraic equations and a single non-linear algebraic equation.

Scheme 2. Now let's change the left part of the iteration Scheme 1 to

$$\frac{a(\widehat{\phi}^{m+1})\widehat{\rho}^{m+1} - a(\phi)\rho}{\tau_j} = \frac{\partial}{\partial x}\left(K(\widehat{\phi}^{m+1})b(\widehat{\rho}^{m+1})\frac{\partial}{\partial x}\widehat{\rho}^{m+1}\right).$$

In order to realize the above iteration process, we need an *inner iteration* to approximate the term $b(\widehat{\rho}^{m+1})\frac{\partial}{\partial x}\widehat{\rho}^{m+1}$as follows

$$\frac{a(\widehat{\phi}^{m+1})\widehat{\rho}^{m+1} - a(\phi)\rho}{\tau_j} = \frac{\partial}{\partial x}\left(K(\widehat{\phi}^{m+1})b(\widehat{\rho}^{n})\frac{\partial}{\partial x}\widehat{\rho}^{n+1}\right).$$

Then, by treating the updated ρ^{n+1} as ρ^{m+1} and plugging it back into $b(\widehat{\rho}^{n+1})$ we organize an inner iteration process . In a similar way is treated the right-hand side. Next, we use cell-centered finite difference scheme (CCFDS) to the ODEs systems to obtain iterative full discretizations.

We use *Kirchhoff transformation* for linearization of the equation (1) and then we discretize in time:

$$\frac{a(\widehat{\phi})R(\widehat{\psi}) - a(\phi)R(\psi)}{\tau_j} = \frac{\partial}{\partial x}\left(K(\widehat{\phi})\frac{\partial \psi}{\partial x}\right), \quad \psi(\rho) = \int_{\rho_0}^{\rho} b(s)ds \leftrightarrow \rho = R(\psi),$$

where in the computation we take $\rho_0 = \min \rho(x), \quad x \in (0,1)$. Next, after spatial CCFD discretization one solves system of algebraic equations with diagonal nonlinearity with respect to ψ.
Some numerical results for 1D isothermal motion of magma in porous rock media are analyzed. We choose fluid parameters, matrix parameters and take typical rock parameters [1]

$$k(\phi) = \frac{\bar{k}}{\mu}\phi^n, \quad \xi(\phi) = \nu\phi^{-m}, \quad m \in [0,2], \quad n = 3, \quad p'(\rho) = \frac{1}{\beta_f \rho^0},$$

where ν is the bulk viscosity coefficient, $\overline{k}$ is the permeability porosity (m^2), μ is the fluid viscosity (Pa.s), β_f is the fluid compressibility (Pa^{-1}), ρ_s (used for deriving the dimensionless variables of (1), (2), see [2]) is the density of the solid phase (g/cm^3).
Computational results, obtained by Schemes 1,2 and Kirchhoff transformation linearization scheme are compared and discussed.

Acknowledgments. The research is supported by the Bulgarian National Science Fund under Bilateral Project DNTS/Russia 02/12 "Development and investigation of finite-difference schemes of higher order of accuracy for solving applied problems of fluid and gas mechanics, and ecology" from 2018.

References

[1] J.A.D. Connolly, Y.Y. Podladchikov, Compaction-driven fluid flow in viscoelastic rock, Geodin. Acta 11, 55–84(1998).

[2] A.A. Papin, M. Tokareva, On local solvability of the system of the equations of one dimensional motion of magma, J. Sib. Fed. Univ. Math. Phys. 10(1), 385–395 (2017).

Finite time blow up of the solutions to nonlinear double dispersive equation with supercritical energy

N. Kolkovska, M. Dimova, N. Kutev

In this paper we study the conditions for finite time blow up of the solutions to the nonlinear double dispersive equation with linear restoring force

$$\begin{aligned} &u_{tt} - u_{xx} - u_{ttxx} + u_{xxxx} + u = f(u), && (t,x) \in \mathbb{R}\times\mathbb{R},\\ &u(0,x) = u_0(x), \quad u_t(0,x) = u_1(x), && x \in \mathbb{R},\\ &u_0 \in \mathrm{H}^1(\mathbb{R}),\ (-\Delta)^{-1/2}u_0 \in \mathrm{L}^2(\mathbb{R}), && u_1 \in \mathrm{L}^2(\mathbb{R}),\ (-\Delta)^{-1/2}u_1 \in \mathrm{L}^2(\mathbb{R}). \end{aligned} \tag{1}$$

Here $(-\Delta)^{-s}v = \mathcal{F}^{-1}(|\xi|^{-2s}\mathcal{F}(v))$ for $s > 0$, $\mathcal{F}(v)$, $\mathcal{F}^{-1}(v)$ are the Fourier and the inverse Fourier transform, respectively. The nonlinearity $f(u)$ has one of the following two forms:

$$\begin{aligned} f(u) &= \sum_{k=1}^{l} a_k|u|^{p_k-1}u - \sum_{j=1}^{s} b_j|u|^{q_j-1}u,\\ f(u) &= a_1|u|^{p_1} + \sum_{k=2}^{l} a_k|u|^{p_k-1}u - \sum_{j=1}^{s} b_j|u|^{q_j-1}u, \end{aligned} \tag{2}$$

where the constants a_k, p_k and b_j, q_j satisfy the conditions $a_1 > 0$, $a_k \geq 0$, $k = 2,\dots,l$, $b_j \geq 0$, $j = 1,\dots,s$, $1 < q_s < \dots < q_1 < p_1 < \dots < p_l < \infty$.

For example, problem (1), (2) appears in mathematical models of propagation of longitudinal strain waves in an isotropic cylindrical compressible elastic rod [1].

The global existence or finite time blow up of the solution to (1), (2) is fully investigated for nonpositive energy $E(0) \leq 0$ and for subcritical energy $0 < E(0) < d$ by means of the potential well method [2].

When the initial energy is supercritical, i.e. $E(0) \geq d$, there are a few results, which guarantee finite time blow up of the solutions. For example, the solution $u(t,x)$ of (1), (2) blows up in a finite time if the following condition is satisfied, see [3]

$$\langle u_0, u_1\rangle \geq 0, \qquad 0 < E(0) \leq \frac{1}{2}\frac{\langle u_0,u_1\rangle^2}{\langle u_0,u_0\rangle} + \frac{p_1-1}{2(p_1+1)}\langle u_0,u_0\rangle. \tag{3}$$

Here $(u,v) = (u(t,\cdot),v(t,\cdot))$ is the standard scalar product and $\langle u,v\rangle$ is defined as

$$\langle u,v\rangle = \langle u(t,\cdot),v(t,\cdot)\rangle = \Big((-\Delta)^{-1/2}u, (-\Delta)^{-1/2}v\Big) + (u,v).$$

Condition (3) generalizes the well-known conditions for finite time blow up of the solutions to the nonlinear double dispersive equation without linear restoring force [4]

$$\langle u_0, u_1\rangle > 0, \qquad 0 < E(0) < \frac{1}{2}\frac{\langle u_0,u_1\rangle^2}{\langle u_0,u_0\rangle}. \tag{4}$$

The sign condition $\langle u_0, u_1\rangle \geq 0$ plays very important role for finite time blow up of the solutions to nonlinear dispersive equations, see for example assumptions (3) - (4). The case $\langle u_0, u_1\rangle < 0$ is investigated only for the solutions to the Klein-Gordon equation with critical initial energy, i.e. $E(0) = d$, see [5].
In this paper we obtain sufficient conditions for finite time blow up of the solutions to (1), (2) for supercritical initial energy and *without any restrictions on the sign of the scalar product* $\langle u_0, u_1\rangle$. The lack of sign condition on $\langle u_0, u_1\rangle$ allows us to prove finite time blow up of the solutions when $t \to +\infty$ and $t \to -\infty$. More precisely, we have the following result.

Theorem 1. *Suppose $u(t, x)$ is the weak solution to* (1)*,* (2) *defined in the maximal existence time interval (t_m, T_m), $-\infty \leq t_m < 0 < T_m \leq +\infty$. If*

$$0 < E(0) < \frac{\sqrt{p_1 - 1}}{p_1 + 1}\langle u_0, u_1\rangle + \frac{p_1 - 1}{2(p_1 + 1)}\langle u_0, u_0\rangle,$$

then $-\infty < t_m < T_m < +\infty$, i.e. the solution $u(t, x)$ blows up in a finite time at t_m and T_m.

Acknowledgments. This work is partially supported by the Bulgarian National Science Fund under grants DNTS /Russia 02/7 and DFNI 12/5.

References

[1] A. Porubov, Amplification of nonlinear strain waves in solids, World Scientific, 2003.

[2] L.E. Payne, D.H. Sattinger, Saddle points and instability of nonlinear hyperbolic equations, *Israel Journal of Mathematics* 22(3-4) (1975) 273–303.

[3] N. Kutev, N. Kolkovska, M. Dimova, Nonexistence of global solutions to new ordinary differential inequality and applications to nonlinear dispersive equations, *Math. Meth. Appl. Sci.* 39(9) (2016) 2287–2297.

[4] S. Wang, G. Chen, Cauchy problem of the generalized double dispersion equation, *Nonlinear Anal.* 64 (2006) 159–173.

[5] J. Esquivel-Avila, Blow up and asymptotic behavior in a nondissipative nonlinear wave equation, *Appl. Anal.* 93(9) (2014) 1963–1978.

Spike Timing Neural Model of Eye Movement Motor Response with Reinforcement Learning

Petia Koprinkova-Hristova, Nadejda Bocheva

The paper presents a hierarchical spike timing neural network model developed in NEST simulator that reproduces the eye movements' behavior of humans. It includes multiple layers starting from retina ganglion cells via thalamic relay including lateral geniculate nucleus (LGN) and thalamic reticular nucleus (TRN) which mediates connections to the higher brain areas. The subsequent areas, visual cortex (V1), middle temporal (MT) and medial superior temporal (MTS) are involved in processing of spatial and dynamic visual information. Next lateral intraparietal cortex (LIP) is responsible for decision making and organization of the motor response [1]. Its reaction is biased by the upper brain areas - Basal ganglia (BG), including Striatum, Globus Pallidus externa (GPe), Subthalamic Nucleus (STN), Substantia Nigra pars reticulata (SNr) and Substantia Nigra pars compacta (SNc) [2, 3]. The output of BG modulates the activity of Superior Colliculus (SC) which in turn modulates the LIP activity and thus the voluntary saccades. The BG is regarded as Reinforcement Learning (RL) engine that uses reward information from the environment to inform and modulate sensory-motor cortex engaged in motor function In particular, the neurotransmitter dopamine released by SNc is thought to represent Temporal Difference (TD) error signal influencing via dopamine-energetic synapses the Stratum activity and thus the BG reaction to external reward stimuli. The model connectivity is designed according to available literature sources. Adaptation of dopamine-energetic synapses in dependence on external binary reinforcement signal is investigated. Our aim for future work is to compare the model behavior with experimental data from planed reinforcement learning experiments with humans observing visual stimuli and receiving external feedback about their response correctness.

Acknowledgement The reported work is supported by the project DN02/3/2016 "Modelling of voluntary saccadic eye movements during decision making" funded by the Bulgarian Science Fund.

References

[1] Koprinkova-Hristova, P., Bocheva, N., Nedelcheva, S., Stefanova, M.: A model of self-motion perception developed in NEST, NEST Conference 2018: A Forum for Users and Developers, 25-26 June 2018, NMBU, As, Norway (2018)

[2] Krishnan, R., Ratnadurai, S., Subramanian, D., Chakravarthy, V.S., Rengaswamyd, M.: Modeling the role of basal ganglia in saccade generation: Is the indirect pathway the explorer?. Neural Networks 24, 801–813 (2011)

[3] Igarashi, J., Shounob, O., Fukai, T., Tsujino, H.: Real-time simulation of a spiking neural network model of the basal ganglia circuitry using general purpose computing on graphics processing units. Neural Networks 24, 950–960 (2011)

Mathematical modeling and numerical simulation of nanoindentation accounting for material heterogeneity

Vladyslav Kyrychok, Roumen Iankov, Maria Datcheva, Petr Yukhymets

The instrumented indentation (IIT), also known as nanoindentation is a relatively new and promising technique used for characterization of materials in a local area [1,2,3]. Moreover, nanoindentation has become a commonly approved tool for the determination of mechanical properties at small scales, but may have even greater importance as a technique for experimental study of fundamental processes related to materials physics. It is well accepted that using the nanoindentation procedure it is possible to determine the hardness value and the Young's modulus of homogeneous bulk materials with a good accuracy. However, the applicability of the nanoindentation technique to assess the material characteristics of layered, coated and, in general, heterogeneous materials is still under investigation.

In the frames of this research we tried to obtain the stress-strain diagram for the material subject to nanoindentation and using the measured during the test force and displacements as input data. For verification of the procedure and the resulted stress-strain diagrams, we used the real true stress-strain diagram of the same bulk material obtained via standard tensile testing. In oredr to consider the relationship between the stress and strains after necking, we applied an approximated exponential relation. If the actual material hardening in the local area where the indenter penetrates the sample and plastic deformations take place was homogeneous, we would get good agreement between the measured during the tensile test stress-strain diagram and the computed relationship based on the force-displacement curve from the nanoindentation. However, we realized that it is impossible to have a good agreement between the nanoindentation and tensile test data if we keep the assumption that the sample obeys homogeneous material model.

Therefore, for ovecoming this drawback, we propose here a procedure, consisting in building a mathematical model and performing 3d numerical simulations of the nanoindentation tests accounting in the mathematical model the heterogeneous property of the structure of in the neighborhood of the penetrated by the indenter tip zone. Moreover, we have developed an automated procedure, which finds the converged solution for the plastic yield stress distribution iteratively. The results obtained confirm the ability of the developed numerical procedure to identify the heterogeneous material properties induced by the nanoindentation providing good agreement with the tensile test data.

Acknowledgements

The authors gratefully acknowledge the financial support within the bilateral project between the Institute of Mechanics, Bulgarian Academy of Scineces and the Paton Welding Institute, Kiev, Ukraine.

References

1. Oliver, Warren Carl, and George Mathews Pharr. "An improved technique for determining hardness and elastic modulus using load and displacement sensing indentation experiments." Journal of materials research 7, no. 6 (1992): 1564-1583.
2. Iankov, R., S. Cherneva, and D. Stoychev. "Investigation of material properties of thin copper films through finite element modelling of microindentation test." Applied Surface Science254, no. 17 (2008): 5460-5469.
3. Datcheva, Maria, Sabina Cherneva, Maria Stoycheva, Roumen Iankov, and Dimitar Stoychev. "Determination of anodized aluminum material characteristics by means of nano-indentation measurements." Materials Sciences and Applications 2, no. 10 (2011): 1452.

Coupled hydro-mechanical finite element simulation of loess slope under atmospheric boundary conditions

Lingyun Li, Maria Datcheva

Slopes in acid area usually exist in unsaturated situation, which might be unstable under rainfall. Loess landslide during rainfall period is a catastrophic problem in loess covered region. Every year, tremendous economic and life loess because of this hazard. In the paper, a case study of Baqiao landslide [1], which caused by the rainfall during in September 2011 is studied by coupled hydromechanical finite element method (CODE_BRIGHT [2]) to investigate the failure and deformation mechanisms of slopes. The viscoplastic Barcelona Basic Model (BBM) [3], is used to represent the deformation behavior of the unsaturated collapsible loess. Different to the other studies where it is used positive flux to simulation rainfall, in our case, we apply atmospheric boundary conditions which include temperature, atmospheric relative humidity, gas pressure and rainfall. These type of boundary conditions gives a realistic representation of the environmental reasons for the rainfall induced slope instability. The effect of antecedent rainfall and cyclic evaporation and infiltration are taken also into consideration. The numerical results demonstrated that the coupled hydro-mechanical analysis satisfactorily predicted the failure and deformation characteristics of the unstable slopes. The spatial and temporal variations of deformation (Fig. 2), stresses and pore water pressure under the atmospheric boundary condition are depicted in Figure 1. The numerical results show that pore water pressure varied at shallow depths and an excessive plastic deformation is developed under consecutive wetting and drying cycles at deeper depth, Figure 3. The corresponding hydrological data revealed a positive correlation between the slope deformation and accumulated rainfall. The coupled hydro mechanical simulation analyses give us some recommendations for practical solutions.

Acknowledgement

The first author acknowledges the support of the Erasmus++ program for supporting her stay at the Bulgarian Academy of Sciences for performing this study.

References

1. Zhuang, J. Q., & Peng, J. B. (2014). A coupled slope cuttingá prolonged rainfall-induced loess landslide: a 17 October 2011 case study. Bulletin of Engineering Geology and the Environment, 73(4), 997-1011.
2. Jamei, M., Guiras, H., & Olivella, S. (2015). Analysis of slope movement initiation induced by rainfall using the Elastoplastic Barcelona Basic Model. European Journal of Environmental and Civil Engineering, 19(9), 1033-1058.
3. Alonso, E. E., Gens, A., & Josa, A. (1990). A constitutive model for partially saturated soils. Géotechnique, 40(3), 405-430.

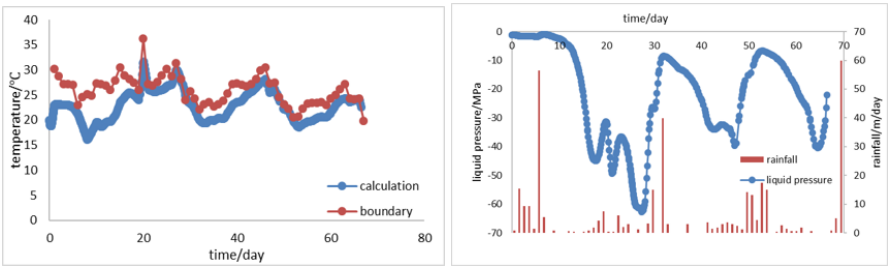

Figure 1. Temperature and liquid pressure distribution on the top surface

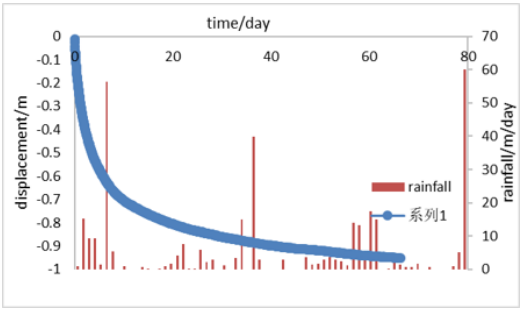

Figure 2. Displacement distribution on the top surface

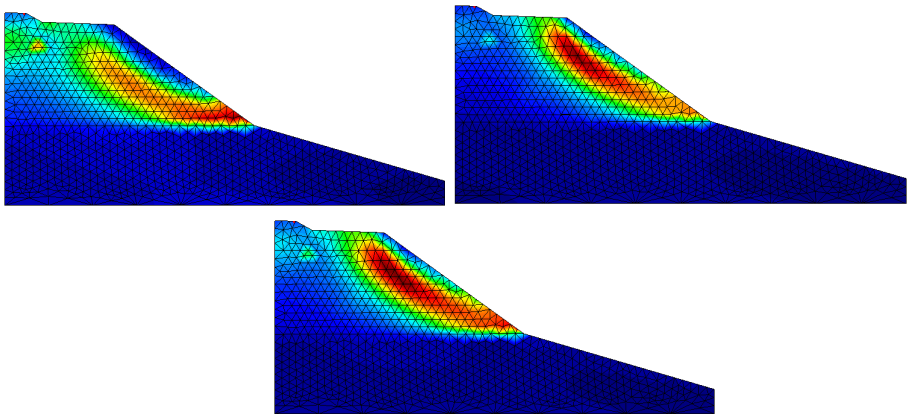

Figure 3. EDP distribution on the initial and after 20 days

Molecular dynamics simulations of His_6-FLAG-hIFNγ fusion glycoproteins

E. Lilkova, N. Ilieva, P. Petkov, E. Krachmarova, G. Nacheva, L. Litov

Human interferon-gamma (hIFNγ) is a secretory glycoprotein, which plays a key role in the regulation of innate and adaptive immunity. Under physiological conditions, IFNγ forms non-covalent homodimers, which represent the biologically active form of the cytokine, where the two monomers are bound in a globule of intertwining α-helices. hIFNγ exerts its effects on cells by a high-affinity interaction with a species-specific receptor complex (IFNγR).

Natural cytokine is a glycoprotein with two N-glycosylation sites in each monomer chain – Asn^{25} and Asn^{97}, which are independently and differentially glycosylated. Glycosylation is not necessary for the activity of the cytokine, but was shown to promote the folding and dimerization of the recombinant protein. Glycosylation also protects hIFNγ from proteolytic degradation, thus extending its circulatory half-life.

In order to obtain glycosylated human hIFNγ and its highly prone to aggregation mutant K88Q, a technology has recently been developed for their secretory expression in insect cells. In addition, to facilitate recombinant proteins purification and detection, the proteins were labeled with specific tag peptides added to their N-termini. Although the obtained proteins were glycosylated, we found that their biological activity was 100 times lower than expected. Moreover, if the labeled hIFNγ was glycosylated, the marker could not be removed due to enterokinase resistance of the tag.

We develop *in silico* models of glycosylated fusion His_6-FLAG-hIFNγ proteins and employ long-scale molecular dynamics (MD) simulations (1.5 μs total simulation time) to explain these unexpected experimental results and to study in detail the effect of glycosylation on the structure and dynamics of the fusion glycoproteins.

Based on experimental data about the glycosylation of hIFNγ and glycosylation patterns in insect cells, two different models of the glycosylated cytokine were developed. In either model the two protein monomers were diglycosylated. In the first model, the glycans were just the bi-antennary tri-mannose core glycans (left pane in Fig. 1). In order to explore the effect of heavier and longer carbohydrates, a second model of the tagged hIFNγ glycoprotein was constructed — with tri-antennary 9-mannose glycans (right panel in Fig. 1). A model of the non-glycosylated fusion His_6-FLAG-hIFNγ homodimer was also developed.

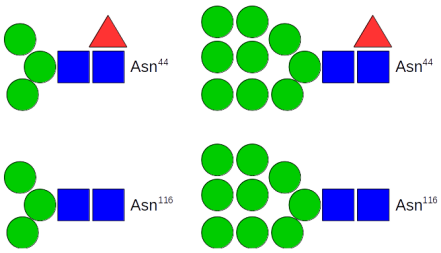

Figure 1: Chemical structure of the glycans for the two glycosylated systems: bi-antennary (left panels) and tri-antennary (right panels) glycans attached to Asn^{44} (top) and Asn^{116} (bottom). The blue squares represent N-acetyl-D-glucosamine, green circles – D-mannose, and red triangles – L-fucose.

The glycan cores were modelled using the GlyProt server and the Glycan Reader module of CHARMM-GUI. The glycoprotein structures were parameterized using the CHARMM 36 force field. The three systems were solvated in rectangular boxes with a minimal distance to the box walls of 2 nm under periodic boundary conditions, their net charge was neutralized and then energy minimization and equilibration simulations were performed. The production MD simulations were run in the NPT ensemble at 310 K temperature and 1 atm pressure, maintained by a v-rescale thermostat with a coupling constant of 0.25 ps and a Parrinello-Rahman barostat with a coupling constant of 1 ps. The leapfrog integrator was used with a time-step of 2 fs, whith constraints imposed on bonds between heavy atoms and hydrogens using the PLINCS algorithm. Van der Waals interactions were smoothly switched off from a distance of 1.0 nm and truncated at 1.2 nm. Electrostatics was treated by the smooth PME method with a direct PME cut-off of 1.2 nm. The simulations had a duration of 500 ns. Trajectory frames were recorded every 200 ps.

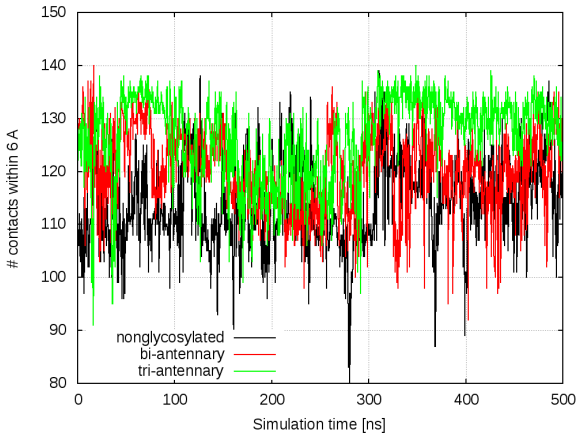

Figure 2: Number of contacts within 0.6 nm between the Asp-Asp-Asp-Asp-Lys pentapeptides in the tags and the hIFNγ glycoprotein. The reference simulation (nonglycosylated cytokine) is shown with the black curve, the glycosylated with bi-antennary glycans protein simulation – with the red curve, and the simulation with the tetra-antennary glycans – with the green curve.

Our initial hypothesis was, that the glycans cover much of the surface of the cytokine and the His_6-FLAG tag and thus completely or partially protect the tag peptide from proteases. Contrary to these expectations, the solvent accessible surface area (SASA) of the tag does not decrease upon glycosylation. However, the pentapetide Asp-Asp-Asp-Asp-Lys, which the enteropeptidase recognizes and cleaves in the FLAG, does form on average about 10% more contacts with the amino acid residues and the sugars of the glycoproteins, that with the reference nonglycosylated fusion cytokine (Fig. 2). Apparently, the presence of the glycan chain in the proximity of the Asp-Asp-Asp-Asp-Lys pentapeptides is sufficient to hinder sterically the access of the massive enzyme (1018 residues and 150 kDa molecular weight), thus preventing a cleavage of the tag.

Acknowledgements This work was supported in part under the Programme for young scientists' career development at the Bulgarian Academy of Sciences (DFNP-17-146/2017) and under Grant DN-11/20/2017 of the Bulgarian Science Fund. Computational resources were provided by the supercomputer Avitohol@BAS and the HPC Cluster at the Faculty of Physics of Sofia University "St. Kl. Ohridski".

A Monte Carlo based stochastic numerical approach for contaminant removal in constructed wetlands

Konstantinos Liolios, Krassimir Georgiev, Ivan Georgiev

Constructed wetlands (CW) are recently used as an ecological and economic alternative solution for the municipal wastewater treatment in small settlements. The purpose of their use is to improve the groundwater quality and the removal of groundwater pollutants in contaminated soils [1]. The traditional numerical simulation of CW operation is usually a $deterministic$ one, based on the solution of the following system of Partial Differential Equations (PDE) [2,3].

The three-dimensional groundwater flow equation, providing as solution the hydraulic head $h = h(x_i; t)$, is written, using tensorial notation ($i, j = 1, 2, 3$):

$$\frac{\partial}{\partial x_i}(K_{ij}\frac{\partial h}{\partial x_j}) + q_s = S_s\frac{\partial h}{\partial t} \tag{1}$$

where K_{ij} is a component of the hydraulic conductivity tensor; h is the hydraulic head; S_y is the specific yield of the porous materials; and q_s is the volumetric flow rate per unit area of aquifer representing fluid sources (positive) and sinks (negative). The velocity field is computed through the Darcy relationship:

$$q_i = -K_{ij}\frac{\partial h}{\partial x_j} \tag{2}$$

The partial differential equation, which describes the fate and transport of a contaminant with adsorption in 3-D, transient groundwater flow systems, is:

$$\varepsilon R_d\frac{\partial C}{\partial t} = \frac{\partial}{\partial x_i}\left(\varepsilon D_{S_{ij}}\frac{\partial C}{\partial x_i}\right) - \frac{\partial}{\partial x_i}(q_i C) + q_s C_s + \sum_{n=1}^{N} R_n, \tag{3}$$

where ε is the porosity of the subsurface medium; R_d is the retardation factor; C is the dissolved concentration of solute; $D_{S_{ij}}$ is the solute hydrodynamic dispersion coefficient tensor; C_s is the concentration of the source or sink flux; and $\sum R_n$ is the chemical reaction term, in [ML^{-3}T^{-1}]. The reaction term $\sum R_n$, for the usual linear reaction case is, given by the formula:

$$\sum R_n = -\lambda R_d C, \tag{4}$$

where λ is the first-order removal coefficient.

The above system of PDE (1)-(4), combined with appropriate initial and boundary conditions, describe the 3-dimensional flow of groundwater and the transport and removal of contaminants in a heterogeneous and anisotropic medium. Thus, the unknowns of the problem are the following six space-time functions: The hydraulic head: $h = h(x_i; t)$; the three velocity components: qi; the temperature: $T = T(x_i; t)$; and the concentration: $C = C(x_i; t)$.

The input parameters concerning the various coefficients of the above system of eqs. (1)-(4), are rarely known in a safe way, which usually requires detailed in-situ measurements. So, the

numerical treatment of the problem is usually realized in the praxis by using a mean-value estimate of the various coefficients. The present paper deals with a computational approach for solving the above problem under input parameters uncertainty. A stochastic methodology is applied, in which the various coefficients are considered as random variables. Probability density functions are used, based on lower and upper bounds for reliable estimates known either from praxis or in-situ measurements.
For the quantitative estimation of the various uncertainties, a Monte Carlo simulation is applied. As well-known, see e.g. [2-4,7-9], Monte Carlo simulation is simply a repeated process of generating deterministic solutions to a given problem. Each solution corresponds to a set of deterministic input values of the underlying random variables. A statistical analysis of the so obtained simulated solutions is then performed. The computational methodology consists of solving first the deterministic problem for each set of the random input variables and finally realizing a statistical analysis.
Details concerning the numerical solution of the deterministic problem are given in [5,6]. Finally, in a numerical example, concerning Biochemically Oxygen Demand (BOD) removal in a pilot-scale horizontal subsurface flow constructed wetland (HSF CW), stochastic computational results are compared with available experimental ones [5].

References

[1] Kadlec, R.H., Wallace, S.: Treatment Wetlands. CRC Press, Boca Raton (2009)

[2] Chen, S., Wang, G.D.: Applied Contaminant Transport Modelling. Wiley, New York (2002)

[3] Bear, J., Chend, A.D.: Modelling Groundwater Flow and Contaminant Transport. Springer, Berlin (2010)

[4] De Marsily, G.: Quantitive Hydrogeology. Academic Press, London (2010)

[5] Liolios, K., Tsihrintzis, V., Moutsopoulos, K., Georgiev, I., Georgiev, K.: A computational approach for remediation procedures in horizontal subsurface flow constructed wetlands. In: Lirkov, I., Margenov, S., Wasniewski, J. (eds.) LNCS, 7116, 299-306 (2012)

[6] Liolios K., Tsihrintzis V., Georgiev K., Georgiev I.: Geothermal effects for BOD removal in horizontal subsurface flow constructed wetlands: A numerical approach. In: Georgiev K., Todorov M., Georgiev I. (eds). Advanced Computing in Industrial Mathematics. Studies in Computational Intelligence, 681, 115-125 (2017)

[7] Kottegoda, N., Rosso, R.: Statistics, Probability and Reliability for Civil and Environmental Engineers. McGraw-Hill, London (2000).

[8] Papadrakakis, M., Stefanou, G.: Multiscale Modeling and Uncertainty Quantification of Materials and Structures. Springer Cham Heidelberg, New York (2014)

[9] Dimov, I.T.: Monte Carlo Methods for Applied Scientists. World Scientific Publishing Co. (2008)

Several results concerning the barnes G-function, a cosecant integral, and some other special functions

Lubomir Markov

The Barnes G-function is defined (cf. [1], [6]) by the Weierstrass canonical product

$$G(1+z) \,=\, (2\pi)^{z/2}\,\mathrm{e}^{-\dfrac{(1+\gamma)z^2+z}{2}}\prod_{n=1}^{\infty}\left\{\left(1+\frac{z}{n}\right)^n\mathrm{e}^{\,-z+\dfrac{z^2}{2n}}\right\}.$$

This function is an interesting relative to the classical Γ-function of Euler, as it satisfies the functional equation $G(z+1) \,=\, \Gamma(z)G(z)$ with the normalization $G(1) \,=\, 1$. It has the special value $G(\frac{1}{2}) \,=\, 2^{\frac{1}{24}}\cdot\pi^{-\frac{1}{4}}\cdot\mathrm{e}^{\frac{1}{8}}\cdot A^{-\frac{3}{2}}$, which may be compared to $\Gamma(\frac{1}{2}) \,=\, \sqrt{\pi}$. (As usual, A denotes the Glaisher-Kinkelin constant.) Another property of the Barnes function is the following formula of reflection type which is due to Kinkelin:

$$\int_0^z \pi t\cot\pi t dt \,=\, z\log(2\pi)+\log\frac{G(1-z)}{G(1+z)}.$$

The G-function is not included in the classical reference by Erdélyi *et al.* [2] on special functions, and it appears only as an exercise in Whittaker and Watson's book [7], but in recent years there has been renewed interest in it, and the literature on it has been growing steadily (see the bibliography in [6]).

In the present work we give simple new proofs of some known properties of the Barnes function, and prove several results which, to the best of our knowledge, are new. In particular, we correct an error in one of the known formulas involving $G(\cdot)$. We also study an integral involving the cosecant function, and prove several relations with the G-function and some other special functions related to polylogarithms (see Lewin's book [5]). These relations allow us to calculate several integrals which are not found in Gradshteyn and Ryzhik [3].

References

[1] E.W. Barnes, The theory of the *G*-function, *Quart. J. Math.* **31** (1899), 264-314

[2] A. Erdélyi, W. Magnus, F. Obberhettinger and F.G. Tricomi, *Higher Transcendental Functions*, Vol. I, McGraw-Hill Book Company, New York, Toronto and London, 1953

[3] I.S. Gradshteyn and I.M. Ryzhik, *Table of Integrals, Series, and Products*, Seventh Ed., Academic Press, New York, 2007

[4] H. Kinkelin, Ueber eine mit der Gammafunction verwandte Transcendente und deren Anwendung auf die Integralrechnung, *J. Reine Angew. Math.* **57** (1860), 122-158

[5] L. Lewin, *Polylogarithms and Associated Functions*, Elsevier (North-Holland), New York, London and Amsterdam, 1981

[6] H.M. Srivastava and J. Choi, *Series Associated with the Zeta and Related Functions*, Kluwer Academic Publishers, Dordrecht, Boston and London, 2001

[7] E.T. Whittaker and G.N. Watson, *A Course of Modern Analysis: An Introduction to the General Theory of Infinite Processes and of Analytic Functions; With an Account of the Principal Transcendental Functions*, Fourth Ed., Cambridge University Press, Cambridge, London and New York, 1963

Monte Carlo simulation of light scattering by hexagonal prisms with rough surface

Maya Mikrenska, Jean-Baptiste Renard

Monte Carlo (MC) ray-tracing is fast and flexible technique for computer modeling and simulation of the light scattering by variously shaped non-absorbing or slightly absorbing particles with sizes larger than the wavelength [1]–[3].
In this work we propose MC computational model of light scattering by hexagonal prisms with either smooth or rough surface. The model is based on geometric optics approximation and MC algorithm for ray path tracing. The model is capable to calculate scattering and polarization phase functions at single scattering by hexagonal particles with given refractive index, degree of roughness, size and aspect ratio distributions.
The software implementation was tested by comparison with available numerical solutions for hexagonal prisms with smooth surface. A series of numerical simulations was performed to study the effect of surface roughness. The computational model was validated by comparison with PROGRA2 experimental results [4] .The experiment has been conducted in microgravity conditions during parabolic flights onboard A300 Zero-G aircraft to ensure random orientation of the observed particles. The ensemble of hexagonal crystals of Na_2 SO_3 was illuminated by red and green He-Ne laser and values of scattering and polarization phase functions at scattering angle from 0^0 to 180^0 have been measured. Computer simulations closely reproduce experimental results.

Acknowledgement. This work was partially supported by the National Science Fund of Bulgaria (BNSF), Grant DFNI 12/5, Project "Effective Stochastic Methods and Algorithms for Large-Scale Computational Problems".

References

[1] M. Mikrenska, P. Koulev, E. Hadamcik, Direct simulation Monte Carlo of light scattering by cube, Dokladi na B lgarskata akademiÃ¢ na naukite 57 (11), 39–44 (2004).

[2] M. Mikrenska, P. Koulev, JB Renard, E. Hadamcik, JC Worms, Direct simulation Monte Carlo of light scattering by rounded cubes,C. R. Acad. Bulg. Sci.58, 275–280 (2005).

[3] M. Mikrenska, P. Koulev,Simulation of light scattering by large particles with randomly distributed spherical or cubic inclusions, Journal of Quantitative Spectroscopy and Radiative Transfer 110 (14-16), 1411–1417 (2009).

[4] http://www.icare.univ-lille1.fr/progra2/instrumentation/index.html

Multicriteria Assessment Approach for Future Digital Security Trends Dynamics

Zlatogor Minchev

The future digital society is going to transcend the present security issues dynamics related to the assumptions of space and data personality together with reality mixing, establishing a new environment of existence and governance [1]. The present study tries to give a light shed towards the possible validation of this complex and not quite certain mixed digital phenomena. A set of ad-hoc defined criteria is used for a priori three-fold (risk, utility and effectiveness) multi-attribute, probabilistic assessing over a weighted graph model [2]. Further on, the trends dynamic modelling towards the future security necessities is outlined, using structural analysis. Some a posteriori corrections of the initial expectations are also performed, implementing empirical information, delivered from interactive simulations [3], [4] and future trends modelling scenario support [5]. The outlined findings, are finally explored towards the development trends, selected evolutional scenarios, giving a holistic outlook of the presented approach towards the new security transcends dynamics expectations.

References

[1] Z. Minchev, (Ed) Future Digital Society Resilience in the Informational Age, Institute of ICT, Bulgarian Academy of Sciences, 2018 (in press)

[2] Z. Minchev, L. Boyanov, A. Georgiev, & A. Tsvetanov, An Analytical Outlook towards Digital Training Security Transformations, In Proc. of ICAICTSEE – 2017, UNWE, Sofia, Nov 3-4, 2017, https://dx.doi.org/10.13140/RG.2.2.20333.28645 [30.11.2018]

[3] Cyber Research Exercise – CYREX 2018 Web Page, http://cleverstance.com/CYREX_2018/cyrex_2018.html [30.11.2018]

[4] Towards Future Society 5.0: Modelling, Exploration & Understanding, Experimental Training, https://goo.gl/Crn4ym [30.11.2018]

[5] A. Frank, J. Carroll-Nellenback, M. Alberti, & A. Kleidon, The Anthropocene Generalized: Evolution of Exo-Civilizations and Their Planetary Feedback, Astrobiology, vol. 18, no. 5, May, 2018, https://doi.org/10.1089/ast.2017.1671 [30.11.2018]

Influence of the temperature on Simulated Annealing Method for Metal Nanoparticle Structures Optimization

V. Myasnichenko, S. Fidanova, R. Mikhov, L. Kirilov, N. Sdobnyakov

Metal, including gold, nanowires (filamentary nanocrystals, nanofibers) is a rapidly expanding field of research. Gold nanowires can be used in transparent electrodes for flexible displays. A particularly important point related to electrodes is the stability of nanowires at a thermal load. The minimization of surface energy caused by thermally activated diffusion leads to the rupture of nanowires. This was observed for copper, for silver, for gold, and also for platinum. The behavior of nanostructures at elevated temperatures can be very different from the macroscopic material. It is well known that small nanoparticles/nanowires will melt at a much lower temperature, which depends on their size

The structure of nanoclusters plays an important role in the study of the thermodynamic characteristics determined in the course of phase transitions (melting/crystallization). The description of the mechanisms of formation and dynamics of changes in the internal structure of nanoparticles can allow predicting the properties of these nanoparticles. Despite the modern development of the experimental base and theoretical approaches, certain tasks in the study of structural characteristics, including the search for stable configurations, the description of the criteria for thermal stability, etc., are not being solved. This problem has an exceptional importance in studying the properties of nanomaterials. The stable configuration is when the potential energy is minimal. It can be solved as a global optimization problem.

Finding global minimum of the potential energy of the surface is NP optimization problem. So searching through all possible minimum is impractical as well as applying traditional numerical methods, because they need huge amount of computational resources like time and memory. The global minimum is approximated using time-efficient optimization strategies, so called metaheuristics. A lot of methods are available for the prediction of nanoalloy structures.

In this paper we apply Simulated Annealing Method for metal nanoparticle structures optimization. Successfulness application of the method depends of algorithm parameters. One of the most important parameters is the value of the initial temperature. By the literature the initial temperature need to have high value. The question is which value is high. A fixed value can be high for some initial data and not high for other. Our idea is the value of the initial temperature to be function of the value of the objective function according the initial solution. Thus the value of the initial temperature will be related with the input data. We propose several variants of calculation of the value of initial temperature and study their influence on algorithm performance.

The experiments are performed with real data as follows. Two sets of mono metal clusters are chosen for investigation: Silver (Ag) and Cobalt (Co) that belong to different groups from the table of Mendeleev. The size of clusters for Ag varies from Ag141 (atoms) to Ag310 (atoms) and for Co varies from Co2 (atoms) to Co200 (atoms) resp. Several dependencies are derived between type of metal and number of atoms in the cluster on the one hand, and starting temperature, the way the temperature is changed and stopping rule on the other hand.

Numerical solution of nonlinear Fredholm fuzzy integral equation by fuzzy neural network

Iva Naydenova

The solutions of integral equations have a major role in the field of science and engineering. A physical even can be modelled by the differential equation, an integral equation. Since few of these equations cannot be solved explicitly, it is often necessary to resort to numerical techniques which are appropriate combinations of numerical integration and interpolation. Borzabadi and Fard in [2] obtained a numerical solution of nonlinear Fredholm integral equations of the second kind.

Fuzzy neural network have been extensively studied [1, 3] and recently, successfully used for solving fuzzy polynomial equation and systems of fuzzy polynomials, approximate fuzzy coefficients of fuzzy regression models, approximate solution of fuzzy linear systems and fully fuzzy linear systems. In [4] is used artificial neural networks to solve linear Fredholm fuzzy integral equations of the second kind.

In this paper, we extend the artificial neural networks to solve the following nonlinear Fredholm fuzzy integral equations

$$y(x) = g(x) \oplus (FR) \int_a^b k(x,t) \odot G(y(t))dt,$$

where $g : [a,b] \to E^1$ is continuous fuzzy-number valued function, $k : [a,b] \times [a,b] \to R_+$ is continuous function and $G : E^1 \to E^1$ is continuous functions on E^1. The set E^1 is the set of all fuzzy numbers.

The ability of neural networks in function approximation is our main objective. We present very simple numerical method based upon neural networks for solving nonlinear Fredholm fuzzy integral equations. In the proposed method, fuzzy neural network model is applied as universal approximator. We use fuzzy trial function, where contains the fuzzy neural network adjustable parameters to be calculated. Moreover, we illustrate how fuzzy connection weights are adjusted in the learning of fuzzy neural networks by the back-propagation-type learning algorithms [5]. Our fuzzy neural network is a three layers feedforward neural network where connection weights and biases are fuzzy numbers. Numerical example is provided to demonstrate the proposed method.

References

1. Bernard J.: Use of rule-based system for process control, IEEE Contr. System Mag., **8**, 3-13, (1988).

2. Borzabadi A. and Fard O.: A numerical scheme for a class of nonlinear Fredholm integral equations of the second kind, Journal of Computational and Applied Mathematics, **232**, 449-454, (2009).

3. Chen Y., Teng C.: A model reference control structure using a fuzzy neural network, Fuzzy Sets and Systems, **73**, 291-312, (1995).

4. Fadravi H., Buzhabadi R., Nik H: Solving linear Fredholm fuzzy integral equations of the second kind by artificial neural networks, Alexandria Engineering Journal, **53**, 249-257, (2014).
5. Ishibuchi H., Morioka K. and Turksen I.: Learning by fuzzified neural networks, International Journal of Approximate Reasoning, **13**, 327-358, (1995).

Rank data clustering based on Lee distance

Nikolay I. Nikolov, Eugenia Stoimenova

Rank data commonly occurs in consumer questionnaires, voting forms or other inquiries of preferences. A full ranking of N items simply assigns a complete ordering to the items. Any such ranking vector can be viewed as an element π of the permutation group $\mathcal{S}_N$ generated by the first N positive integers. In this research we consider a cluster analysis of full ranking data that aims to identify typical groups of rank choices. The "K-means" procedure based on Lee distance is studied in details and some asymptotical results for large values of N are derived. In order to compare the clustering procedure based on Lee distance to those based on some of the most commonly used distances on $\mathcal{S}_N$, we apply the presented algorithms to several illustrative examples.

Suppose that there are n observations of complete rankings $\pi^{(1)}, \pi^{(2)}, \ldots, \pi^{(n)} \in \mathcal{S}_N$. Marden [2] considered a "K-means" clustering procedure for finding K centers (rankings) about which the observations are clustered in K groups. For fixed number of groups K, the centers $\hat{\sigma}^{(1)}, \hat{\sigma}^{(2)}, \ldots, \hat{\sigma}^{(K)} \in \mathcal{S}_N$ are estimated to be those that minimize the mean distance between the observations and the closest corresponding group centers, i.e.

$$\left(\hat{\sigma}^{(1)}, \hat{\sigma}^{(2)}, \ldots, \hat{\sigma}^{(K)}\right) = \underset{\sigma^{(1)}, \sigma^{(2)}, \ldots, \sigma^{(K)}}{\operatorname{argmin}} C_K\left(\sigma^{(1)}, \sigma^{(2)}, \ldots, \sigma^{(K)}\right), \quad \text{where} \tag{1}$$

$$C_K\left(\sigma^{(1)}, \sigma^{(2)}, \ldots, \sigma^{(K)}\right) = \frac{1}{n} \sum_{i=1}^{n} \min_{1 \le j \le K} d\left(\pi^{(i)}, \sigma^{(j)}\right),$$

for some distance $d(\cdot, \cdot)$ on $\mathcal{S}_N$. When the values of n, N and K are small the rankings given in (1) can be found by exhaustive search. The quantity C_K indicates how tightly the data are clustered about the estimated centers. The value of C_K decreases when the number of groups K increases. In order to adjust C_K to account the number of clusters K, Marden [2] considered the quantity

$$t_K = 1 - \frac{C_K\left(\hat{\sigma}^{(1)}, \hat{\sigma}^{(2)}, \ldots, \hat{\sigma}^{(K)}\right)}{C_K^0},$$

where $K = 1, 2, \ldots$ and

$$C_K^0 := \min_{\sigma^{(1)}, \sigma^{(2)}, \ldots, \sigma^{(K)}} \frac{1}{N!} \sum_{\pi \in \mathcal{S}_N} \min_{1 \le j \le K} d\left(\pi, \sigma^{(j)}\right) \tag{2}$$

is the value of C_K under uniform distribution over all possible $N!$ rankings. It is not hard to see that $0 \le t_K \le 1$, where $t_K = 0$ when the observations are uniformly distributed over the $N!$ rankings, i.e. there are no groups in the data, and $t_K = 1$ when the observations coincide with the cluster centers, i.e. the cluster centers are sufficient to describe the variety in the data. Thus, the coefficient t_K indicates how tightly the observations are clustered and can be considered as a measure of "tightness". Since the normalizing coefficient C_K^0 in (2) depends

on the distance $d(\cdot,\cdot)$, it is not reasonable to compare the values of t_K which are based on different distances on $\mathcal{S}_N$. However, it is useful to study t_K for fixed distance and different values of K.

The value of C_K^0 does not depend on the observations and can be computed for fixed distance $d(\cdot,\cdot)$ and value K. Since there are $\binom{N!}{K}$ possible choices for cluster centers, the complete search in (2) becomes computationally demanding for $N \geq 10$ and it is helpful to approximate C_K^0 by using some properties of $d(\cdot,\cdot)$. For instance, when $K = 2$ and $d(\cdot,\cdot)$ is Kendall's tau, the value of C_K^0 can be calculated by an iterative procedure described in [2]. An extensive review of the properties and applications of the most widely used distances on $\mathcal{S}_N$ can be found in [1] and [2]. In this study we focus on the properties of the Lee distance $d_L(\cdot,\cdot)$, defined by

$$d_L(\pi,\sigma) = \sum_{i=1}^{N} \min\Big(\mid \pi(i) - \sigma(i) \mid, N - \mid \pi(i) - \sigma(i) \mid \Big), \quad \text{for } \pi,\sigma \in \mathcal{S}_N.$$

By making use of the properties of Lee distance described in [3], we propose an efficient algorithm for finding the cluster centers in (1) and computing the values of C_K^0 based on $d_L(\cdot,\cdot)$. In the case when $K = 2$ and N is even, we show that C_K^0 based on Lee distance can be approximated by

$$C_2^0 \approx \frac{N^2}{4} - \sqrt{\frac{N^4 + 8N^2}{24\pi(N-1)}},$$

for large values of N.

Acknowledgements: This work was supported by grant I02/19 of the Bulgarian National Science Fund and by grant 17-95/2017 from the "Young Scientists and PhD Students Support Programme" of the Bulgarian Academy of Sciences.

References

[1] Diaconis P. (1988). *Group Representations in Probability and Statistics.* IMS Lecture Notes - Monograph Series, Vol. **11**, Hayward, California.

[2] Marden J. I. (1995). *Analyzing and Modeling Rank Data.* Monographs on Statistics and Applied Probability, No. **64**, Chapman & Hall.

[3] Nikolov N. I., Stoimenova E. (2018). Asymptotic properties of Lee distance. Metrika. https://doi.org/10.1007/s00184-018-0687-7

Blood flow instabilities related to the elasticity and asymmetry of an abdominal aorta aneurysm

Nikola Nikolov, Sonia Tabakova, Stefan Radev

It is known that the blood flow in arteries is in some cases turbulent. However, it is not clear to what extent the turbulence is well accepted by the cardio-vascular system, e.g. by the big arteries such as the aorta. Also to what extent the interaction of the aorta elasticity and blood flow velocity could compensate the turbulence and/or recover the laminar flow regime, at which the blood quality could be preserved during its transport to the tissues.

In this work the interaction between an oscillatory blood flow and an abdominal aorta aneurysm (AAA) is numerically modeled using the fluid-structure interaction (FSI) software of ANSYS. The AAA is modeled as an elastic tube with a symmetric (as previously discussed in [1]) or asymmetric sac (similar geometrical cases studied in [2]), situated at the middle section of the tube. For both geometrical cases, the established laminar flow regimes depend on the elasticity modulus values. It occurs that the laminarity loss corresponds to higher values of the elastic modulus for the asymmetric sac than for the symmetric one. This effect is connected with the development of ring-shaped vortices inside the sac. In the asymmetric shaped AAA, the vortices are ejected from the sac and travel upstream, while these vortices remain recirculating inside the sac in the symmetrical case. The vortex dynamics has a significant role for increasing the rupture risk and thrombus formation. However, it is interesting to note that although the blood flow becomes unstable, no rupture of the artery is still observed.

As results, the displacement and Von Mises wall stress distributions are presented for the two geometrical cases, as well as the velocity, pressure and wall-shear stress distributions correspondent to laminar and unstable flow regimes.

The influence of both types of aneurysm sac on the flow regimes is shown in correspondence with the similar one for a straight tube (without aneurysm). It can be concluded, that the asymmetry changes the inlet flow without its recovery far away from the aneurysm sac, while after the symmetric sac the inlet flow recovers completely its oscillatory character.

References

[1] N. Nikolov, S. Tabakova and St. Radev (2019) Gaussian Model Deformation of an Abdominal Aortic Aneurysm Caused by the Interaction between the Wall Elasticity and the Average Blood Pressure, *In: Georgiev K., Todorov M., Georgiev I. (eds), Advanced Computing in Industrial Mathematics, BGSIAM 2017, Studies in Computational Intelligence* **793**, pp. 305-316.

[2] Ch. M. Scotti, A. D. Shkolnik, S. C. Muluk and E. A. Finol (2005) Fluid-structure interaction in abdominal aortic aneurysms: effects of asymmetry and wall thickness, *BioMedical Engineering OnLine* **4:64**, 22 pages.

Analysis of Swing Oscillatory Motion

Svetoslav G. Nikolov, Vasil M. Vasilev and Daniela T. Zaharieva

Dynamical systems can be separated into two classes – integrable and nonintegrable systems. A system of differential equations of n^{th} order is completely integrable if it has n independent integrals of motion. According to the Arnold-Liouville theorem, for Hamiltonian (canonical) systems the existence of only $N = n/2$ integrals of motion is sufficient for integrability. The intersections (of level manifolds) of these *n* independent first integrals in involution are invariant for the flow associated to the integrable Hamiltonian system. Moreover, the Liouville-Arnold theorem ensures that these invariant objects are diffeomorphic to either N-dimensional: *tori* – $\boldsymbol{T}^N$=$S^1 \times ... \times S^1$, or *cylinders* – $\boldsymbol{C}^N$=$T^m \times R^l$, where $m \neq l$ and $m + l = N$.

For a completely integrable Hamiltonian system, its Hamiltonian $H\,(q,\,p)$ can be reduced in the form $H\,(P)$, where $P = P\,(q,\,p)$ is the generalized momentum vector and all its components are constants. It is well-known that the motion of an integrable Hamiltonian system is regular (periodic or quasi-periodic), as the regular component of this system has positive Lebesgue measure under quite general conditions.

For general Hamiltonian systems with two degrees of freedom, two extreme degenerate cases are typical: 1) *integrable one* – when KAM (Kolmogorov-Arnold-Moser) curves form smooth families filling all phase space; 2) *wholly chaotic one* – when one large stochastic zone occupies the whole phase space. Note, that in the case of higher degrees of freedom the situation is similar, but KAM tori do not divide the phase space, as stochastic (ergodic) layers (closures generated by periodic hyperbolic trajectories) are tied together in one large everywhere penetrating – stochastic web.

In this paper we investigate a model of a swing pumped from the seated position. Many authors modeled the rider and the swing as a compound pendulum, with a massive bob, m_1 at the rider's position on the seat and the rest of the body by two other bobs, m_2 that account for the extension of the body due to the rest of the body parts-arms, legs, head and so on. The two other bobs (for simplicity) of equal mass are represented as dumbbells that are positioned symmetrically about the scat of the swing. Since the model uses a symmetrical dumbbell, the center of mass of the swing is always at the position of the central mass, and therefore the parametric mechanism – periodically varying the center of mass relative to the pivot – does not apply. However, if the dumbbell is allowed to be asymmetric, then the center of mass will change and a parametric energizing mechanism does come into play.

The aim of this paper is to find new integrable case(s) of a Hamiltonian system with two degrees of freedom describing the rider and the swing pumped (from the seated position) as a compound pendulum. In result of our analytical calculations we can conclude that this system has two integrable cases when: both dumbbell lengths and point-masses are equal; the gravitational force is neglected.

Non–linear waves of interacting populations with density–dependent diffusion

Elena V. Nikolova, Denislav Z. Serbezov, Ivan P. Jordanov, Nikolay K. Vitanov

In this study we consider a mathematical model based on diffusion-reaction type PDEs to describe the spatio–temporal behaviour of interacting populations. We extend the generalized reaction–diffusion model for spatio–temporal dynamics of interacting (competing) populations, proposed in [1], by adding density–dependent diffusive terms to the equations therein. The new density–dependent terms describe the intra– and inter–specific spatial interactions among individuals leading to formation of aggregation structures or individual repulsion. We are interested in the particular case of one population migrating in one spatial direction. Then the generalized model is reduced to one degenerate diffusion–reaction PDE. We extract a general analytical solution of the considered equation applying the modified method of simplest equation [2]–[4]. The ordinary differential equation of Bernoulli is used as simplest equation. Numerical tests of the obtained analytical solution are performed. We show that the population density wave can vary in its profile depending on assumptions made about density–depending diffusion coefficients.

Acknowledgments. This work contains results, which are supported by the UNWE project for scientific researchers with grant agreement No. NID NI-21/2016.

References

[1] N. K. Vitanov, I. P. Jordanov, Z. I. Dimitrova, On nonlinear population waves, Applied Mathematics and Computation 215, 2950–2964 (2009).

[2] N. K. Vitanov, Application of simplest equations of Bernoulli and Riccati kind for obtaining exact traveling-wave solutions for a class of PDEs with polynomial nonlinearity, Communications in Nonlinear Science and Numerical Simulation 15 (8), 2050–2060 (2010).

[3] N. K. Vitanov, On modified method of simplest equation for obtaining exact and approximate solutions of nonlinear PDEs: the role of the simplest equation, Communications in Nonlinear Science and Numerical Simulation 16 (11), 4215–4231 (2011).

[4] N. K. Vitanov, On modified method of simplest equation for obtaining exact and approximate solutions of nonlinear PDEs: the role of the simplest equation, Communications in Nonlinear Science and Numerical Simulation 16 (11), 4215–4231 (2011).

Critical Points in the Optimization of a Parallel Code for Air Pollution Modelling

Tzvetan Ostromsky

The environmental modelling and air pollution modelling in particular is one of the toughest problems of computational mathematics (together with the meteorological modelling). All relevant physical and chemical processes in the atmosphere should be taken into account, which are mathematically represented by a complex PDE system. To simplify it a proper splitting procedure is applied. As a result the initial system is replaced by several simpler systems (submodels), connected with the main physical and chemical processes. These systems should be calculated in a large spatial domain, as the pollutants are moved quickly by the winds on a long distance, especially in the upper layers of atmosphere. Here they are exposed to temperature, light and other condition changes in extremely wide range, so does the speed of most chemical reactions. One of the major sources of difficulty is the dynamics of the atmospheric processes, which require small time-step to be used (at least – for the chemistry submodel) in order to get a stable numerical solution of the corresponding system. All this makes the treatment of large-scale air pollution models a heavy and time-consuming computational task. It has always been a serious challenge, even for the fastest and most powerful supercomputers nowadays [2, 6]. Parallel architectures and algorithms must be used to solve efficiently this task.

The first crucial point on the way to this goal is the domain decomposition technique. This is a natural way to achieve an efficient distributed memory parallelization of any numerical problem over a large spatial domain. For some of them however, like the advection-diffusion equations in our case, there is always certain overhead due to the boundary conditions. Minimizing this overhead is the next critical point towards the efficient optimization. On the other hand, optimization should not restrict the portability of the parallel implementation, as the intensive development in the computer technology inevitably leads to regular updates or complete replacement of the outdated hardware. Standard parallel programming tools (as MPI /OpenMP/ for distributed /shared/ memory models) are to be used in order to preserve portability of the code. Another important parallel optimization issue is the load-balance. MPI barriers, used to force synchronization between the processes in data transfer commands, often do not allow good load-balance. This obstacle can be avoided to some extent by using non-blocking communication routines from the MPI standard library.

How to overcome in practice these and other common optimization problems will be shown in relation with the optimization of the Danish Eulerian Model (DEM). DEM is a powerful and sophisticated large scale air pollution model, with some 30-year development history [5, 4, 6]. Over the years it was successfully applied in different long-term environmental studies in various areas (including environment protection, human health care, agricultural production, forestry, wildlife, and culture heritage protection). By processing a huge amount of data (most of it - for the quickly changing meteorological conditions), the model is able to calculate the variable concentrations of a number of pollutants and other chemically active species interacting with them (precursors), over a long time period. Moreover, various accumulative quantities (AOT40, AOT60, etc.) are calculated on yearly basis.

During these heavy calculations huge work arrays appear and are to be processed along with the computational work. Even after the partitioning of the large computational domain for parallel execution the main work arrays are too large to fit into the fastest cache memory (closer to the processors). Reuse of data already loaded into the cache is another key point in the optimization of the model. With the rising power of the modern supercomputers and the novel developments in the up-to-date parallel implementation of the model (UNI-DEM), great improvement has been achieved in the speed of calculations. As far as the transfer and I/O processing of the huge data sets is concerned, this lately become a strong bottleneck for the overall performance of the code. A way to deal efficiently with this problem will be shown also.

For some applications it is highly desirable to simplify as much as possible the model, keeping the reliability of its output results. A careful sensitivity analysis is needed in order to decide how to do such simplifications. On the other hand, it is important to analyze the influence of variations of the initial conditions, the boundary conditions, the rates of some chemical reactions, etc. on the model results in order to make right assumptions about the possible simplifications, which could be done. Such analysis can give valuable information about the performance of reliable and reasonable simplifications. It can also help in identifying the accuracy-critical parameters. Thus the sensitivity analysis version of DEM – SA-DEM was created [1, 3]. Its optimization faces similar, but often more severe problems, as its complexity is of higher order.

References

[1] I. Dimov, R. Georgieva, S. Ivanovska, Tz. Ostromsky, Z. Zlatev, Studying the Sensitivity of the Pollutants Concentrations Caused by Variations of Chemical Rates, *Journal of Computational and Applied Mathematics Vol. 235, No. 2* (2010), pp. 391–402.

[2] I. Dimov, K. Georgiev, Tz. Ostromsky, Z. Zlatev, Computational challenges in the numerical treatment of large air pollution models, *Ecological Modelling* **179**, Elsevier (2004), pp. 187-203.

[3] I. Dimov, R. Georgieva, Tz. Ostromsky, Monte Carlo Sensitivity Analysis of an Eulerian Large-scale Air Pollution Model, *Reliability Engineering and System Safety* **107**, Elsevier (2012), pp. 23–28.

[4] Tz. Ostromsky, Z. Zlatev, Parallel Implementation of a Large-scale 3-D Air Pollution Model, Large Scale Scientific Computing (S. Margenov, J. Wasniewski, P. Yalamov, Eds.), LNCS-2179, Springer (2001), pp. 309–316.

[5] Z. Zlatev, Computer treatment of large air pollution models, Kluwer, 1995.

[6] Z. Zlatev, I. Dimov, Computational and Numerical Challenges in Environmental Modelling, Elsevier, Amsterdam (2006).

Mechanical properties assessments for cellular materials and light alloys with predominant embedded phases

L. Parashkevova, L. Drenchev, P. Egizabal

Objectives:
The present report concerns three - phase composites with high volume fraction of non-matrix phases. The elastic properties assessments of such materials are calculated by analytical approach based on the variant of Differential Effective Medium (DEM) method. Here in the methodology from [1] is further developed for two cases: composite type A and composite type B. The composite A consists of matrix and two inclusion phases. The matrix is much softer than the inclusions material of first kind and at the same time is much harder than the inclusions of second kind. Composite B is a closed cell porous material. It is assumed that the high porosity is induced by spherical pores of two sets very different by size: $D_i \gg d_i$. At high volume fraction of pore space the average diameter of small pores is comparable to the inter-pores distance (cell's wall). For both composites A an B a two-step homogenization procedure [1] is applied. The initial plastic state of composites is supposed to start according to the corresponding yield condition. Hill's energy balance and leading role of matrix are taken into account describing the transition point from elastic to plastic state.

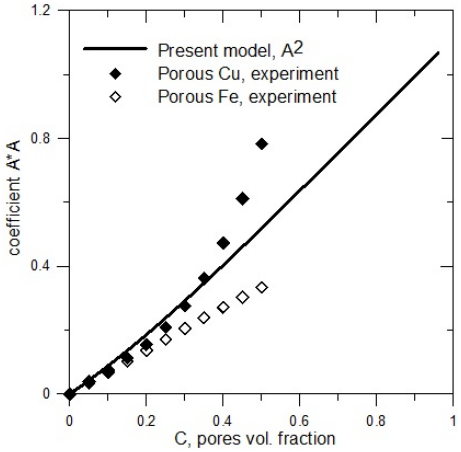

Figure 1: Comparison of the parameters of the yield condition (2) for porous composite with experimental data from [4]: coefficient A^2

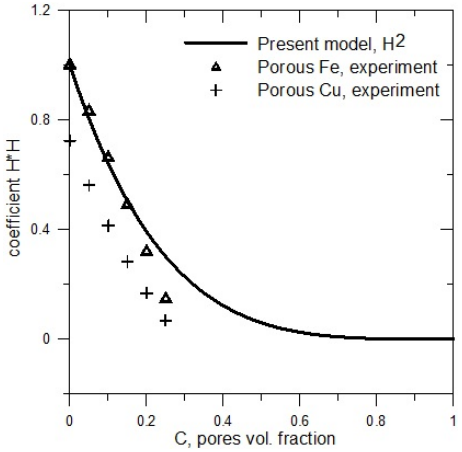

Figure 2: Comparison of the parameters of the yield condition (2)for porous composite with experimental data from [4]: coefficient H^2.

Results:
New explicit formulae are developed for overall elastic properties of the three-phase composites considered. These properties are incorporated into newly defined yield conditions. The size- sensitive variant of DEM used herein gives rise to additional opportunities to gain

in knowledge of microstructure - properties relationship. As a representative of the composites A Mg based alloys AZ , modified by TiC particles are investigated. At specific cooling conditions these alloys demonstrate discontinuous distribution of the harder gamma phase Mg17Al12 and TiC particles around the grains, formed by softer alpha Mg.
Equations (1) and (2) represent the yield condition suggested for porous composites. The evolution of the parameters representing the influence of mean macro-stress (A^2) and the relative composite yield limit (H^2) at increasing porosity are illustrated on Fig.1 and Fig. 2, respectively. Presented experimental data are recalculated from [4].

$$A^2 = \frac{2\left[(1-c) - \frac{K_c}{K_m}\right]}{\left[(1-c) - \frac{2}{3}\frac{G_c}{K_m}\right]} \frac{{G_c}^2}{{K_c}^2}, \quad H^2 = \frac{(1-c)\left[1 - \frac{2}{3}\frac{G_m}{K_m}\right]}{\left[(1-c) - \frac{2}{3}\frac{G_c}{K_m}\right]} \frac{{G_c}^2}{{G_m}^2} \tag{1}$$

$$\frac{\frac{3}{2}S_{ij}S_{ij}}{(\sigma_{pm})^2} + A^2\frac{(\Sigma_{kk})^2}{9(\sigma_{pm})^2} = H^2. \tag{2}$$

In (1) and (2) $K_x, G_x,\ x = m, c$ are bulk and shear moduli of the matrix (composite) and σ_{pm} is the initial yield stress of matrix material. The models of composite B are proper for gasars [2] and cellular structures as metal foams, obtained by space holders. Theoretical predictions of presented models are compared with other theories, [3], and experimental data available in the literature, [4].

Acknowledgements: This research is carrying out in the frame of KMM-VIN, European Virtual Institute on Knowledge-based Multifunctional Materials AISBL. Partial support from BG FSI through the grant DH 07/17/2016 is gratefully acknowledged.

References

[1] Parashkevova, L., Bontcheva, N., Babakov, V., Comp Mater Sci, **50**, 527–537 (2010)

[2] Drenchev, L., Sobczak, J., Malinov, S., Sha, W., Mater Sci Tech-Lond, **22**, 10, 1135–1147 (2006)

[3] Giordano, S., Eur J Mech A-Solid, **22**, 885–902 (2003)

[4] Shestakov, N.A., Subich, V.N., Demin, V.A., *Compaction, consolidation and fracture of porous materials*, (Fizmatlit, Moscow, 264 p.), (2011)

Symmetries and Conservation Laws of the Timoshenko Beam Equations for Double-Wall Carbon Nanotubes

Svilen I. Popov, Vassil M. Vassilev

In 2004, Yoon, Ru and Mioduchowski [1] studied a model describing the Timoshenko-beam effects on transverse wave propagation in multi-wall carbon nanotubes regarded as a system of separate nested tubes. In the case of a double-wall carbon nanotube, the suggested system of equations read

$$\begin{aligned}
-KGA_1\left(\frac{\partial\phi_1}{\partial x}-\frac{\partial^2 w_1}{\partial x^2}\right)+c\,(w_2-w_1)&=\rho I_1\frac{\partial^2 w_1}{\partial t^2},\\
EI_1\frac{\partial^2\phi_1}{\partial x^2}-KGA_1\left(\phi_1-\frac{\partial w_1}{\partial x}\right)&=\rho I_1\frac{\partial^2\phi_1}{\partial t^2},\\
-KGA_2\left(\frac{\partial\phi_2}{\partial x}-\frac{\partial^2 w_2}{\partial x^2}\right)-c\,(w_2-w_1)&=\rho I_2\frac{\partial^2 w_2}{\partial t^2},\\
EI_2\frac{\partial^2\phi_2}{\partial x^2}-KGA_2\left(\phi_2-\frac{\partial w_2}{\partial x}\right)&=\rho I_2\frac{\partial^2\phi_2}{\partial t^2}.
\end{aligned}\tag{1}$$

In Eqs. (1) x is the axial coordinate; t is the time variable; E, ρ and G are Young's modulus, mass density per unit length and shear modulus, which are assumed to be identical for both nested nanotubes; K is a shear coefficient. The dependent variables w_j and ϕ_j ($j=1,2$) are the total deflection and the slope due to bending of the j-th nanotube, respectively, I_j, A_j are the moments of inertia and the cross-section areas of the j-th nantube. Here, the subscripts $(1,2)$ are used to denote the quantities of the inner and the outer tubes; c is the intertube interaction coefficient due to the van der Waals interaction between the tubes.

Eqs. (1) turned out to be the Euler-Lagrange equations associated with the functional, defined on an appropriate two-dimensional smooth manifold, whose Lagrangian density can be taken in the form

$$L=K-P,$$

where

$$K=\frac{1}{2}\rho\left(A_2\frac{\partial w_2}{\partial t}^2+I_1\frac{\partial\phi_1}{\partial t}^2+I_2\frac{\partial\phi_2}{\partial t}^2+A_1\frac{\partial w_1}{\partial t}^2\right)$$

is the kinetic energy density of the system, while

$$\begin{aligned}
P=\frac{1}{2}\left[E\left(I_1\frac{\partial\phi_1}{\partial x}^2+I_2\frac{\partial\phi_2}{\partial x}^2\right)+c\,(w_1-w_2)^2\right]+\\
+\left[KG\left(A_1\left(\phi_1-\frac{\partial w_1}{\partial x}\right)^2+A_2\left(\phi_2-\frac{\partial w_2}{\partial x}\right)^2\right)\right]
\end{aligned}$$

is the potential energy density of the latter.

In the present paper we study the invariance of this functional with respect to local Lie groups of local point transformations of the respective dependent w_j, ϕ_j and independent variables x, t (see, e.g., [2]). We have found all variational symmetries of the considered functional as well as the densities and fluxes of the corresponding linearly independent conservation laws. We intend to use the obtained results in the analysis of the dynamic behaviour of the considered system of nested carbon nanotubes described by Eqs. (1).

References

[1] Yoon, J., Ru, C.Q., Mioduchowski, A.: Timoshenko-beam effects on transverse wave propagation in carbon nanotubes. Composites Part B: Engineering **35** (2), 87–93 (2004)

[2] Olver, P.: Applications of Lie Groups to Differential Equations, 2nd ed. Springer-Verlag, New York (1993)

Novel Application of Interval Analysis in Strength of Materials

Evgenija D. Popova, Isaac Elishakoff

Considering uncertainties is inevitable in a realistic analysis or design of mechanical structures. The uncertain parameters are represented by interval-valued parameters and interval analysis is applied when the available data do not allow applying the probabilistic approach. Most of the interval models considered so far are based on classical interval analysis [1]. Within this setting a lot of effort is put and a variety of special methods are proposed aiming at eliminating the interval dependency problem and thus obtaining sharp bounds for the unknowns. However, even the exact ranges of the unknowns within the models based on classical interval arithmetic may violate some physical laws of the deterministic model. Therefore, some recent works, [2, 3, 4] for example, emphasize the need of interval analysis in engineering context.

In [4], [5] the focus is on a mathematical model which is more precise than any model based on classical interval arithmetic. It relates the dependency of interval quantities to the physics of the problem being considered, e.g., linear equilibrium equations. The new model (called algebraic) represents any vector model parameter (possessing magnitude and direction) by a directed interval (range + direction) and requires that all kinds of linear equilibrium equations be completely satisfied. Thus, the new interval model is embedded in an isomorphic algebraic extension of classical interval arithmetic which is known under a variety of names: Kaucher arithmetic [6], modal arithmetic [7], directed arithmetic [8], generalized (proper and improper) intervals, reflecting some of its aspects. The generalized interval arithmetic structure possesses group properties with respect to the operation addition and the operation multiplication of intervals not involving zero. This allows the newly proposed interval algebraic model to resemble the corresponding deterministic model, to be applied straightforward to the latter, as well as to yield exact bounds for the unknowns without any overestimation.

In this work we further develop the interval algebraic approach by applying it to strength of material problems, in particular for bounding the uncertainties in axial forces, strains and stresses of truss elements considered as functions of the primary obtained variations of the displacements. Our current work continues [9]. As in the previous works, here the results obtained by the interval algebraic approach are compared theoretically and by numerical results to various interval models of truss structures based on classical interval arithmetic.

References

[1] Moore, R.E.: Interval Analysis. Prentice-Hall, Englewood Cliffs, N.J. (1966)

[2] Verhaeghe, W., Dempstet, W., Vanderpitte, D., Moens, D.: Interval fields to represent uncertainty on the output side of a static FE analysis. Computer Methods in Applied Mechanics and Engineering **260** 50-62 (2013)

[3] Qiu, Z.P., Wang, L.: The need for introduction of non-probabilistic interval conceptions into structural analysis and design. Science China: Physics, Mechanics and Astronomy, **59**, 11, article 114632 (2016)

[4] Elishakoff I., Gabriele, S., Wang, Y.: Generalized Galileo Galilei problem in interval setting for functionally related loads. Archive of Applied Mechanics **86**, 7, 1203–1217 (2016)

[5] Popova, E.D.: Improved solution to the generalized Galilei's problem with interval loads. Archive of Applied Mechanics **87** 1, 115–127 (2017)

[6] Kaucher, E.: Interval analysis in the extended interval space IR. Computing Suppl. **2**, 33–49 (1980)

[7] Sainz, M.A., Armengol J., Calm R., Herrero P., Jorba L., Vehi J.: Modal Interval Analysis: New Tools for Numerical Information. Lecture Notes in Mathematics **2091**, Springer (2014)

[8] Markov, S.M.: On directed interval arithmeticand its applications. J. Univers. Comput. Sci. **1**, 7, 514–526 (1995)

[9] Popova, E.D.: Algebraic solution to interval equilibrium equations of truss structures. Applied Mathematical Modelling **65**, 489–506 (2019)

Algorithmic problems in the geometry of polynomials

Blagovest Sendov and Hristo Sendov

The *Geometry of polynomials* study the geometric relations, on the complex plane $\mathcal{C}$, between the zeros of a complex polynomial $p(z)$ and the zeros (called also critical points) of its derivative $p'(z)$. The fundamental fact in this feeld, see [1, p. 69 - 78], is:

Theorem 1 (Gauss-Lucas)**.** *The convex hull $K(p)$ of a polynomial $p(z)$ contain the the zeros of its derivative $p'(z)$.*

To every polynomial

$$p(z) = \sum_{k=0}^{n} a_k z^k; \quad a_n \neq 0$$

correspond a multiaffine, symmetric polynomial in n complex variables:

$$P(z_1, \ldots, z_n) := \sum_{k=0}^{n} \frac{a_k}{\binom{n}{k}} S_k(z_1, \ldots, z_n)$$

where

$$S_k(z_1, \ldots, z_n) = \sum_{1 \leq i_1 < \cdots < i_k \leq n} z_{i_1} \cdots z_{i_k}, \quad k = 1, 2, \ldots, n$$

are the elementary symmetric polynomials of degree k, with $S_0(z_1, \ldots, z_n) := 1$. Obviously, $p(z) = P(z, \ldots, z)$. One say that $P(z_1, \ldots, z_n)$ is the *symmetrization of* $p(z)$.
The n-tuple $\{z_1, \ldots, z_n\}$ is called a *solution* of $p(z)$ if $P(z_1, \ldots, z_n) = 0$.
To study extreme problems in the Geometry of polynomials, we introduce, the following notion, see [2], [3], [4], [5].

Definition 1. *A closed subset Ω of $\mathcal{C}^* = \mathcal{C} \bigcup \infty$ is called a* **locus holder** *of $p(z)$ if Ω contains at least one point from every solution of $p(z)$. A minimal by inclusion locus holder Ω is called a* **locus** *of $p(z)$.*

It was shown in [2] that every locus holder contains a locus. If α is a zero of $p(z)$ and Ω is a locus of $p(z)$, then $\alpha \in \Omega$, since $\{\alpha, \alpha, \ldots, \alpha\}$ is a solution of $p(z)$. It is also shown, see [2], that every locus holder of $p(z)$ contains all zeros of all its derivatives $p^{(s)}(z)$; $s = 1, 2, \ldots, n-1$. A restatement of the classical theorem of Grace, see [1, p. 107], says that every circular domain containing the zeros of $p(z)$ is a locus holder of $p(z)$. In fact, every locus of $p(z)$ allows one to formulate an extreme version of Grace's theorem, see [3].
A corollary of the Grace theorem, see [1, p. 126], is:

Theorem 2 (Grace-Heawood)**.** *Let $p(z)$ be a polynomial of degree $n \geq 2$. If $z_1 \neq z_2$ and $p(z_1) = p(z_2)$, then the disk $D_n(z_1, z_2)$ with center $c = \frac{z_1+z_2}{2}$ and radius $r = \frac{|z_1-z_2|}{2} \cot \frac{\pi}{n}$ contains at least one zero of $p'(z)$.*

In fact $D_n(z_1, z_2)$ is a locus holder of a polynomial $\kappa_{n-1}(z)$ of degree $n-1$, depending only on the points z_1 and z_2, but not from the poliynomial $p(z)$. To sharpen the theorem of Grace-Heawood, we have to find a locus holder of $\kappa_{n-1}(z)$ with smaller area then this of the disk $D_n(z_1, z_2)$, see [5]. The disk $D_n(z_1, z_2)$ is only a locus holder of $\kappa_{n-1}(z)$, but not a locus. The problem to find the sharpest analogue of the Grace-Heawood theorem was formulated by Lubomir Tchakaloff, see [6], more than 80 years ago.

There are many extreme problems in the Geometry of polynomials, which may be solved by finding a locus of a polynomial.

It is possible to find a locus holder of a given polynomial by analytical methods. But until now, we do not know an analitical method to find the locus with the smallest area of a polynomial of degree $n \geq 4$.

The lecture is devoted to some ideas for constructing numerical algorithms for calculating the locus of a polynomial with smallest area. Observe that every polynomial has a such locus, but the problem of its uniqueness is steel open.

References

[1] RAHMAN, Q. I. AND SCHMEISSER, G., *Analytic Theory of Polynomials*, Oxford Univ. Press Inc., New York, (2002).

[2] SENDOV, BL. AND SENDOV, H.S., Loci of complex polynomials, part I, *Trans. Amer. Math. Soc.*, 10(366) 5155–5184 (2014).

[3] SENDOV, BL. AND SENDOV, H.S., Loci of complex polynomials, part II: polar derivatives, *Math. Proc. Camb. Phil. Soc.*, 159, 253–273 (2015).

[4] SENDOV, BL. AND SENDOV, H.S., Two Walsh-type theorems for the solutions of multi-affine symmetric polynomials, *Progress in Approximation Theory and Applicable Complex Analysis - In the Memory of Q.I. Rahman*, Springer-Verlag series in "Optimization and Its Applications", accepted (2016).

[5] SENDOV, BL. AND SENDOV, H.S., Stronger Rolle's theorem for complex polynomials *Proc. Amer. Math. Soc.*, v. 148, n. 8, 3367–3380 (2018).

[6] TCHAKALOFF, L.: Sur une généralisation du théoreme de Rolle pour polynomiales, C. R. Acad. Sci. Paris, 202 (1936), 1635 - 1637.

Performance analysis of hierarchical semi-separable compression solver for fractional diffusion problems

D. Slavchev, S. Margenov

We study the performance of a hierarchical solver for systems of linear algebraic equations arising from finite elements (FEM) discretization of fractional diffusion problems. There exist different definitions of fractional power of elliptic operators. Here we suppose the integral definition of fractional Laplacian in a bounded domain introduced through the Ritz potential. The problem is non-local and the related FEM system has a dense matrix.
The Structured Matrix Package (STRUMPACK) and its implementation of a Hierarchical Semi-Separable compression is utilized. Our main aim is to evaluate the performance and accuracy of the method by comparing its solution times, speed-up and accuracy with respect to reference solutions obtained by Gaussian Elimination solver from the Math Kernel Library (MKL) and the original MATLAB code.
The hierarchical compression is using the structure of a matrix to transform it into sparser matrix that would take less space and be easier for computations. Gaussian elimination has computational complexity of $O(n^3)$, where n is the number of degrees of freedom of the problem. Many applications produce dense matrices that are *structured* (*low-rank*, *data-sparse*, etc.). These matrices are *compressible* in some sense and for them we could effectively use hierarchical compression. For such problems the hierarchical methods have *nearly optimal* computational complexity of $O(r^2 n)$, where r is the maximum rank of the off-diagonal blocks of the matrix. Typically r is much smaller than n. For some problems r either grows slowly (like $O(\ln n)$) or is a constant.
In this paper we consider the implementation of hierarchically semi-separable compression within the STRUMPACK project [1] for solving *dense* systems of linear algebraic equations arising when discretizing fractional diffusion problems. STRUMPACK uses the following three step method to solve the system of linear algebraic equations:

1. HSS compression. In this step the input matrix is compressed into HSS form using random sampling. It has computational complexity of $O(r^2 n)$.

2. ULV-like factorization. In this step the HSS form of the matrix is factorized. This leaves $O(r)$ unknowns. It has computational complexity of $O(r^2 n)$

3. Solution. The remaining $O(r)$ unknowns are calculated with Gaussian Elimination. This part has computational complexity of $O(rn)$.

In [2] a 2D implementation of a homogeneous Dirichlet problem of a Fractional Laplacian is presented. We use the accompanying MATLAB code to generate systems of linear equation for both square and circular domains, and for various sizes. (Visualization of the FEM solutions could be seen in Fig. 1.) Then we use the arising dense matrices to measure the *parallel* scalability, speed-up and accuracy of STRUMPACK by comparing it to solutions calculated by Intel's native MKL solver.

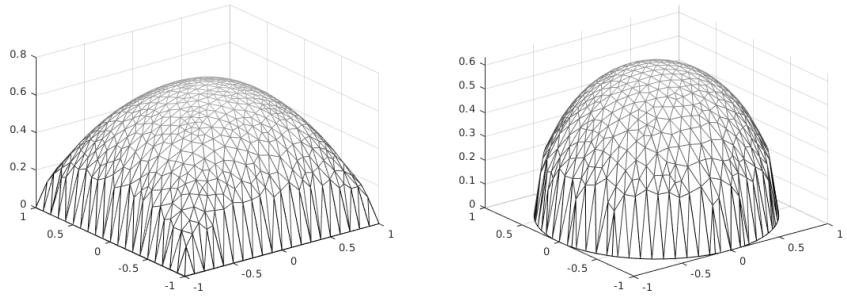

Figure 1: FEM solution of fractional Laplacian in square and circle domains (left and right respectively). The right hand side of the system is a volume force $b_i = \int_{T_l} f\varphi_{i_k}$, where for $k = 1, 2, 3$, i_k denotes the k-th vertex of the triangular polygon $T_l \in \Omega$ (Ω being the domain of the problem) and φ_{i_k} is the basis function corresponding to it. In the examples above $f = 1$. The power of the fractional Laplasian is $\alpha = 0.5$

.

For the Numerical Experiments we are using the HPC Cluster AVITOHOL [3] at the Institute of Information and Communication Technologies at the Bulgarian Academy of Sciences. It has 150 HP Cluster SL250S GEN8 servers (nodes), each with 2 Intel Xeon E2650v2 CPUs and 2 Intel Xeon Phi 7120P MICs. We run the tests on a single node with two CPUs with 8 cores each.

Acknowledgments.

The partial support by the Bulgarian NSF Grant DN 12/2 is acknowledged. The first author is also supported through the Bulgarian Academy of Sciences Program for support of Ph.D. Students.
We acknowledge the opportunity to run the numerical tests on the HPC cluster AVITOHOL [3] of the Institute of Information and Communication Technologies, Bulgarian Academy of Sciences.

References

[1] François-Henry Rouet, Xiaoye S. Li, Pieter Ghysels, and Artem Napov. A distributed-memory package for dense hierarchically semi-separable matrix computations using randomization. *ACM Trans. Math. Softw.*, 42(4):27:1–27:35, June 2016.

[2] Gabriel Acosta, Francisco Bersetche, and Juan Borthagaray. A short fe implementation for a 2d homogeneous dirichlet problem of a fractional laplacian. *Computers Mathematics with Applications*, pages 784–816, 08 2017.

[3] HPC cluster AVITOHOL. http://www.hpc.acad.bg/system-1/.

Desktop application for operational teams support activities suggested in eOUTLAND project

Stefan Stefanov

The article describes how we will implement open source tools into one system having desktop application as a result. This tool will be tested during the life time of the eOUTLAND project which is focused on NATURA 2000 protected areas in south Bulgaria and north Greece. The project idea is funded under the Interreg Greece - Bulgaria call for proposals in the Environmental priority axis. The test zones from Bulgarian side are Zlatograd and Svilengrad municipal areas. Information and Communication Technology (ICT) teams from both countries are combining efforts in order to provide for the respective volunteer groups open source tools for visualization of natural hazards affected zones. For Zlatograd we are going to use the system with predefined wildland fires risk maps and for Svilengrad we will use predefined flood risk maps. The fire part of the desktop application will have the ability to show any active fires on the test area inserted from operators on the interactive map. The second part of our desktop application will have the ability to present flood endangered zones located at the area of Svilengrad municipality. This maps visualization will be an option in GIS (Geographic Information System) environment and depending on the available layers every concerned team can have that information available online.

The desktop application will have open GIS layers focused on POIs (Points of Interests). They will be divided in two main groups. The first is going to describe administrative and vulnerable objects which need to be evacuated or protected with priority. The second will give locations of logistic centers from where volunteers and firefighter teams can get their tools and supplies. The reality nowadays when it comes to volunteer groups in Bulgaria is that they have significant lack of basic trainings, knowledge and tools to support them battle better with the nature on the field. Points of Interest (POIs) which this people need to know like logistic centers for water supplies and firefighting tools are usually well done instructions on a paper documents. There are no Information and Communication Technologies that can ease their orientation or provide them with information what type of equipment is placed in the nearby locations. Thus in our article we will present an idea for a system that can be used on the field and in operational rooms by firefighting and volunteer groups acting in cases of wildland fires and floods. For our application we will use different open source software solutions as Geoserver, Qgis, Web App Builder and Boundless WEBSDK: Geoserver allows the user to display spatial information to the world; QGIS is a professional GIS (Geographic Information System) cross-platform application that is Free and Open Source Software (FOSS); Web App Builder is a plugin for QGIS that allows easy creation of web applications; Boundless WEB-SDK which provides tools for easy-to-build JavaScript-based web mapping applications.

The presented idea for a desktop application can be used by the firefighting and volunteer groups teams in the tests areas. It can help reduction of time for response, by giving GIS based maps instead of paper instructions to the response teams.

Keywords: Wildland fires, floods, open source software, Qgis, Geoserver.

On the spectral properties of Lax operators and soliton equations

A. Streche-Pauna, A. Florian, V. S. Gerdjikov

It is well known [1, 2, 3] that the multicomponent nonlinear Schrödinger equations (MNLS) allow Lax representation $[L, M] = 0$. Here L and M are ordinary differential operators given by:

$$\begin{aligned} L\psi(x,t,\lambda) &\equiv i\partial_x\psi + (Q(x,t) - \lambda J)\psi(x,t,\lambda) = 0. && (1)\\ M\psi(x,t,\lambda) &\equiv i\partial_t\psi + (V_0(x,t) + \lambda V_1(x,t) - \lambda^2 J)\psi(x,t,\lambda) = 0, && (2)\\ V_1(x,t) &= Q(x,t), \qquad V_0(x,t) = i\mathrm{ad}\,_J^{-1}\frac{dQ}{dx} + \frac{1}{2}\left[\mathrm{ad}\,_J^{-1}Q, Q(x,t)\right]. && (3) \end{aligned}$$

For the generic BD.I VNLS (5) we have to choose Q and J to be $(2r+1)\times(2r+1)$ matrices with different block-matrix structure:

$$Q(x,t) = \begin{pmatrix} 0 & \vec{q}^T & 0 \\ \vec{q}^* & 0 & s_0\vec{q} \\ 0 & \vec{q}^\dagger s_0 & 0 \end{pmatrix}, \qquad J = \mathrm{diag}(1, 0, \dots 0, -1). \tag{4}$$

Kulish and Sklyanin [2] constructed an important integrable system which later was established as a model for spin-1 Bose-Einstein condensate. It is related to the **BD.I**-type symmetric spaces $SO(5)/S(O(2)\otimes O(3))$ [3] and can be written in the form:

$$i\vec{q}_t + \vec{q}_{xx} + 2(\vec{q}^\dagger, \vec{q})\vec{q}(x,t) - (\vec{q}, s_0\vec{q})s_0\vec{q}^*(x,t) = 0, \tag{5}$$

where $\vec{q}(x,t)$ is a 3-component vector function vanishing fast enough for $|x| \to \infty$ and the constant matrix $s_0 = \sum_{k=1}^{5}(-1)^{k+1}E_{k,6-k}$. The Hamiltonian for the Kulish-Sklyanin model (5) is given by

$$H_{\mathrm{KS}} = \int_{-\infty}^{\infty} dx \left((\partial_x\vec{q}^\dagger, \partial_x\vec{q}) - (\vec{q}^\dagger, \vec{q})^2 + \frac{1}{2}(\vec{q}^\dagger, s_0\vec{q}^*)(\vec{q}^T, s_0\vec{q}) \right). \tag{6}$$

Our first aim in this paper is to construct the kernel of the resolvent of the Lax operator. To this end we will use the fundamental analytic solutions $\chi^{\pm}(x,\lambda)$ of L, where $+$ (resp. $-$) means analyticity for $\lambda \in \mathbb{C}_+$ (resp. for $\lambda \in \mathbb{C}_-$). Thus we state that

$$\begin{aligned} &R^{\pm}(x,y,\lambda) = \frac{1}{i}\chi^{\pm}(x,\lambda)\Theta^{\pm}(x-y)\hat{\chi}^{\pm}(y,\lambda),\\ &\Theta^{+}(x-y) = \mathrm{diag}\,(-\theta(y-x), \theta(x-y)\mathbb{1}, \theta(x-y)) = -E_{11} + \theta(x-y)\mathbb{1},\\ &\Theta^{-}(x-y) = \mathrm{diag}\,(\theta(x-y), \theta(x-y)\mathbb{1}, -\theta(y-x)) = -E_{55} + \theta(x-y)\mathbb{1}, \end{aligned} \tag{7}$$

is the proper kernel of the resolvent. The next theorem generalizes results of [4] and [5]:

Theorem 1. *Let $q(x)$ be such that $T_{11}(\lambda)$ has finite number of second order zeroes at $\lambda_j^{\pm} \in \mathbb{C}_{\pm}$ Then*

1. *$R^{\pm}(x,y,\lambda)$ is an analytic function of λ having second order pole singularities at $\lambda_j^{\pm}$;*

2. *$R^{\pm}(x,y,\lambda)$ is a kernel of a bounded integral operator for $\mathrm{Im}\,\lambda \neq 0$;*

3. *$R(x,y,\lambda)$ is uniformly bounded function for $\lambda \in \mathbb{R}$ and provides a kernel of an unbounded integral operator;*

4. *$R^{\pm}(x,y,\lambda)$ satisfy the equation:*

$$L(\lambda)R^{\pm}(x,y,\lambda) = \mathbb{1}\delta(x-y). \tag{8}$$

This theorem has been proven earlier for generic Lax operators of the form (1) but with non-degenerate J, see [4, 5] and the references therein. In our case J above is degenerate; indeed, it has three vanishing eigenvalues. A consequence of this fact is that the algebra acquires a nontrivial $\mathbb{Z}_2$-grading:

$$\mathfrak{g} = \mathfrak{g}^{(0)} \oplus \mathfrak{g}^{(1)}, \qquad X^{(k)} \in \mathfrak{g}^{(k)} \quad \text{iff} \quad AX^{(k)}A^{-1} = (-1)^k X^{(k)}, \tag{9}$$

where the automorphism $A = \exp(\pi i J)$.
Our main result here is that the fundamental analytic solutions of L satisfy the completeness relation only in $\mathfrak{g}^{(1)}$. This result is valid also for the MNLS with non-local reductions: $Q(x,t) = Q(-x,t)^{\dagger}$.

Acknowledgements

Two of us (ASP and VSG) have been partially supported by network SEENET-MTP. ASP acknowledges financial support of Craiova and New Bulgarian Universities in the framework of Erazmus programm, and also by the project "Computational Methods in Astrophysics and Space Sciences", no. 181/20.07.2017, of the Romanian National Authority for Scientific Research, Program for Research Space Technology and Advanced Research.

References

[1] V. S. Gerdjikov. *Basic Aspects of Soliton Theory.* Eds.: I. M. Mladenov, A. C. Hirshfeld. "Geometry, Integrability and Quantization", pp. 78-125; Softex, Sofia 2005. **nlin.SI/0604004**

[2] P. P. Kulish, E. K. Sklyanin. $O(N)$-invariant nonlinear Schrodinger equation - a new completely integrable system. *Phys. Lett.* **84A**, 349-352 (1981).

[3] V. S. Gerdjikov, G. G. Grahovski. Multi-component NLS Models on Symmetric Spaces: Spectral Properties versus Representations Theory. SIGMA **6** (2010), 044, 29 pages.

[4] V. S. Gerdjikov. *On the spectral theory of the integro–differential operator Λ, generating nonlinear evolution equations.* Lett. Math. Phys. **6,** n. 6, 315–324, (1982).

[5] V. S. Gerdjikov. Algebraic and Analytic Aspects of N-wave Type Equations. **nlin.SI/0206014**; *Contemporary Mathematics* **301**, 35-68 (2002).

InterCriteria Analysis of the Human Factor Assessment in a Mobile Company

Velichka Traneva, Stoyan Tranev

In this paper is presented an application of the recently proposed approach for multicriteria decision making – InterCriteria Analysis (ICA) – to the assessmen of the human factor in a mobile company. ICA is a new method [3] for detecting positive and negative consonance coefficients between the different criteria for evaluation of objects. The ICA method employs the apparatus of intuitionistic fuzzy sets (IFSs) and index matrices (IMs). IFSs is first defined by Atanassov (IFSs, [2]) as an extension of the concept of fuzzy sets defined by Zadeh [5]. The concept of IMs is introduced in [1].
Here, the proposed method is applied to establish the relations and dependencies between pairs of criteria referred to the assessment in a mobile company of Bulgaria. The open dependencies between the evaluation criteria will lead to optimization of the company's staff rating system by removing part of the evaluation criteria and will support the decision-making process. In the paper presented here the authors have applied the ICA method to the real datasets with the evaluations of the human factor in the surveyed company. The main contribution of the paper is that it shows the effectiveness of the proposed hybrid method combining fuzzy logic with classic correlation analysis [4] to optimize the staff rating system of a mobile company. The outlined approach for ICA, can be applied to both the crisp parameters and the fuzzy ones and can be expanded to retrieve information to other types of multi-dimensional data. The comparative analysis of the correlation dependencies between the evaluation criteria in a mobile company has been performed in the paper after application of the ICA, the Pearson's and Spearman's correlation analyzes. It is observed that considerable divergence of the ICA results from those obtained by the Pearson's and Spearman's analyzes is only found when the input data contain mistakes. That is, ICA is less sensitive, so the use of them together can be used as a way of detecting errors in the input data.

References

[1] Atanassov, K.: Generalized index matrices. Comptes rendus de l'Academie Bulgare des Sciences **40**(11), 15-18 (1987)

[2] Atanassov, K.: On Intuitionistic Fuzzy Sets Theory. STUDFUZZ, vol. 283. Springer, Heidelberg (2012). doi.org/10.1007/978-3-642-29127-2

[3] Atanassov, K., Mavrov, D., Atanassova, V.: InterCriteria decision making. A new approach for multicriteria decision making, based on index matrices and intuitionistic fuzzy sets. Issues in Intuitionistic Fuzzy Sets and Generalized Nets **11**, 1-8 (2014)

[4] Doane, D., Seward, L.: Applied statistics in business and economics. McGraw-Hill Education, New York, USA (2016)

[5] Zadeh, L.: Fuzzy Sets. Information and Control 8(3), 338-353 (1965)

Using DLT in Software Lifecycle Management

Biser Tsvetkov, Hristo Kostadinov

Since the original work on Bitcoin of Satoshi Nakamoto [1] was published the blockchain technologies and their natural generalization - the distributed ledger technologies (DLT) are used in many areas beyond their original intent to support distributed cash systems. Establishing trust between several parties without relying on a trusted intermediary is a common goal of modern DLTs [2, 3]. Some of the popular Bitcoin's successors could be classified are either public/ permisionless blockchains (such as Ethereum [4] and EOS [5]), enterprise/ permissioned blockchain systems (such as MultiChain [6], and Hyperledger Fabric [7]), or DLTs that are no longer considered blockchains (such as Corda, Tangle, and Nano). The original application of DLT in Bitcoin to act as a trustless peer-to-peer digital cash system is extended in many directions in the recent years. Some of the directions in which DLTs are evolving are improvements of the processing speed, scalability, power consumptions, consensus mechanisms, and many security and integration features [7]. The introductions of smart contracts and blockchain oracles in Ethereum created an environment suitable to support more complicated scenarios for various industries such as finance, supply chain [8], insurance, healthcare, government and many more [2, 9, 10]. The rapid development of the DLTs in the recent years solved many of the shortcomings of original Bitcoin network and extended the areas and problems they were used to address. As result one of the new issues that architects have to decide on is which DLT is best suited for the specific tasks they are solving. In this article different DLTs and DLT features will be reviewed regarding their suitability to solve current problems in the area of the software lifecycle management (SLM). Software lifecycle management is the process of managing procedures that are executed at customer site, in their cloud, IoT devices and for edge computing landscapes. Some of these procedures are software products installation, upgrade, transport customized code and data, system copy, configuration, and many other. In the Enterprise world these procedures may be very complex as they involve coordination and configuration for usage of many tools and many different parties on different landscapes and clouds. Often many involved parties need to cooperate to successfully complete complex set of mutually dependent software lifecycle management procedures with minimal risk, downtimes and resource usage. Some of the parties that could be involved in a complex software lifecycle management project are:

- Customer(s)
- Software Provider(s)
- Consulting Partner(s)
- Hardware Vendor(s)
- Software Vendors(s)

The parties involved are not hierarchically organized and may not fully trust each other. Their goal is often project-based, temporary, and not strictly formalized in detailed legal frames.

Anyway, the success of the project often depends on the results of their collaboration and proper sharing of knowledge and resources. This makes usage of a DLT a good candidate to handle and automate the collaboration and sharing aspects of their interactions. In this session a DLT-based system will be described that could streamline and automate processes that are currently manual and time consuming. The tooling used during the software lifecycle management procedures could be DLT-enabled and most of the data will automatically be shared with the participants that the data is relevant to. And since the DLT is by design temper proof it may be used as a single source of truth by all involved parties providing a single solution to various current issues such as data visibility, security, prediction of downtimes and resource usage, and risk evaluation.

References

[1] S. Nakamoto. Bitcoin: A Peer-to-Peer Electronic Cash System, (2008). https://bitcoin.org/bitcoin.pdf

[2] R. Etwaru. Blockchain: Trust Companies, ISBN: 9781457556623, (2017)

[3] W. Mougayar, The Business Blockchain, ISBN: 9781119300311, (2016).

[4] V. Buterin, A Next-Generation Smart Contract and Decentralized Application Platform, (2013). https://github.com/ethereum/wiki/wiki/White-Paper

[5] D. Larimer, EOS.IO Technical White Paper, (2017). https://eoscollective.org/papers/

[6] G. Greenspan, MultiChain Private Blockchain-White Paper, (2015). http://www.multichain.com/white-paper/

[7] Hyperledger/Fabric: Blockchain Fabric Incubator Code. https://github.com/hyperledger/fabric

[8] R. Bee. Asset Management: 3 ways Blockchain will Enhance your Asset Management Efforts, (2018). https://www.ibm.com/blogs/internet-of-things/iot-blockchain-enhances-asset-management/

[9] A. Boudguida, Towards Better Availability and Accountability for IoT Updates by means of a Blockchain, IEEE European Symposium on Security and Privacy, April 2017

[10]] B. Morrell, How to Strengthen Product Lifecycle Management using Blockchain, (2017).

The logical model of unify, innovative Platform for Automation and Management of Standards (PAMS)

Toddor Velev, Nina Dobrinkova

The subject of the article is a study of a high-tech innovative product in the field of information technologies – unified platform for administration, automation and management of internationally recognized standards. Platform for Automation and Management of Standards (PAMS) is a modern, integrated information and communication system that models, digitizes, registers, manages, stores and controls work processes and related information and documentation, in accordance with a variety of internationally recognized standards. The logical model of the platform is the result of a research process with the following steps:

1. Profound research and analysis of the information sources for internationally recognized standards in aspects - content, infrastructure, superstructure and resources such as: International Standards Organization (ISO), Hazard Analysis Critical Control Point (HACCP), British Standard Occupational Health and Safety Assessment Series (BS OHSAS), etc.;
2. Defining evaluation criteria;
3. Selection of the common set of information identifiers, constituting the information content of the platform;
4. Structure of information identifiers (fields) in object-oriented information classes and subclasses, in accordance with their functional orientation in the description of the standards;
5. Research and analysis of relationships and dependences between information objects and definition of a logical model.

PAMS modifies and revives the company's document matrix and turns it into a powerful real-time management tool. By modeling the different sets of standards implemented by the company with he unified objects and processes, the platform is a highly effective in monitoring, control and operational management and can assure the requirements of the standards and their real utility. The resulting logical model is represented by a class diagrams of the information classes and subclasses and their attributes and is described by the Unified Modelling Language (UML) syntax.
Implementation of a management systems built in conformance to an organization's applicable ISO standards can bring a host many benefits. After becoming ISO certified, it is likely that an organization will achieve process improvement, lower defect and scrap costs, and increased customer satisfaction. That is why the presented idea have potential for many Bulgarian and international companies to improve their everyday work.

Keywords: Information technology, ICT, Platform, Integrated system, Document system, Standards, Modelling, Automation.

Study of a flow of reacting substances in a channel of network

Nikolay K. Vitanov, Kaloyan N. Vitanov, Zlatinka I. Dimitrova

Complex systems often have features that can be modeled by advanced mathematical tools [1]. Of special interests are the features of complex systems that have a network structure as such systems are important for modeling technological and social processes [3, 4]. In our previous research we have discussed the flow of a single substance in a channel of network. It may happen however that two substances flow in the same channel of network. In addition the substances may react and then the question arises about the distribution of the amounts of the substances in the segments of the channel. A study of the dynamics of the flow of the substances as well as a study of the distribution of the substances is presented in this paper on the base of a discrete - time model of flow of substances in the nodes of a channel of a network.

References

[1] Nikolay K. Vitanov. Science dynamics and research production. Indica- tors, indexes, statistical laws and mathematical models. Springer, Cham, (2016)

[2] Nikolay K. Vitanov, Kaloyan N. Vitanov. Box model of migration chan- nels. *Mathematical Social Sciences* **80**, 108 - 114 (2016).

[3] Nikolay K. Vitanov, Kaloyan N. Vitanov. On the motion of substance in a channel of network and human migration. *Physica A* **490**, 1277 - 1294 (2018).

Convergence of the minimum L_p-norm networks as $p \to \infty$

Krassimira Vlachkova

Scattered data interpolation is a fundamental problem in approximation theory and CAGD with applications in a variety of fields such as automotive, aircraft and ship design, architecture, medicine, computer graphics, and more. Recently, the problem has become particularly relevant in bioinformatics and scientific visualization for surface reconstruction.

We consider the extremal problem of interpolation of scattered data in $\mathbb{R}^3$ by smooth curve networks with minimal L_p-norm of the second derivative for $1 < p \leq \infty$. The problem for $p = 2$ was set and solved by Nielson [1]. Andersson et al. [2] gave a new proof of Nielson's result by using a different approach. Vlachkova [3] extended the results in [2] and solved the problem for $1 < p \leq \infty$. The minimum L_p-norm network for $1 < p < \infty$ is obtained from the solution to a system of nonlinear equations with coefficients determined by the data. The solution in the case $1 < p < \infty$ is unique. We denote the corresponding minimum L_p-norm network by F_p. In the case where $p = \infty$ the existence of a solution of the same type as in the case where $1 < p < \infty$ is established in [3]. This solution on each edge of the underlying triangulation is a quadratic spline function with at most one knot. We denote this solution by F_∞.

The following question arises naturally. Does the solutions for $1 < p < \infty$ converge to F_∞ as $p \to \infty$? Here we answer positively to this question. We prove the following theorem.

Theorem 2. *The minimum L_p-norm networks F_p converge to the minimum L_∞-norm network F_∞ as $p \to \infty$.*

Example 1. The data are $(-1/2, -\sqrt{3}/6, 0)$, $(1/2, -\sqrt{3}/6, 0)$, $(0, \sqrt{3}/3, 0)$, $(0, 0, -1/2)$. The minimum L_p-norm networks F_p and the corresponding L_p-norms of the second derivatives $\|F_p''\|_p$ for $p = 2,\ 6,$ and ∞ are shown in Fig. 1.

Acknowledgments. This work was supported by Sofia University Science Fund Grant No. 80-10-145/2018, and by European Regional Development Fund and the Operational Program "Science and Education for Smart Growth" under contract No BG05M2OP001-1.001-0004 (2018-2023).

References

[1] G. M. Nielson. A method for interpolating scattered data based upon a minimum norm network. *Mathematics of Computation*, 40(161):253–271, 1983.

[2] L.-E. Andersson, T. Elfving, G. Iliev, K. Vlachkova. Interpolation of convex scattered data in $\mathbb{R}^3$ based upon an edge convex minimum norm network. *Journal of Approximation Theory*, 80(3):299–320, 1995.

[3] K. Vlachkova, Interpolation of scattered data in $\mathbb{R}^3$ using minimum L_p-norm networks, $1 < p \leq \infty$, *submitted to Elsevier*.

$p = 2,\ \|F_2''\|_2 = 14.1636$

$p = 6,\ \|F_6''\|_6 = 3.40846$

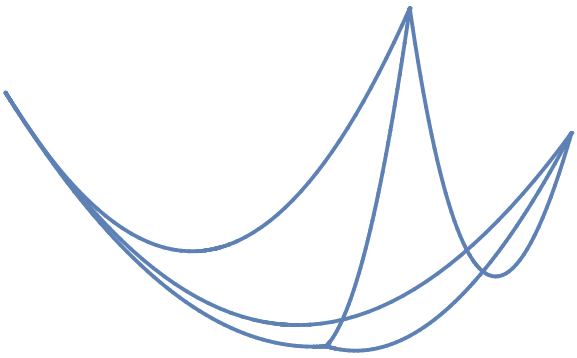

$p = \infty,\ \|F_\infty''\|_\infty = 3.$

Figure 1: The minimum L_p-norm networks F_p and the corresponding L_p-norms of the second derivatives $\|F_p''\|_p$ for $p = 2,\ 6,\ \text{and}\ \infty$ for the data in Example 1.

A Symplectic Numerical Method for Sixth Order Boussinesq Equations

Veselina Vucheva, Natalia Kolkovska

In this talk we consider two finite difference schemes for the Boussinesq Equation with a sixth order dispersion term (SOBE):

$$\frac{\partial^2 U}{\partial t^2} = \Delta U + \beta_1 \Delta \frac{\partial^2 U}{\partial t^2} - \beta_2 \Delta^2 U + \beta_3 \Delta^3 U - \alpha \Delta U^p,\ x \in (-\infty, \infty)\,,\ t > 0.$$

SOBE appears in various models of real processes, for example, in some micro-structure problems and in the bidirectional propagation of small amplitude on the surface of shallow water .

We rewrite the SOBE as a Hamiltonian system

$$\begin{aligned} \frac{\partial U}{\partial t} &= \frac{\partial V}{\partial x}, \\ \frac{\partial V}{\partial t} &= (I - \beta_1 \Delta)^{-1} \left(\frac{\partial U}{\partial x} - \beta_2 \frac{\partial^3 U}{\partial x^3} + \beta_3 \frac{\partial^5 U}{\partial x^5} - \alpha \frac{\partial U^p}{\partial x} \right), \end{aligned}$$

apply the leap-frog method and construct a symplectic scheme, which preserves the symplectic structure of the SOBE ([1], [2], [3]).

This scheme is explicit, conditionally stable and has second order of approximation to SOBE. For deriving of the second energy preserving scheme, we keep the linear terms in the symplectic scheme intact and appropriately approximate the nonlinearity. We prove that the solution of this scheme preserves the discrete Hamiltonian (equivalently, the discrete energy) exactly. The new scheme is implicit and the evaluation of the numerical solution is done via an iteration process.

Both finite difference schemes, the symplectic one and the energy preserving one, conserve the discrete mass exactly. Moreover, the solution to the symplectic scheme approximates with accuracy $O(h^2 + \tau^2)$ the discrete Hamiltonian.

Various numerical experiments are provided for the solution of SOBE with quadratic ($p = 2$) and cubic ($p = 3$) nonlinearity. The numerical simulations illustrate the efficiency of the schemes and are in a good agreement with the theoretical results.

Acknowledgment

This work is partially supported by the project DFNP 17-30 of the Program for young scientists' career development of Bulgarian Academy of Sciences and the Bulgarian Science Fund under grant DNTS/Russia 02/7.

References

[1] A. Aydin, B. Karasözen (2008), *Symplectic and multisymplectic Lobato methods for the 'good' Boussinesq Equation*, Journal of Mathematical Physics.

[2] V. Vucheva, N. Kolkovska, *A symplectic numerical method for Boussinesq equation*, AIP Conference Proceedings, 2025, 10.1063-1.5064941.

[3] N. Kolkovska, V. Vucheva, *Invariant preserving schemes for double dispersion equations*, Advances in Difference Equations, submitted for publications.

Part B

List of participants

A.Alexandrov
Institute of Information and
Communication Technologies
Bulgarian Academy of Sciences
Akad. G. Bonchev, Str., Bl. 2
Sofia, Bulgaria
akalexandrov@iit.bas.bg

Petko Alov
Institute of Biophysics and
Biomedical Engineering
Bulgarian Academy of Sciences
105 Acad G. Bonchev Str., 1113
Sofia, Bulgaria

Slav Angelov
Department of Informatics
New Bulgarian University
Montevideo str., 21
1618 Sofia, Bulgaria
sangelov@nbu.bg

Vera Angelova
Institute of Information and
Communication Technologies
Bulgarian Academy of Sciences
Akad. G. Bonchev, Str., Bl. 2
1113 Sofia, Bulgaria
vangelova@iit.bas.bg

Krassimir Atanassov
Institute of Biophysics and
Biomedical Engineering
Bulgarian Academy of Sciences
Acad. G. Bonchev str., bl.105
1113 Sofia, Bulgaria
krat@bas.bg

Owe Axelsson
Institute of Geonics, AS CR
Studentska 1768
70800 Ostrava, Czech Republic
owe.axelsson@it.uu.se

Tsonka Baicheva
Institute of Mathematics and Informatics,
Bulgarian Academy of Sciences
78, Nikola Gabrovski Str., P.O.Box 323
5000 Veliko Tarnovo, Bulgaria
tsonka@math.bas.bg

Todor Balabanov
Institute of Information and
Communication Technologies
Bulgarian Academy of Sciences
acad. G. Bontchev Str., block 2
1113 Sofia, Bulgaria
todorb@iinf.bas.bg

Mauro Ballicchia
Polytechnic University of Marche
Via Brecce Bianche 12
60131 Ancona, Italy
m.ballicchia@univpm.it

Majid Benam
TU Wien – Institute for Microelectronics
Gußhausstraße 27-29 / E360
A-1040 Vienna, Austria
benam@iue.tuwien.ac.at

Gergana Bencheva
Institute of Information and
Communication Technologies
Bulgarian Academy of Sciences
Acad. G. Bonchev Str., bl. 25A
1113 Sofia, Bulgaria
gery@parallel.bas.bg

Milen K. Borisov
Institute of Mathematics and Informatics,
Bulgarian Academy of Sciences
Acad. Georgi Bonchev Str., Block 8
1113 Sofia, Bulgaria
milen_kb@math.bas.bg

Stefan Bushev
Institute of Metal Science
Equipment and Technologies
with Center for Hydro and Aerodynamics
Bulgarian Academy of Sciences
Shipchenski prohod Str., 67
1574 Sofia, Bulgaria
stbushev@abv.bg

Hristo Chervenkov
National Institute of
Meteorology and Hydrology
Bulgarian Academy of Sciences
Tsarigradsko Shose blvd. 66
1784 Sofia, Bulgaria
hristo.tchervenkov@meteo.bg

Maria Datcheva
Institute of Mechanics
Bulgarian Academy of Sciences
Acad. G. Bonchev Str., Bl. 4
1113 Sofia, Bulgaria
datcheva@imbm.bas.bg

Miroslav Dimitrov
Institute of Mathematics and Informatics
Bulgarian Academy of Sciences
Acad. G. Bonchev str., bl. 8
1113 Sofia, Bulgaria
mirdim@math.bas.bg

Neli S. Dimitrova
Institute of Mathematics and Informatics,
Bulgarian Academy of Sciences
Acad. G. Bonchev Str., bl. 8
1113 Sofia, Bulgaria

Zlatinka I. Dimitrova
"G. Nadjakov" Institute of
Solid State Physics,
Bulgarian Academy of Sciences,
Blvd. Tzarigradsko Chaussee 72,
1782 Sofia, Bulgaria

Ivan Dimov
Institute of Information and
Communication Technologies,
Bulgarian Academy of Sciences
Acad. G. Bonchev Str., bl. 25A
1113 Sofia, Bulgaria
ivdimov@bas.bg

Milena Dimova
University of National and World Economy
Student Town
1700 Sofia, Bulgaria
mkoleva@math.bas.bg

Nina Dobrinkova
Institute of Information and
Communication Technologies
Bulgarian Academy of Sciences
Acad. G. Bontchev str., bl. 2
1113 Sofia, Bulgaria
ninabox2002@gmail.com

Violeta Dutcheva
Institute of Mathematics and Informatics
Bulgarian Academy of Sciences
78, Nikola Gabrovski Str., P.O.Box 323
5000 Veliko Tarnovo, Bulgaria

Isaac Elishakoff
Department of Ocean and
Mechanical Engineering
Florida Atlantic University
Boca Raton, FL
333434-0991, USA
elishako@fau.edu

Georgi Evtimov
Institute of Information and
Communication Technologies
Bulgarian Academy of Sciences
Acad. G. Bontchev str., bl. 25A
1113 Sofia, Bulgaria
gevtimov@abv.bg

Stefka Fidanova
Institute of Information and
Communication Technologies
Bulgarian Academy of Sciences
Acad. G. Bontchev str., bl. 25A
1113 Sofia, Bulgaria
stefka@parallel.bas.bg

A. Florian
Craiova University
Craiova, Romania

Tatiana Gateva-Ivanova
Max Planck Institute for
Mathematics in the Sciences (MiS), Leipzig
Inselstraße 22
4103 Leipzig, Germany
tatyana@aubg.edu

Jordan Genoff
Technical University of Sofia
branch Plovdiv
63 Sankt Petersburg Blvd
4000 Plovdiv, Bulgaria
jgenoff@tu-plovdiv.bg

Ivan Georgiev
Institute of Information and
Communication Technologies
Bulgarian Academy of Sciences
Acad. G. Bonchev Str., bl. 2
and
Institute of Mathematics and Informatics
Bulgarian Academy of Sciences
Acad. G. Bonchev str., bl. 8
1113 Sofia, Bulgaria

Krassimir Georgiev
Institute of Information and
Communication Technologies
Bulgarian Academy of Sciences
Acad. G. Bontchev str., bl. 25A
1113 Sofia, Bulgaria
georgiev@parallel.bas.bg

Petar Georgiev
Technical University of Varna
1, Studentska Str.
9010 Varna, Bulgaria
petar.ge@tu-varna.bg

Slavi Georgiev
Angel Kanchev University of Ruse
8 Studentska Str.
7017 Ruse, Bulgaia
georgiev.slavi.94@gmail.com

Atanaska Georgieva
Faculty of Mathematics and Informatics
University of Plovdiv "Paisii Hilendarski"
24 Tzar Asen
4000 Plovdiv, Bulgaria
afi2000@abv.bg

Vladimir Gerdjikov
Institute of Mathematics and Informatics
Bulgarian Academy of Sciences
Acad. G. Bonchev str., bl. 8
1113 Sofia, Bulgaria
vgerdjikov@math.bas.bg

Andrey Gizdov
National High School of Mathematics
and Natural Sciences "Acad. L. Chakalov"
52 Bigla str.
1164 Sofia, Bulgaria

Stanislav Harizanov
Institute of Information and
Communication Technologies
Bulgarian Academy of Sciences
Acad. G. Bonchev Str., bl. 25A
1113 Sofia, Bulgaria
sharizanov@parallel.bas.bg
and
Institute of Mathematics and Informatics
Bulgarian Academy of Sciences
Acad. G. Bonchev str., bl. 8
1113 Sofia, Bulgaria

Snezhana Hristova
Faculty of Mathematics and Informatics
University of Plovdiv Paisii Hilendarski
Tzar Asen 24,
4000 Plovdiv, Bulgaria
snehri@gmail.bg

Roumen Iankov
Institute of Mechanics
Bulgarian Academy of Sciences
Acad. G. Bonchev Str., Bl. 4
1113 Sofia, Bulgaria

Nikolay Ikonomov
Institute of Mathematics and Informatics
Bulgarian Academy of Sciences
Acad. G. Bonchev str., bl. 8
1113 Sofia, Bulgaria

Nevena Ilieva
Institute of Information and
Communication Technologies
Bulgarian Academy of Sciences
Acad. G. Bonchev Str, Block 25A
1113 Sofia, Bulgaria
nevena.ilieva@parallel.bas.bg

Vesselin Iossifov
School of Energy and
Information technology
University for Applied Sciences (HTW)
Berlin, Germany
Vesselin.Iossifov@htw-berlin.de

Vladimir Ivanov
National Institute of Geophysics,
Geodesy and Geography
Bulgarian Academy of Sciences
Acad. G. Bonchev str., bl. 3
1113 Sofia, Bulgaria
vivanov@geophys.bas.bg

Violeta N. Ivanova-Rohling
Bulgarian Academy of Sciences
Schneckenburgstrasse 3a
784621 Konstanz, Deutschland
violeta@math.bas.bg

Dessislava Jereva
Institute of Biophysics and
Biomedical Engineering
Bulgarian Academy of Sciences
105 Acad G. Bonchev Str., 1113
Sofia, Bulgaria

Juri Kandilarov
Ruse University
8 Studentska Str.
7017 Ruse, Bulgaria
ukandilarov@uni-ruse.bg

Kristina Kapanova
Institute of Information and
Communication Technologies
Bulgarian Academy of Sciences
Acad. G. Bonchev Str., bl. 25A
1113 Sofia, Bulgaria
kapanova@parallel.bas.bg

Leoneed Kirilov
Institute of Information and
Communication Technologies
Bulgarian Academy of Sciences
Acad. G. Bontchev str., bl. 2
1113 Sofia, Bulgaria
lkirilov@iinf.bas.bg

Natalia Kolkovska
Institute of Mathematics and Informatics
Bulgarian Academy of Sciences
Acad. G. Bonchev Str., Bl. 8
1113 Sofia, Bulgaria

Petia Koprinkova-Hristova
Institute of Information and
Communication Technologies
Bulgarian Academy of Sciences
Acad. G. Bontchev str., bl. 25-A
1113 Sofia, Bulgaria
pkoprinkova@bas.bg

Hristo Kostadinov
Institute of Mathematics and Informatics
Bulgarian Academy of Sciences
Acad. G. Bonchev str., bl. 8
1113 Sofia, Bulgaria

Mikhail I. Krastanov
Institute of Mathematics and Informatics,
Bulgarian Academy of Sciences and
Faculty of Mathematics and Informatics,
Sofia University "St. K. Ohridski"

V.Kyrychok
Paton Welding Institute
Kiev, Ukraine

Raytcho Lazarov
Department of Mathematics
Texas A&M University
77843-3368 College Station, TX, USA
lazarov@math.tamu.edu

Lingyun Li
Chair of Foundation Engineering
Soil and Rock Mechanics
Ruhr Universität Bochum
Geb. IC E5-115, Universitätstr.150,
44780, Bochum, Germany

Elena Lilkova
Institute of Information and
Communication Technologies
Bulgarian Academy of Sciences
25A, Acad. G. Bonchev Str. , Block 25A
1113 Sofia, Bulgaria
elilkova@parallel.bas.bg

Konstantinos Liolios
Institute of Information and
Communication Technologies,
Bulgarian Academy of Sciences
Sofia, Bulgaria
kostisliolios@gmail.com

Svetozar Margenov
Institute of Information and
Communication Technologies
Bulgarian Academy of Sciences
Acad. G. Bonchev Str., bl. 25A
1113 Sofia, Bulgaria
margenov@parallel.bas.bg

Pencho Marinov
Institute of Information and
Communication Technologies
Bulgarian Academy of Sciences
Acad. G. Bontchev str., bl. 25-A
1113 Sofia, Bulgaria
pencho@parallel.bas.bg

Lubomir Markov
Department of Mathematics and CS
Barry University
11300 N.E. Second Avenue
Miami Shores, FL 33161, USA
lmarkov@barry.edu

Rossen Mikhov
Institute of Information and
Communication Technologies
Bulgarian Academy of Sciences
Acad. G. Bontchev Str., Bl. 2
1113 Sofia, Bulgaria
rmikhov@abv.bg

Maya Mikrenska
UNWE
Studentski grad
1700 Sofia, Bulgaria
mikr@unwe.bg

Zlatogor Minchev
Institute of Information and
Communication Technologies
Bulgarian Academy of Sciences
Acad. G. Bontchev Str., Bl. 25A
1113 Sofia, Bulgaria
zlatogor@bas.bg
and
Institute of Mathematics and Informatics
Bulgarian Academy of Sciences
Acad. G. Bonchev Str., Bl. 8
1113 Sofia, Bulgaria

V. Monov
Institute of Information and
Communication Technologies
Bulgarian Academy of Sciences
Acad. G. Bontchev Str., Bl. 2
1113 Sofia, Bulgaria
vmonov@iit.bas.bg

Vladimir Myasnichenko
Tver State University
Tver, Russia
viplabs@yandex.ru

Iva Naydenova
Faculty of Mathematics and Informatics
University of Plovdiv Paisii Hilendarski
24 Tzar Asen
4000 Plovdiv, Bulgaria
iva.naydenova@asm32.info

Maya Neytcheva
Department of Information Technology
Uppsala University, Sweden,
maya.neytcheva@it.uu.se

Nikolay I. Nikolov
Institute of Mathematics and Informatics
Bulgarian Academy of Sciences
Acad. G.Bontchev str., block 8
1113 Sofia, Bulgaria
n.nikolov@math.bas.bg

Svetoslav G. Nikolov
Institute of Mechanics
Bulgarian Academy of Sciences
Acad. G. Bonchev Str., Bl. 4
1113 Sofia, Bulgaria

Elena V. Nikolova
Institute of Mechanics
Bulgarian Academy of Sciences
Acad. G. Bonchev Str., Bl. 4
1113 Sofia, Bulgaria
elena@imbm.bas.bg

Silviya Nikolova
Department of Anthropology
and Anatomy
Institute of Experimental Morphology,
Pathology and Anthropology
with Museum
Bulgarian Academy of Sciences
Acad. G. Bonchev Str., bl. 25
1113 Sofia, Bulgaria
sil_nikolova@abv.bg

Tzvetan Ostromsky
Institute of Information and
Communication Technologies,
Bulgarian Academy of Sciences
Acad. G. Bonchev Str., bl. 25A
1113 Sofia, Bulgaria
ceco@parallel.bas.bg

Ilza Pajeva
Institute of Biophysics and
Biomedical Engineering
Bulgarian Academy of Sciences
105 Acad G. Bonchev Str., 1113
Sofia, Bulgaria

Ludmila Parashkevova
Institute of Mechanics
Bulgarian Academy of Sciences
Acad. G. Bontchev str., bl. 4
1113 Sofia, Bulgaria
lusy@imbm.bas.bg

Albena Pavlova
Department of MPC
Technical University-Sofia, Plovdiv Branch
4000 Plovdiv, Bulgaria
akosseva@gmail.com

Tania Pencheva
Institute of Biophysics and
Biomedical Engineering
Bulgarian Academy of Sciences
105 Acad G. Bonchev Str., 1113
Sofia, Bulgaria
tania.pencheva@biomed.bas.bg

Nedyu Popivanov
Institute of Information and
Communication Technologies
Bulgarian Academy of Sciences and
Sofia University "St. Kliment Ohridski"
nedyu@parallel.bas.bg

Svilen I. Popov
Institute of Mechanics
Bulgarian Academy of Sciences
Acad. G. Bonchev Str., Bl. 4
1113 Sofia, Bulgaria

Evgenija D. Popova
Institute of Mathematics and Informatics
Bulgarian Academy of Sciences
Acad. G. Bonchev str., block 8
1113 Sofia, Bulgaria
epopova@math.bas.bg

Stefan Radev
Institute of Mechanics
Bulgarian Academy of Sciences
Acad. G. Bontchev str., bl. 4
1113 Sofia, Bulgaria
stradev@imbm.bas.bg

Nikolay Sdobnyakov
Tver State University
Tver, Russia

Blagovest Sendov
Institute of Information and
Communication Technologies
Bulgarian Academy of Sciences
Acad. G. Bontchev Str., Bl. 25A
1113 Sofia, Bulgaria
bsendov@bas.bg

Dimitar Slavchev
Institute of Information and
Communication Technologies,
Bulgarian Academy of Sciences
Acad. G. Bonchev Str., bl. 25A
1113 Sofia, Bulgaria
dimitargslavchev@parallel.bas.bg

Stefan Stefanov
Institute of Information and
Communication Technologies
Bulgarian Academy of Sciences
Acad. G. Bontchev str., bl. 2
1113 Sofia, Bulgaria
stefans.stefanov303@gmail.com

Miroslav Stoenchev
Technical University of Sofia
Bul."Kl. Ohridski" 8
1000 Sofia, Bulgaria
MATHEMATICSMIROSLAV@gmail.com

Eugenia Stoimenova
Institute of Mathematics and Informatics
Bulgarian Academy of Sciences
Acad. G. Bontchev str., bl. 8
1113 Sofia, Bulgaria
jeni@math.bas.bg

A. Streche-Pauna
Craiova University
Craiova, Romania

Sonia Tabakova
Institute of Mechanics
Bulgarian Academy of Sciences
Acad. G. Bontchev str., bl. 4
1113 Sofia, Bulgaria
stabakova@gmail.com

Radoslava Terzieva
Faculty of Mathematics and Informatics
University of Plovdiv Paisii Hilendarski
Tzar Asen 24,
4000 Plovdiv, Bulgaria
radoslavaterzieva@abv.bg

Michail D. Todorov
Department of Applied
Mathematics and Computer Science
Technical University of Sofia
1000 Sofia, Bulgaria
mtod@tu-sofia.bg

Venelin Todorov
Institute of Information and
Communication Technologies
Bulgarian Academy of Sciences
Acad. G. Bonchev Str., bl. 25A
1113 Sofia, Bulgaria

Diana Toneva
Department of Anthropology
and Anatomy
Institute of Experimental Morphology,
Pathology and Anthropology
with Museum
Bulgarian Academy of Sciences
Acad. G. Bonchev Str., bl. 25
1113 Sofia, Bulgaria

Stoyan Tranev
"Prof. Asen Zlatarov" University
"Prof. Yakimov" Blvd 1
8000 Burgas, Bulgaria

Velichka Traneva
"Prof. Asen Zlatarov" University
"Prof. Yakimov" Blvd 1
8000 Burgas, Bulgaria

Lozanka Trenkova
Faculty of Mathematics and Informatics
University of Plovdiv "Paisii Hilendarski"
24 Tzar Asen
4000 Plovdiv, Bulgaria
lozanka@hotmail.com

Ivanka Tsakovska
Institute of Biophysics and
Biomedical Engineering
Bulgarian Academy of Sciences
105 Acad G. Bonchev Str., 1113
Sofia, Bulgaria

Biser Tsvetkov
Institute of Mathematics and Informatics
Bulgarian Academy of Sciences
Acad. G. Bonchev Str., Bl. 8
1113 Sofia, Bulgaria

Vassil M. Vassilev
Institute of Mechanics
Bulgarian Academy of Sciences
Acad. G. Bonchev Str., Bl. 4
1113 Sofia, Bulgaria

Toddor Velev
Institute of Information and
Communication Technologies,
Bulgarian Academy of Sciences
Acad. G. Bonchev Str., bl. 2
1113 Sofia, Bulgaria
toddorv@gmail.com

Kaloyan N. Vitanov
Institute of Mechanics
Bulgarian Academy of Sciences
Acad. G. Bonchev Str., Bl. 4
1113 Sofia, Bulgaria

Nikolay K. Vitanov
Institute of Mechanics
Bulgarian Academy of Sciences,
Acad. G. Bonchev Str.,Bl. 4
1113 Sofia, Bulgaria
vitanov@imbm.bas.bg

Krassimira Vlachkova
Faculty of Mathematics and Informatics
Sofia University "St. Kl. Ohridski"
Blvd. James Bourchier 5
1164 Sofia, Bulgaria
krassivl@fmi.uni-sofia.bg

Veselina Vucheva
Institute of Mathematics and Informatics
Bulgarian Academy of Sciences
Acad. G. Bonchev Str., Bl. 8
1113 Sofia, Bulgaria

Lubin Vulkov
Ruse University
6 Studentska St
7017 Ruse, Bulgaria
lvalkov@uni-ruse.bg

Yavor Vutov
Institute of Information and
Communication Technologies,
Bulgarian Academy of Sciences
Acad. G. Bonchev Str., bl. 25A
1113 Sofia, Bulgaria
yavor@parallel.bas.bg

P. Yukhimets
Paton Welding Institute
Kiev, Ukraine

Daniela T. Zaharieva
Todor Kableshkov University of Transport
Geo Milev Str. 158
1574 Sofia, Bulgaria